April 24, 1973

To the Graduate Council:

I am submitting herewith a thesis written by John H. Wickman entitled "Internal Cooling Study of Discrete Injector Transpiration Cooled Nosetips." I recommend that it be accepted for nine quarter hours of credit in partial fulfillment of the requirements for the degree of Master of Science, with a major in Mechanical Engineering.

Major Professor

We have read this thesis
and recommend its acceptance:

Accepted for the Council:

Vice Chancellor for
Graduate Studies and Research

INTERNAL COOLING STUDY OF DISCRETE INJECTOR TRANSPIRATION COOLED NOSETIPS

A Thesis

Presented to

the Graduate Council of

The University of Tennessee

In Partial Fulfillment

of the Requirements for the Degree

Master of Science

---

by

John H. Wickman

August 1973

ACKNOWLEDGEMENTS

The author expresses his appreciation to the United States Air Force (SAMSO) for awarding the discrete injector transpiration cooled nosetips research contract number 844001-5401R-95 to The University of Tennessee Space Institute and also to major contractor Aerotherm, Inc. thus allowing him to participate in the program. Appreciation of help received in preparing graphs and sections of the text is given to Juergen Bitte and Walter Harper. Appreciation is also given to Philip Yee who helped prepare this thesis for final printing.

The author wishes to acknowledge Dr. Walter Frost for his extra effort and patience that was required in preparing the thesis due to the author living in Connecticut rather than Tennessee.

1105995

ABSTRACT

The purpose of this investigation was to determine an experimental and analytical program to determine the single phase and two phase flow and heat transfer mechanics in rectangular ducts of 0.005 × 0.02 inch cross-sectional dimensions typical of discrete injector slots on transpiration cooled nosetips. Mass fluxes from 0 to 10 $lb_m/sec\text{-}ft^2$ exhausting to pressurized environments of 0 to 2000 psig were used in the study. Maximum simulated heat fluxes on the order of 500 $Btu/sec\text{-}ft^2$ were achieved.

Results indicated that very little in-depth cooling is achieved and that the primary cooling effects of liquid injection must occur externally in the boundary layer. The mechanics of flow in the slot determine whether the liquid is ejected as a mist or as large globules, with the transition between flow patterns occurring rather suddenly when a critical condition is reached and accompanied with substantial surface temperature excursions. It is conjectured that this phenomenon may be responsible for the sudden failure of nosetips under flight conditions.

TABLE OF CONTENTS

CHAPTER	PAGE
INTRODUCTION	1
I. DESCRIPTION OF TEST APPARATUS	5
Introduction	5
Description of Flow Loop	5
II. DESCRIPTION OF PRESSURE VESSEL AND TEST PACKAGE	10
III. INSTRUMENTATION OF APPARATUS	23
IV. DESCRIPTION OF TEST FACILITY AND TEST PROCEDURES	35
V. RESULTS OF TEST RUNS	39
VI. DISCUSSION OF RESULTS	98
VII. CONCLUSIONS	115
BIBLIOGRAPHY	117
APPENDIXES	119
A. EXPERIMENT PROCEDURE	120
B. SINGLE PHASE FLOW DATA ANALYSIS	125
C. DETERMINATION OF THE HEAT TRANSFER COEFFICIENT AT THE COOLANT-SOLID INTERFACE	129
D. DETERMINATION OF HEAT FLUX FROM HEATER POWER INPUT AND BLOCK TEMPERATURE	132
E. THOMPSON SOLUTION WITHOUT ASSUMPTION $T_s = T_F$	136
VITA	143

LIST OF TABLES

TABLE		PAGE
I.	Test Matrix	40
II.	Test Data from Run 9a	42
III.	Test Data from Run 9b	43
IV.	Test Data from Run 9c	45
V.	Test Data from Run 10a	46
VI.	Test Data from Run 10b	47
VII.	Test Data from Run 11	48
VIII.	Test Data from Run 13a	49
IX.	Test Data from Run 13b	51
X.	Test Data from Run 14	53
XI.	Test Data from Run 15	54
XII.	Test Data from Run 16a	56
XIII.	Test Data from Run 16b	57
XIV.	Test Data from Run 18	58

LIST OF FIGURES

FIGURE		PAGE
1.	Types of Flow Conditions	2
2.	Schematic of Flow Loop	6
3.	Volumetric Flow Versus Discharge Pressure for Feed Pump	8
4.	Mounting of Test Package in Pressure Vessel	11
5.	Photograph of Finned Heat Exchanger and Cooling Jacket	12
6.	Test Package Assembly	14
7.	Plenum Chamber and Manifold	16
8.	Fabrication of Slotted Plate	17
9.	Flange on Test Section	18
10.	Copper Wedge with Electrical Cartridge Heaters	19
11.	Ceramic Clamping Blocks on Test Package	21
12.	Corrosion of Flange on Stainless Steel Plate	22
13.	Temperature Distribution and Location of Mounting of Thermocouples	24
14.	Thermocouple Spacing on Test Slot	25
15.	Junction Box in Test Package	27
16.	Thermocouple at Exit Plane	28
17.	Test Facility Layout	36
18.	Control Panel for TCNT Experiment	37
19.	Single Phase Data, Set 10--Runs 1 and 2	61
20.	Single Phase Data, Set 10--Runs 3 and 4	62

FIGURE PAGE

21. Single Phase Data, Set 10--Runs 5 and 6 63
22. Single Phase Data, Set 10--Runs 7 and 8 64
23. Single Phase Data, Set 10--Run 9, and Set 11--Run 10 65
24. Single Phase Data, Set 11--Runs 11 and 13 66
25. Single Phase Data, Set 11--Run 14 67
26. Single Phase Data, Set 14--Runs 1 and 2 68
27. Single Phase Data, Set 16--Runs 1 and 2 69
28. Single Phase Data, Set 16--Runs 3 and 4 70
29. Single Phase Data, Set 16--Runs 5 and 6 71
30. Single Phase Data, Set 16--Runs 7 and 8 72
31. Single Phase Data, Set 16--Runs 9 and 10 73
32. Single Phase Data, Set 18--Runs 5 and 6 74
33. Pressure Drop and Ratio of Calculated to Measured Mass Flux Versus Elapsed Run Time 76
34. Temperature Distribution, Test 9--Runs 1-6 77
35. Temperature Distribution, Test 9--Runs 7-13 78
36. Temperature Distribution, Test 9--Runs 14-20 . . . 79
37. Temperature Distribution, Test 11--Runs 12, 15, and 16 80
38. Temperature Distribution, Test 13a--Runs 1-8 . . . 81
39. Temperature Distribution, Test 13b--Runs 9-16 . . . 82
40. Temperature Distribution, Test 14--Runs 3, 4, and 5 83

FIGURE PAGE

41. Temperature Distribution, Test 15--Runs 1, 2, 3, and 8 84
42. Temperature Distribution, Test 18--Runs 1-6 85
43. Correlation of Heat Flux with Heater Power, Temperatures of Heater Block--Slot Exit and Vessel Atmosphere and Heat Transfer Coefficient to Chamber Atmosphere 87
44. Consecutive Temperature Profiles During Oscillating Flow 89
45. Temperature at Station 1 Versus Time for Oscillating Flow 90
46. Temperature Profile Excursion 91
47. Single Phase Flow 92
48. Two-Phase Dispersed Flow 93
49. Two-Phase Globule Flow 94
50. Sensitivity to Change in Mass Flux at Pressure = 500 Psig, Power = 640 Watts 96
51. Sensitivity to Change in Mass Flux at Pressure = 1030 Psig, Power = 1407 Watts 97
52. Correlation of Heat Transfer Coefficient for Liquid Water 99
53. Comparison of Single Phase Pressure Drop with Aerojet Design Correlation 101
54. Comparison of The University of Tennessee Space Institute Computer Code Solutions with Data from Test 15, Run 1 106

FIGURE PAGE

55. Transition from Mist Flow to Globule Flow 110

56. Surface Temperature Versus Heat Flux for Stable Flow 112

57. Representation of Actual Temperature Distribution by Mass Flow Iteration 128

58. Qualitative Solutions to Approaches I-III 138

59. Influence of h--Approach I 139

60. Influence of h--Approach II 140

NOMENCLATURE

A_c	Cross-sectional area of solid per unit area of plate
A_s	Channel cross-sectional area
d	Diameter of round slot
D_H	Hydraulic diameter of channel
f	Friction factor
G_{cal}	Calculated mass flux
G_{meas}	Measured mass flux
h	Convective heat transfer coefficient between channel walls and fluid
h_e	Convective heat transfer coefficient between the copper wedge and vessel atmosphere
h_L	Limiting convective heat transfer coefficient between channel wall and fluid
H	Fluid enthalpy
k	Thermal conductivity
K_c	Contraction coefficient
K_e	Expansion coefficient
L	Length of channel
$\dot{m}$	Mass flow rate
p	Pressure
P	Periphery of channel
P	Power input to heaters
q	Heat flux

t	Time
T	Temperature
T_f	Fluid temperature
T_s	Channel wall temperature
v	Specific volume
w	Distance between channels measured from their centers
W	Oxide film thickness
X_{tr}	Quality at which flow changes from equilibrium to non-equilibrium phase change
α	Viscous resistance coefficient
β	Inertia resistance coefficient
σ	Surface tension
μ	Fluid viscosity
η	Fraction of energy transferred to a mixture element used to evaporate liquid
ρ	Density

Subscripts

ℓ	Saturated liquid
g	Saturated vapor

INTRODUCTION

The object of the internal cooling study is to provide an adequate engineering description of significant heat transfer and fluid mechanics phenomena which occur inside the external contour of a discrete injection nosetip.

Figure 1 shows a schematic of the discrete injector concept. A coolant flows through multi-injector slots and exhausts into the high enthalpy and high pressure reentry environment. Interest lies in determining for a given heat flux and external pressure at the surface, the mass flow rate and the fluid state at the slot inlet necessary to avoid melting temperatures on the nosetip. Three types of flow conditions may be encountered in the slots as illustrated in Figure 1. Pure liquid can flow through the slots and exhaust on the surface as a liquid layer. At higher heat flux or inlet temperatures and at the same mass flow rate, the liquid may change phase internally and exhaust as a two phase mixture or as a superheated vapor. With even higher heat fluxes, the phase change may occur upstream in the plenum and pure vapor will flow in the slots; or alternatively, gas injection may be desired and the fluid will enter as a gas.

Under typical flight conditions the nosetip will be exposed to a heat flux range from 0 to 20,000 Btu/sec-ft^2 and to pressures from 1 to 250 atmospheres. At the higher

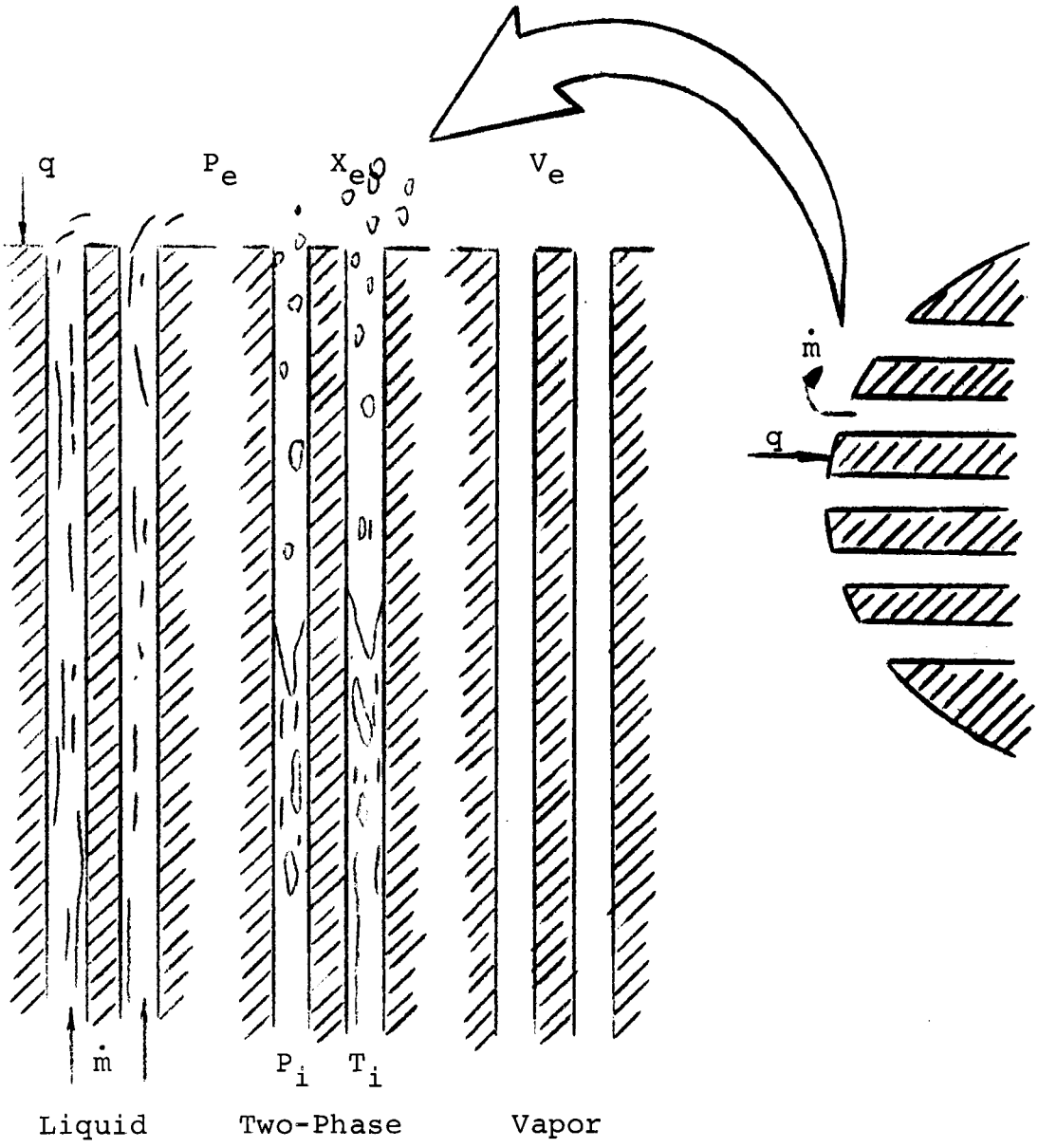


Figure 1. Types of flow conditions.

pressures the water coolant will be near the thermodynamic supercritical state.

The designer of the nosetip will normally require predictions of the slot dimensions and spacing, mass flow rate in each slot, and the internal fluid distributing and pressurizing system to accommodate the anticipated surface heating and pressures during reentry. Knowledge of the local surface heat flux and external pressure will be available from the external cooling study, and of the interaction between the injected fluid with the boundary layer from the combined cooling study. The internal cooling study is thus directed toward providing methods for predicting in a given slot:

1. The flow condition in the slot.

2. The temperature on the surface of the land.

3. The state of the fluid at the exit for determining both cooling efficiency and boundary conditions for the external flow analysis (i.e., temperature, quality, and velocity of fluid plus phase pattern which includes liquid droplets, liquid layer with bubbles, etc.).

4. The inlet pressure necessary to maintain the mass flow rate under the various types of flow expected.

Also of interest are operating conditions which induce sudden flow excursions or oscillations and how these may be avoided.

This report describes an experiment which was carried out to provide an understanding of the mechanism of the

in-depth cooling achieved in thin slots and to verify and develop thermal analysis and flow rate prediction techniques.

CHAPTER I

DESCRIPTION OF TEST APPARATUS

I. INTRODUCTION

The major components of the test apparatus are a flow loop designed to provide steady high pressure flow (0-5000 psig) at very low and accurately measured flow rates (0-28.2 cc/min), a pressure vessel in which the high pressure reentry environment is simulated, and a test package which models the discrete injection slots and the heating on the exit surface as experienced in flight.

II. DESCRIPTION OF FLOW LOOP

A schematic of the flow loop is shown in Figure 2. Initially water is degassed by heating it to 220 °F with the use of an electrical heating element submerged in the stainless steel degassing and storage tank. The temperature of the water in the storage tank is controlled with an adjustable thermostat having a temperature sensing element submerged in the water. A nitrogen bottle and 3000 psi regulator are used to pressurize the storage tank to 30 psi providing sufficient suction head for the downstream pump. The tank is designed to hold pressures up to 300 psi and has a safety valve to prevent over-pressurization. The five gallon capacity of the tank permits eight hours of continuous

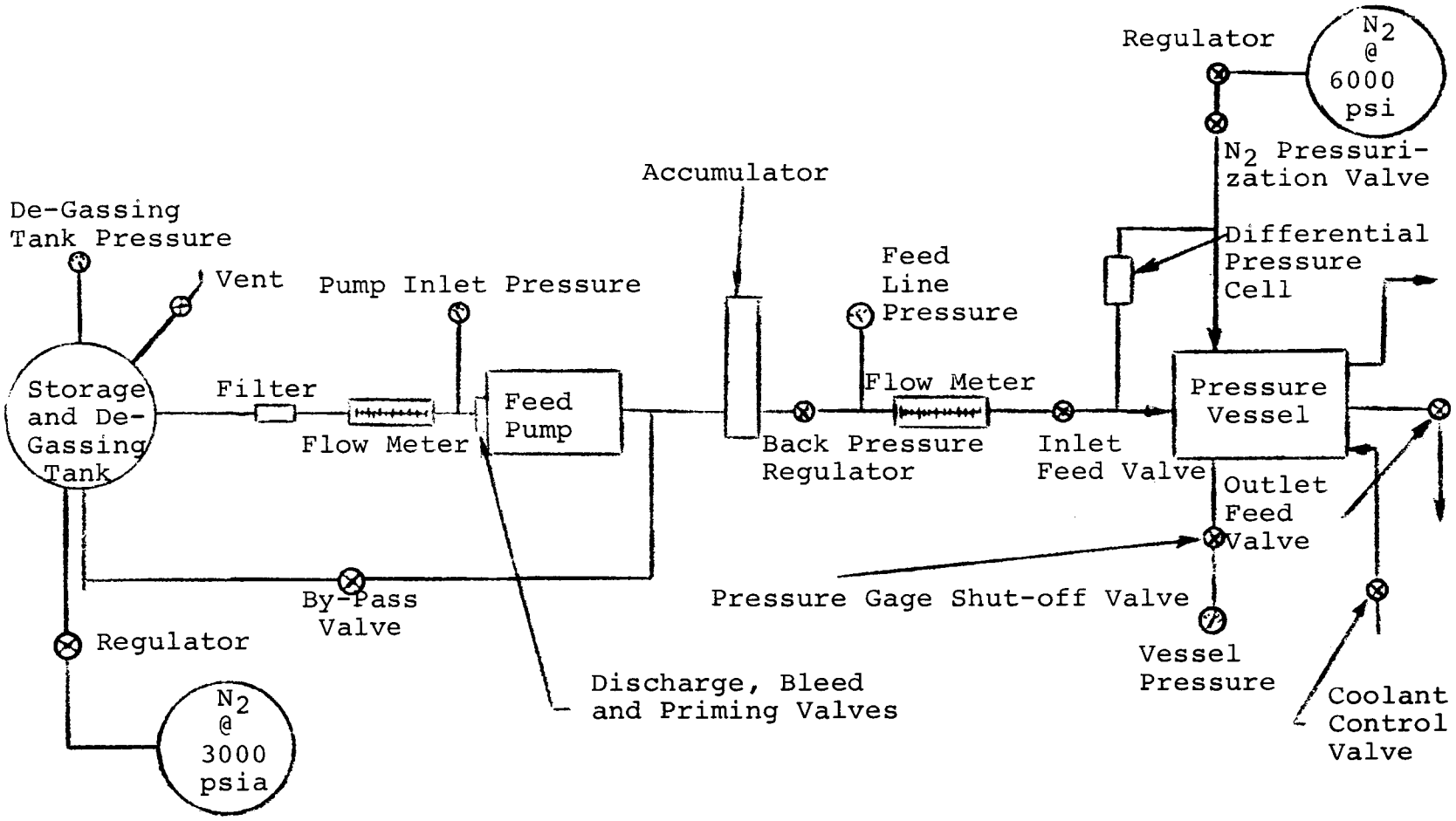


Figure 2. Schematic of flow loop.

operation at the maximum flow rate planned for any test. Due to the low flow rates, the water assumes room temperature very quickly after leaving the storage vessel, in general, by the time it reaches the pump.

The water is pumped by a diaphragm-piston feed pump. A graph of the flow rate as a function of exit pressure is shown in Figure 3. The minimum controllable flow rate is five per cent of the flow rate at zero exit pressure. The flow rate is controlled with a micrometer dial control which adjusts the pump stroke. A by-pass loop was added to the system to permit flows below the five per cent minimum pump flow rate. A stainless steel eight micron filter at the pump inlet eliminates particles from clogging the pump and contaminating the system.

An accumulator is installed downstream from the pump to compensate for the flow pulsations generated by the reciprocating pump. The accumulator in a fluid circuit is the counterpart of a capacitor in an electrical circuit. It consists of a cylindrical tank with a piston or diaphragm separating the tank into two chambers. One chamber of the accumulator is connected to the flow loop while the other is charged with a gas at approximately 90 per cent of the pressure in the flow loop. The piston or diaphragm in the accumulator moves back and forward in phase with the pump piston, accumulating and discharging fluid such that the pulsations are damped out.

A back-pressure regulator is located downstream from

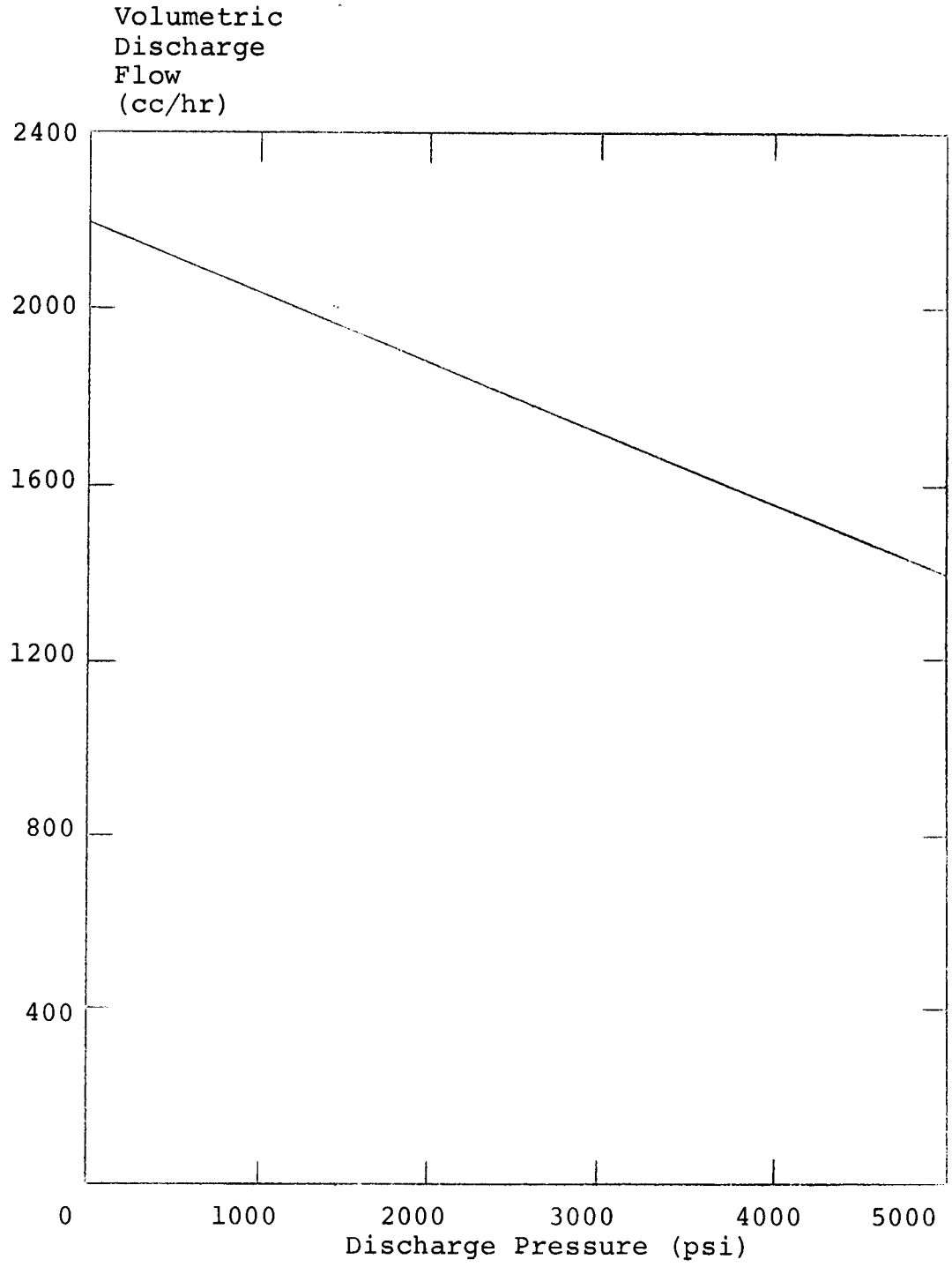


Figure 3. Volumetric flow versus discharge pressure for feed pump.

the accumulator and maintains a constant upstream line pressure. Since the flow rate from the pump is directly proportional to the discharge line pressure, the regulator assures a constant flow rate. Without the back-pressure regulator, the discharge pressure would be equal to the vessel pressure and any pressure variations in the vessel would generate unsteady pumping rates. The regulator can be set to maintain a constant line pressure within a pressure range of 25 to 4000 psi.

A 5000 psi rotameter measures the flow rate of water into the pressure vessel. Three interchangeable, calibrated guide tubes and floats permit flow rate measurements in the 0.1-1.02, 0.5-4.96, and 2.0-28.2 cc/min ranges. An accuracy of one per cent full scale is obtained with this rotameter. A 0 to 5000 psi pressure gage upstream from the rotameter is used to monitor the approximate inlet feed line pressure.

A digital needle valve is located downstream from the rotameter to act as a shut-off and control valve for the water flowing into the vessel. Its main function is to act as a shut-off valve to allow the pressure vessel to be evacuated and pressurized without interfering with the flow loop. A by-pass valve and the diaphragm stroke control on the pump are the primary flow control devices. The by-pass valve is simply a digital needle valve which bleeds off mass flow from the pump exit and returns it to the degassing and storage tank. The maximum flow capacity of both valves is 32 cc/min.

CHAPTER II

DESCRIPTION OF PRESSURE VESSEL AND TEST PACKAGE

A stainless steel pressure vessel 18.5 x 15 in. O.D. with two one inch diameter windows directly opposite to one another for direct viewing and photographic purposes contains the test package and instrumentation. The test package is directly attached to the pressure vessel cover as shown in Figure 4. A copper cooling jacket surrounds the inner walls of the vessel and a finned heat exchanger is positioned on the bottom as shown in Figure 5. The purpose of the heat exchanger and cooling jacket are to condense the steam flowing from the slotted test section, thus eliminating condensate on the observation windows, and to maintain the pressure vessel at a safe operating temperature for structural integrity during high pressure and high heat flux operations. The exchangers, however, were not effective in preventing fog from forming inside the vessel and obscuring the view of the test section at high flow rates. This was unexpected since design analysis indicated that the heat exchanger would condense the maximum steam ejected from the slots. The origin of the fog is believed to occur at the higher flow rates from liquid leaving the slots and running down over the copper heater block and boiling off similar to a sauna bath. Possible methods for eliminating water from

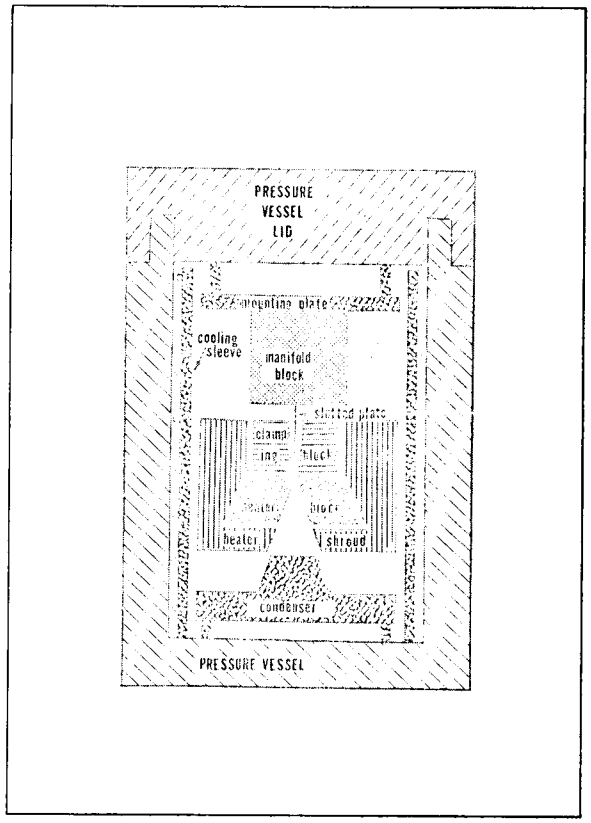


Figure 4. Mounting of test package in pressure vessel.

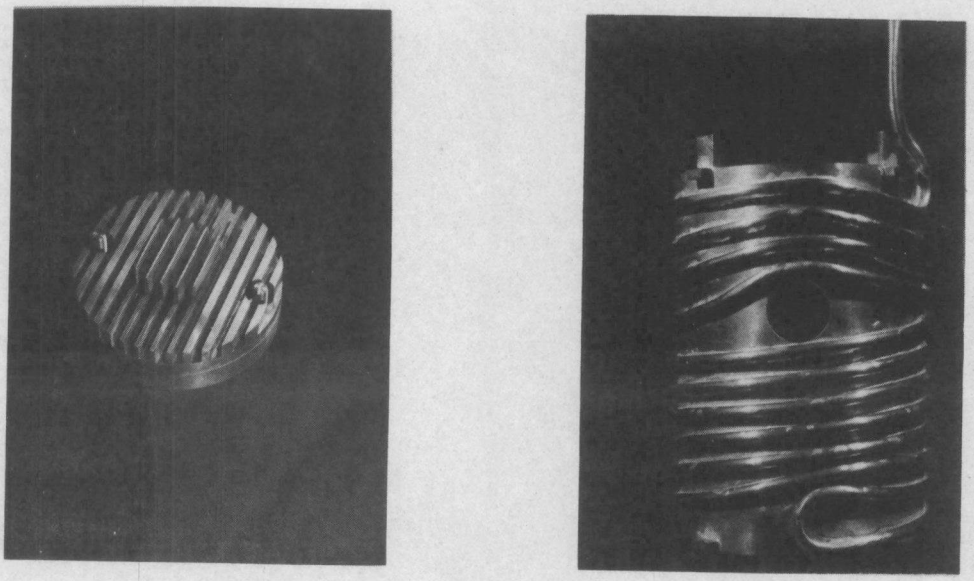


Figure 5. Photograph of finned heat exchanger and cooling jacket.

boiling on the heater are coating the wedge with non-wetting material or using a wick to carry the water away to the sides. Neither of these methods were attempted within the time limits of the program.

Water exhausted from the slotted test section can be drained from the bottom of the vessel through a digital needle valve controlled drain line. The water inlet flow rates are usually so small during test runs, however, that the drain valve is generally closed for the test.

The vessel is pressurized using 6000 psig bottled nitrogen. A regulator and needle shut-off valve control the flow of nitrogen to the vessel. A safety relief valve set at a pressure of 3200 psi prevents over-pressurization of the vessel.

Figure 6 shows the test package assembly. The 1/16 inch diameter tubing shown in the photograph runs out through the vessel cover where it is coupled to a 1/4 inch diameter feed line. The 1/16 inch feed line serves as a capillary tube through which the water flows into a plenum chamber and manifold arrangement. The plenum chamber is made by drilling straight through the steel block to form a cylindrical hole sealed with two end plugs. During test 17 one plug came loose allowing water to flow down the side of the steel block onto the cartridge heater lead wires. All the wires to the electrical heaters on that side broke due to thermal shock. The plug was recemented into place but it is recommended that it eventually be welded in place.

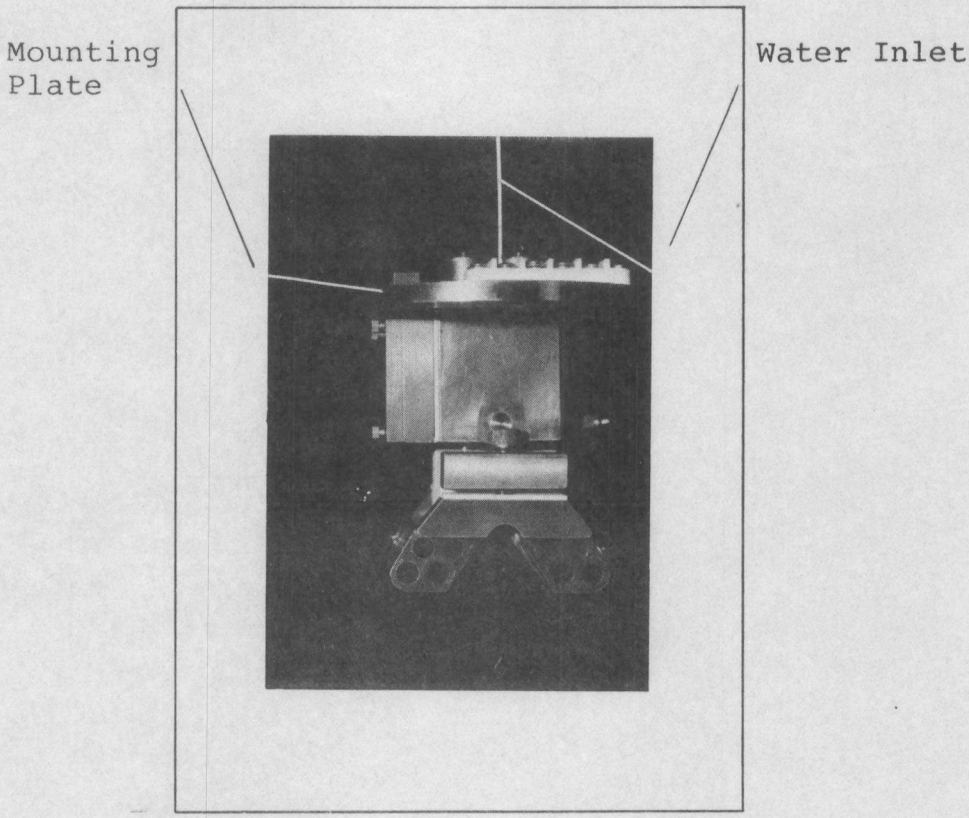


Figure 6. Test package assembly.

The manifold effect is achieved by inserting the slotted plate into the plenum such that the entrance plane is half into the plenum chamber hence the fluid does not flow directly at any single slot but enters the plenum in an axial direction and flows up and over to the slot inlet assuring uniform flow distribution. Figure 7 shows the plenum chamber and manifold arrangement.

The slotted test section consists of 15 rectangular channels, 0.005 x 0.02 inches, machined in a central stainless steel plate which is sandwiched between two 0.035 inch flat stainless steel plates and the complete unit fusion bonded. The size of the slots are typical of those of a transpiration cooled nose tip. The outer plates are bent 90 degrees at one end to form a lip which contacts the copper heater upon installation in the test package (Figures 8 and 9).

The heat flux to the slotted test section is supplied by a triangular shaped copper wedge which focuses the energy of eight 200 watt electrical cartridge heaters imbedded inside the wedge on the lip of the slotted test section. Figure 10 shows the copper heater and the cartridges lying in the background. The cartridges are press fitted into the holes to minimize contact resistance and maximize the transfer of energy to the wedge. The electrical heaters are wired in parallel to obtain the maximum power input from each heater. The maximum block temperature is dictated by the melting temperature of the block, approximately 1200 °F.

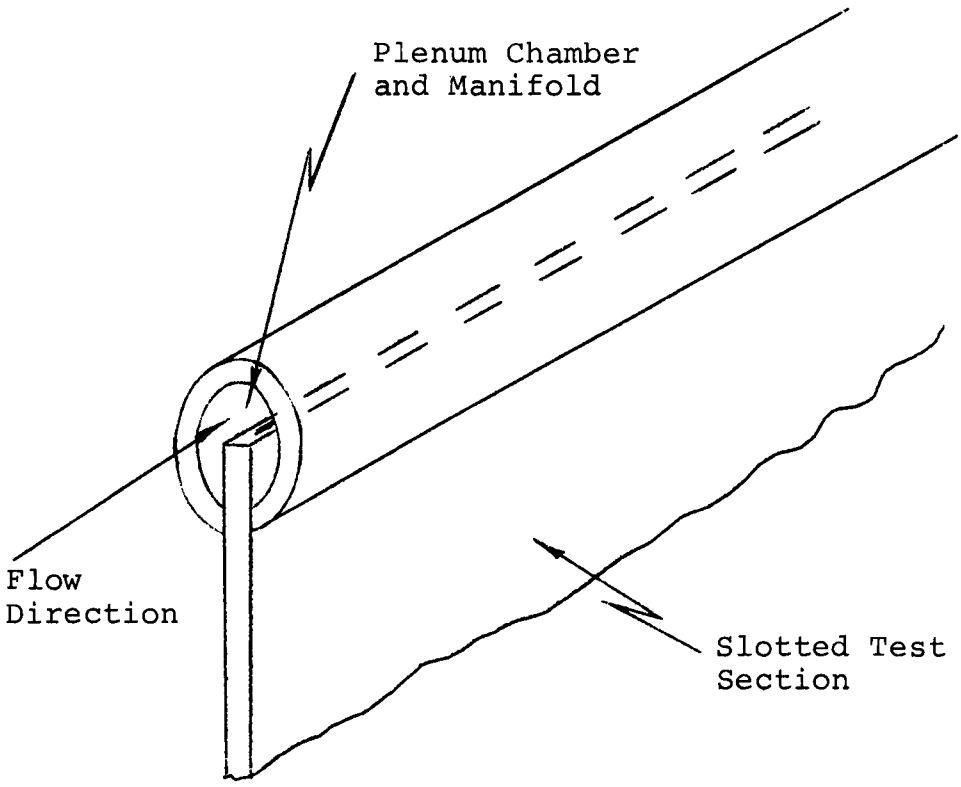


Figure 7. Plenum chamber and manifold.

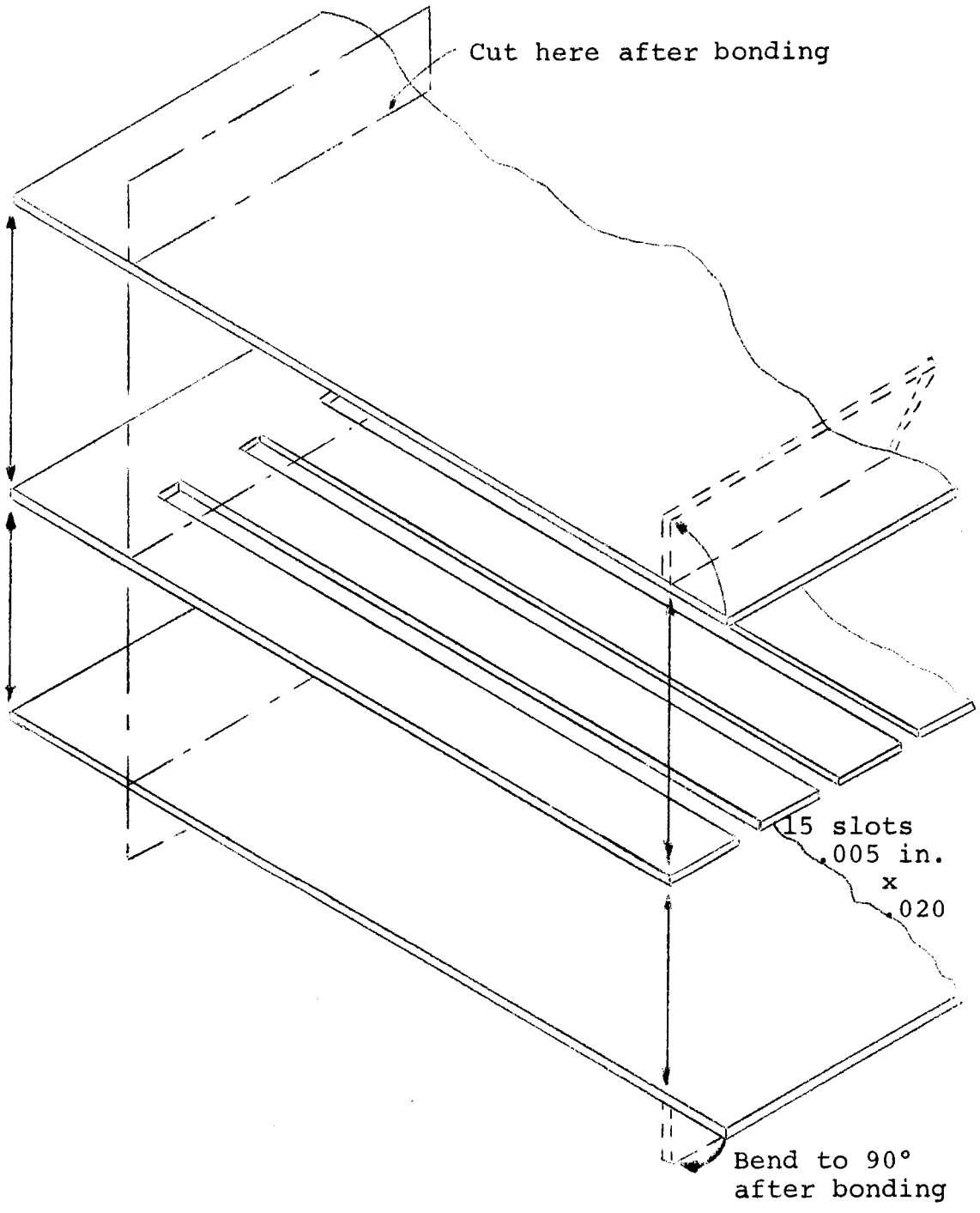


Figure 8. Fabrication of slotted plate.

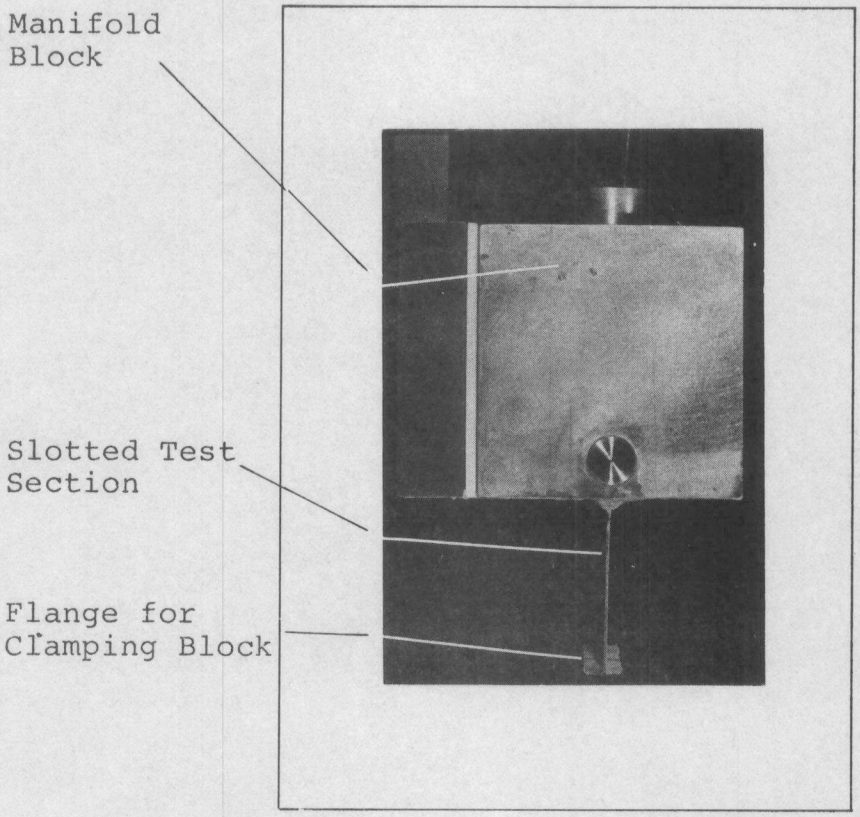


Figure 9. Flange on test section.

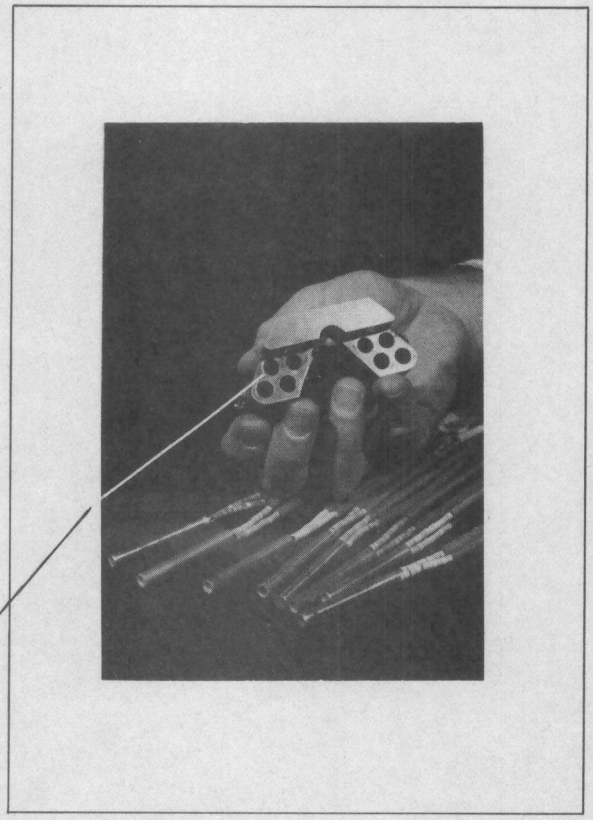


Figure 10. Copper wedge with electrical cartridge heaters.

A significant amount of energy is lost from the exposed areas of the heater by convection. Strong convection currents were actually visible through the observation window. The heat flux steadily increases as the energy flow area decreases until it reaches a maximum valve at the tip of the wedge. The flange of the test section is clamped tightly between the copper heater and two ceramic support blocks shown in Figure 11. The complete assembly is shown in Figure 6, page 14.

Design analysis indicated that heat fluxes to the surface of the lands on the order of 2000 Btu/ft^2-sec were possible with the copper block heater; however, heat fluxes on the order of only 150 Btu/ft^2-sec were achieved. The reason for this is the high contact resistance between the tip of the copper wedge and flange on the test section. Severe corrosion on the flange resulted at high temperatures and pressures despite the 99 per cent pure nitrogen atmosphere. Figure 12 shows a magnified view of the flange showing corrosion so severe the slots are not even visible. This corrosion greatly increases the contact resistance. The ceramic clamping blocks lost considerable structural strength after heating and hence did not allow high clamping pressures between the flange and wedge tip. This further increased the contact resistance. For later runs stainless steel support blocks were machined and replaced the ceramic blocks. Higher heat fluxes were achieved but the 2000 Btu/ft^2-sec value was still not approached.

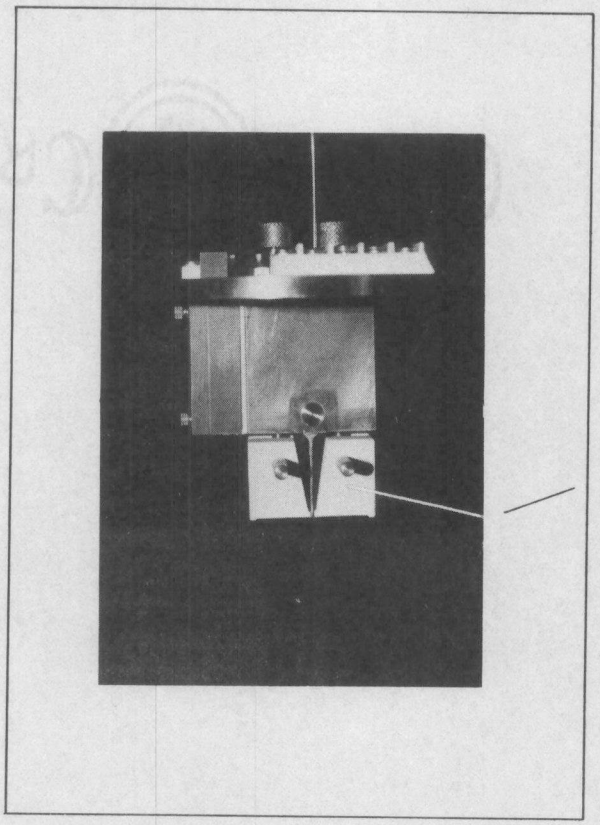


Figure 11. Ceramic clamping blocks on test package.

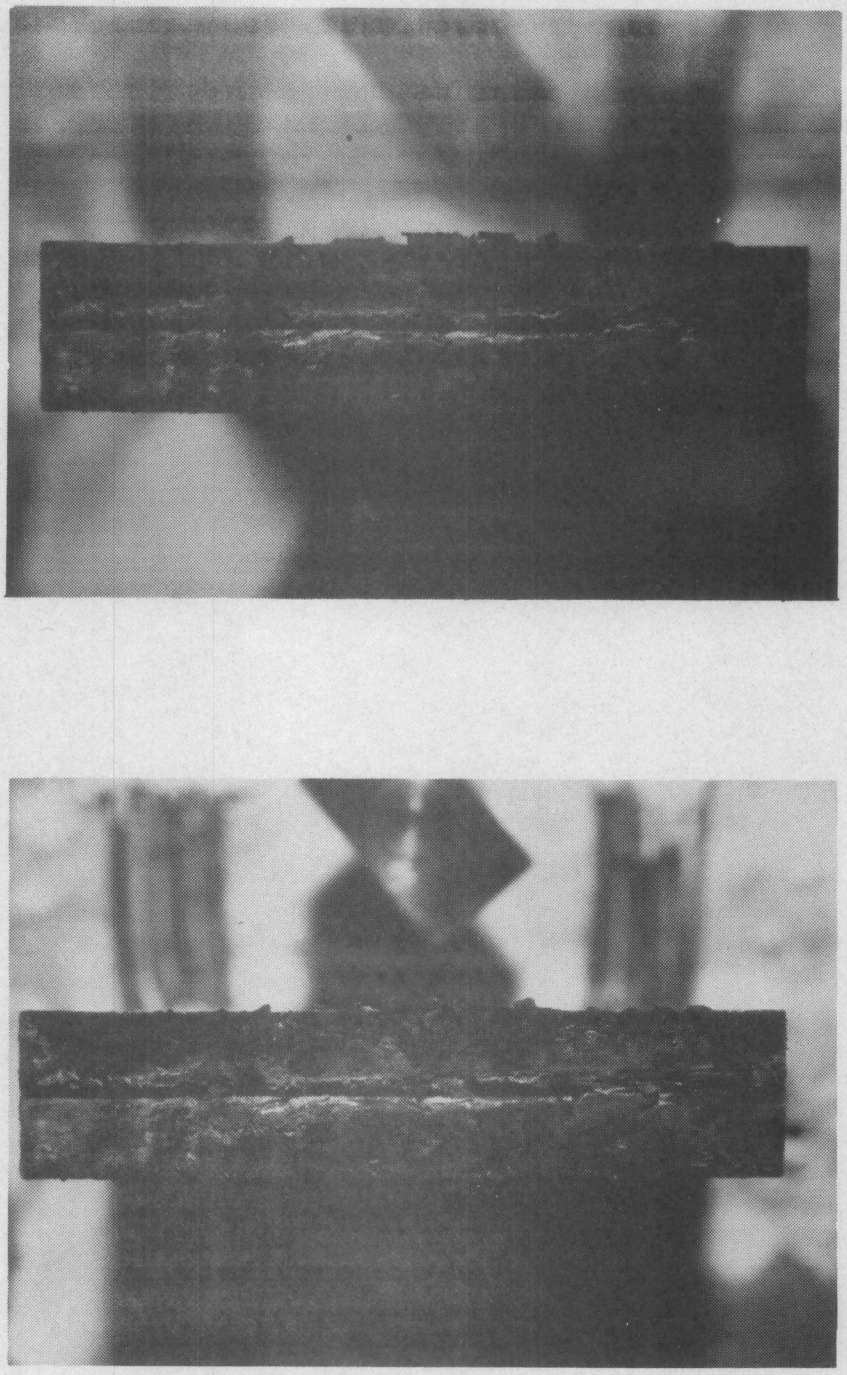


Figure 12. Corrosion of flange on stainless steel plate.

CHAPTER III

INSTRUMENTATION OF APPARATUS

The entire flow loop and test package is instrumented to measure the necessary transpiration cooled nose tip, hereafter referred to as TCNT, design parameters and monitor the test equipment during operation. One of the more critical measurements is the temperature gradient along the beginning of the slot wall since this wall will provide a measurement of the heat flux. Figure 13 indicates the approximate shape of the gradient computed for a typical land. This shows that most of the heat flux transferred from the slot walls to the water is taking place right at the end of the slot.

Five chromel-alumel thermocouples are spot welded along one side of the center slot to measure the temperature gradient at the exit of the slot. The thermocouples are spaced approximately 0.01 inches from one another as shown in Figure 14. The distance between the five thermocouples in the photograph is measured optically from the picture shown by using a photograph to the same magnification of a 1/1000 inch division scale. Two additional chromel-alumel thermocouples are spot welded at positions of 0.25 inches and 0.5 inches upstream of the exit.

Originally one mil wire was used for the thermocouples. The wires were run along one side of the slotted

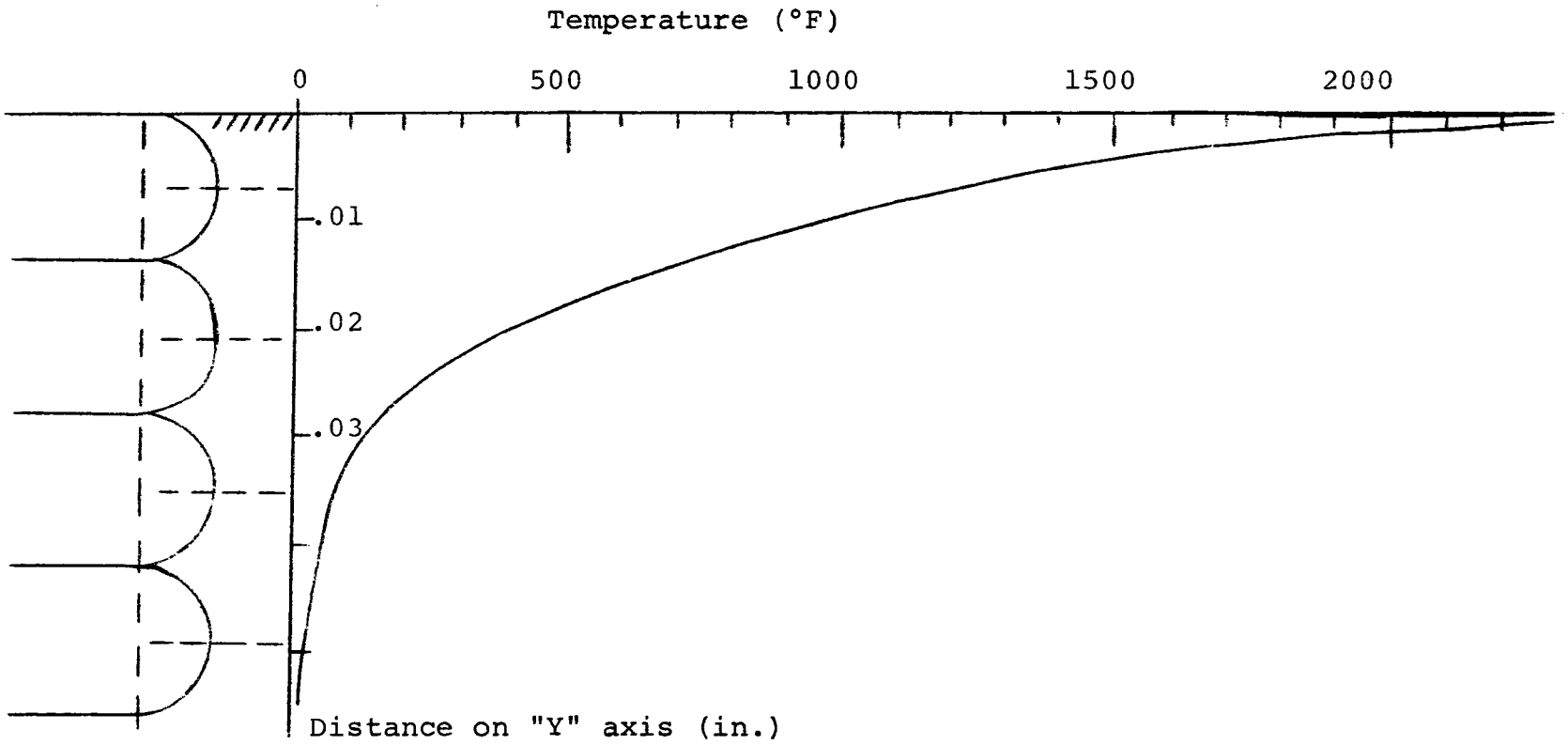
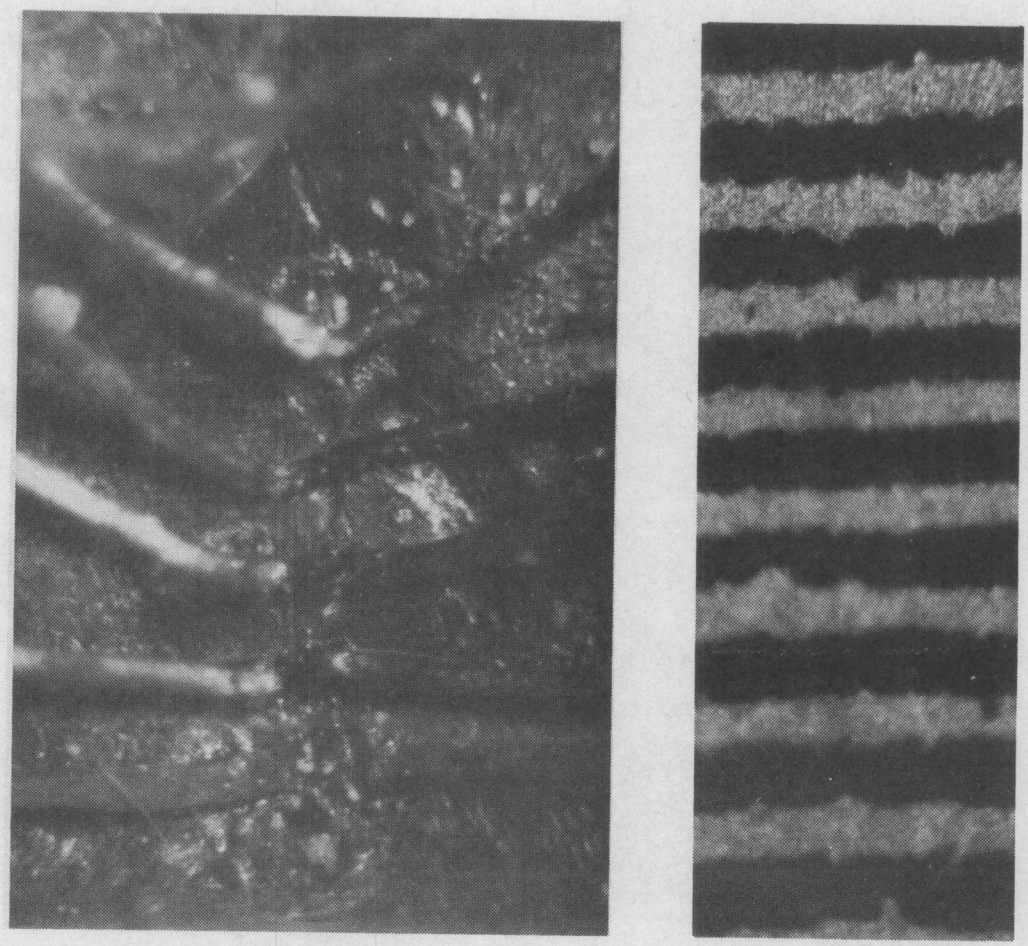


Figure 13. Temperature distribution and location of mounting of thermocouples.



(a) 3 Mil Thermocouples Mounted on Plate

(b) 1/1000 in Divisions of Scale

Figure 14. Thermocouple spacing on test slot.

test section to a junction box in the test section, Figure 15. At the junction box sheathed thermocouple wire was soldered to the one mil wires. The sheathed wires were fed out of the vessel through a fitting. Several of the one mil wires broke by mechanical failure during the first test possibly due to thermal-expansion of the assembly.

The junction box has now been eliminated and three mil wires have replaced the one mil wires. The new wires are spot welded on the plate as before and run along one side of the test section to a point where they are soldered directly to sheathed, chromel-alumel thermocouple wire. With this change, failure during repeated testing and thermal cycling has not occurred.

The temperature of the liquid exhausting from the slots is measured with a thermocouple at the exit plane of the slotted test section as shown in Figure 16. The bead of the thermocouple is placed as close as possible to the exit of the instrumented slot without actually touching it. The thermocouple bead has caused water to collect at that point forming big droplets which block the view of the exit plane. A possible solution would be to coat the bead with a non-wetting material so that water would not collect on the bead.

The thermocouple wire runs along one side of the copper wedge and up to the top of the test package where sheathed thermocouple wire is soldered to it. Since the wire is against the surface of the wedge at 1200 °F, the

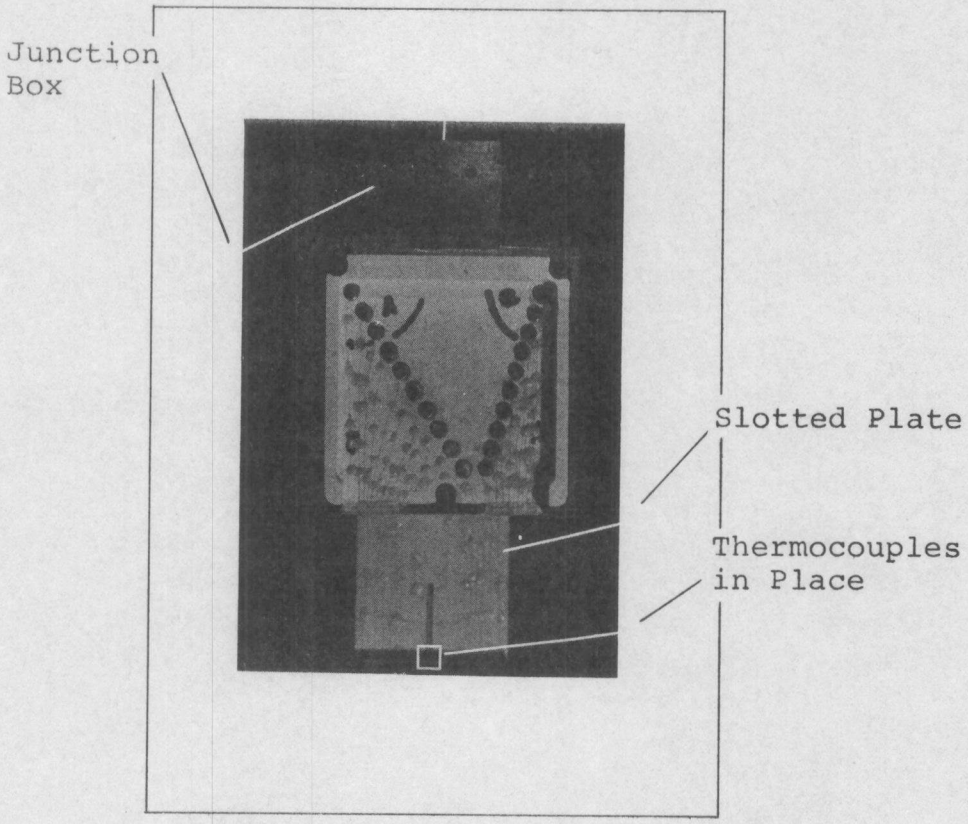


Figure 15. Junction box in test package.

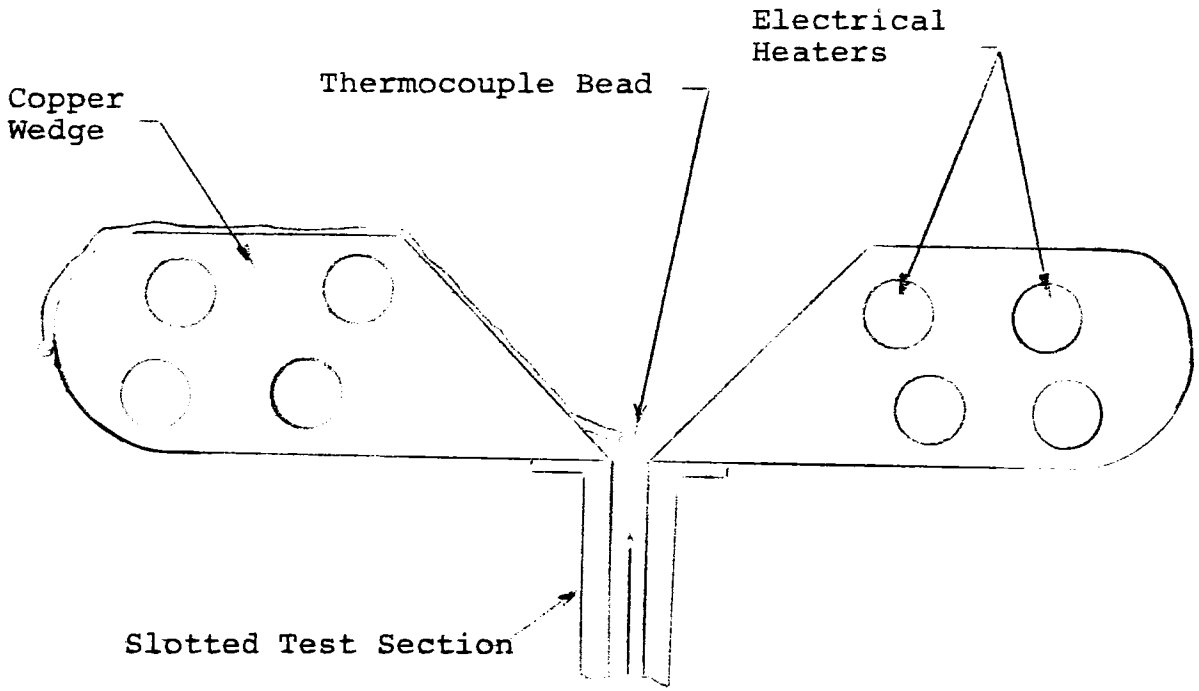


Figure 16. Thermocouple at exit plane.

thermocouple temperature must be corrected for conduction from the block.

Another chromel-alumel thermocouple is located in the plenum chamber to measure water inlet temperatures. Two additional thermocouples are mounted on each side of the copper wedge to determine the symmetry of the heat flux applied to the test section and to monitor the block temperature to avoid exceeding the melting temperature. One of these thermocouples on the wedge failed repeatedly after being thermally cycled. The failure was primarily due to the cement not adhering to the copper heater. Application of new cement appears to have solved the problem.

Thermocouples are also located on the window, cooling jacket, and finned heat exchanger plus the inlets and outlets of the cooling jacket and finned heat exchanger. The thermocouple on the window was broken before the first test from the ceramic shroud around the test package rubbing against it. The cement holding it against the window also failed to hold it in place. The thermocouple has been recemented in place to measure the window temperature. The window temperature is not of interest to the test results but is necessary to safely operate the vessel under pressure and high heat fluxes. If the window temperature reaches approximately 500 °F during high pressure testing, there is a high probability the window will lose its structural integrity and explode. A three foot thick wall of sandbags protect personnel from flying glass fragments should such an

explosion occur.

The temperature of the finned heat exchanger and cooling jacket inside the pressure vessel indicate the internal temperature of the environment.

All thermocouple outputs are recorded in millivolts on a Honeywell Multi-point Strip Chart recorder.[1] This recorder prints each channel approximately every 30 seconds depending on the number of channels being recorded. This is quite adequate during steady state operations which was the case for most of the testing done in this study. However, for studies where unstable flow was encountered a five channel continuous reading recorder would be very useful.

A BLH Differential Pressure transducer[2] is used to measure the pressure difference between the vessel and inlet line which is essentially the pressure drop over the length of the slot. The transducer can measure differential pressures up to 18 psi with an accuracy of 0.25 per cent full scale. A one volt supply is required by the transducer and produces a full scale output of 1.5 millivolts. A calibration data sheet supplied by BLH was confirmed by a recalibration performed at The University of Tennessee Space Institute. A nitrogen bottle and regulator were used in the

---

[1]Honeywell Industrial Products Group, Philadelphia 44, Pennsylvania; Electronik 16-24 channel recorder.

[2]BLH Electronics, Inc., Waltham, Massachusetts, Differential Pressure Transducer Model 1500.

recalibration. The results indicated that a slight hysteresis was present in the transducer. The output from the transducer is displayed on a Texas Instrument Company[3] continuous reading strip chart recorder.

Several anomalies occurred in the measurement system during initial tests. The pressure transducer indicated sudden excursions in differential pressure for no apparent reason. This was subsequently traced to a broken wire in the link between the transducer and recorder. The broken wire has been replaced.

Tubing, 0.25 inches in diameter, connects the pressure vessel atmosphere to a pressure gage to measure the pressure in the vessel. A shut-off valve is located between the pressure gage and vessel to protect the gage during evacuation of the vessel and allow changing of the pressure gage without depressurizing the vessel. Three different pressure gages are used to cover the ranges of 0-100, 0-400, and 0-5000 psi. The accuracy of the gages is 0.25 per cent full scale for 0-100, 0-400 psi and 0.5 per cent full scale for the 0-5000 psi range.

A D.C. power supply is used to energize the electrical heaters in the copper wedge. An A.C. power supply originally planned for use induced an emf in the thermocouples. The power supply now used has a 0-10 ammeter and 0-300 voltmeter

---

[3]Texas Instruments, Inc., Servowriter II two pen servowriter.

as an integral part of the power supply and both are used to measure the power input to the electrical heaters. The ammeter can be read to within ±0.1 ampere and the voltmeter ±1 volt. The power setting is adjusted with one master rheostat control that can vary the power continuously throughout the entire power range. In addition to the D.C. power supply, two arc welder power supplies can be added to the system for high power input requirements. These power supplies are 80 Kw, three phase units which can be connected in series to provide 160 Kw at 2000 amperes and 80 volts.

Initially in the testing program, all of the cartridge heaters were wired in parallel. During one test a sealing plug in the plenum chamber blew out allowing water to run down onto the heater lead wires shorting out one heater which in turn damaged all the remaining heaters on that side of the wedge due to the resultant power surge. As each heater failed, the power increased to the other heaters since the total power input to all heaters is kept constant. Finally when the four heaters in the bank of heater elements had failed the open series circuit between the left and right-hand banks of heaters cut the power. The electrical circuit was changed to prevent this occurrence in the future. All the electrical heaters were wired in series so that if one heater fails the circuit is open and no further power flows. This approach could not be used since the voltage drop required across the series circuit to provide the necessary amperage was excessive. The original electrical

circuit was therefore restored.

A Brooks Instrument 5000 psi pressure level rotameter[4] measures the flow rate of the test fluid. Flow ranges between 0.1-1.0, 0.5-4.96, and 2.0-28.2 cc/min can be measured. All three flow ranges are calibrated by the manufacturer to an accuracy of one per cent full scale and obtained by interchanging guide tubes and floats.

One disadvantage of using a rotameter to measure flow is that impurities in the fluid can cause the float to stick in the guide tube. Only a very small amount of impurity is required to cause float sticking. This problem can be overcome by periodic cleaning of the rotameter and fluid filters. A filter is used in this system and the rotameter is cleaned periodically which takes about 30 to 45 minutes.

A high pressure gage upstream from the rotameter ranging from 0-5000 psi is used to monitor the feed line pressure and let the system operator know when the inlet feed valve can be opened without worry of back-flow.

Photographic coverage of the test section is provided by a 16 mm high speed motion picture camera. The camera can photograph the exit plane at 500 frames/second during selected runs. This is sufficient to measure exit velocities of liquid droplets on the order of 50 ft/sec over a one inch field of view. Lighting is diffuse backlighting through the

---

[4]Brooks Instrument, Hatfield, Pennsylvania, High Pressure Rotameter Model 1452.

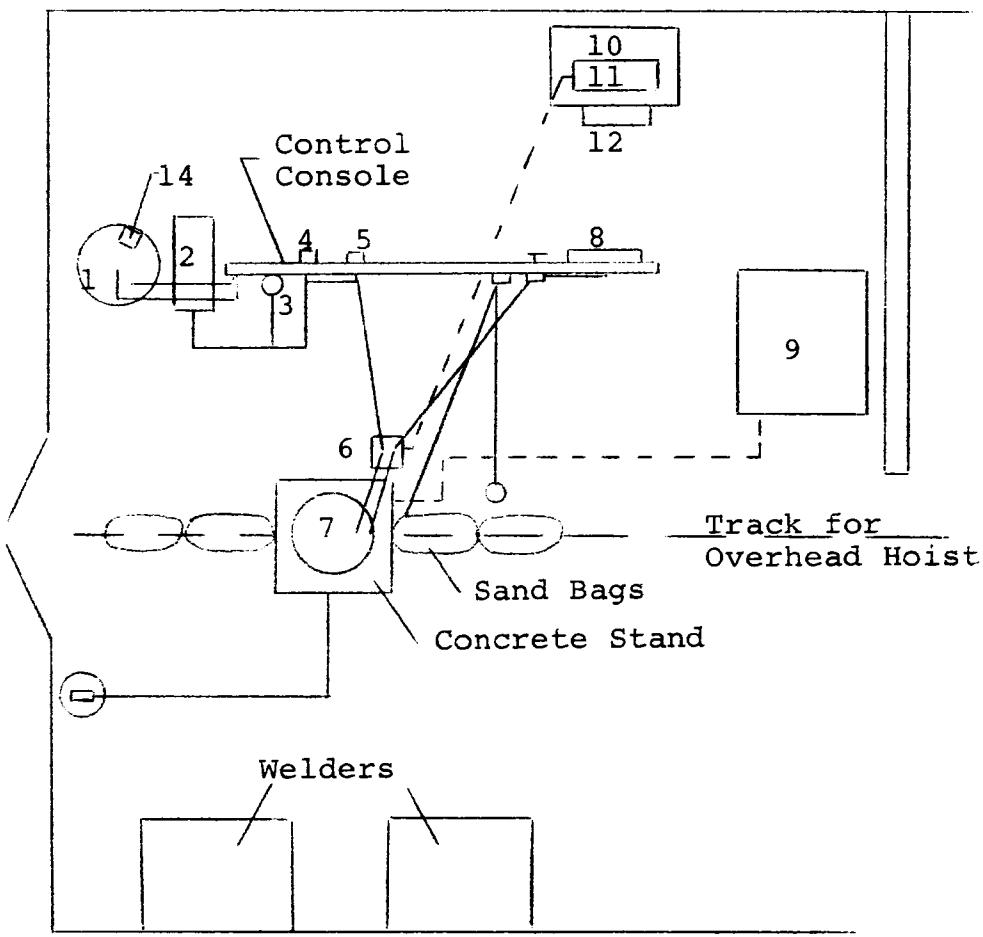
opposite window. Droplet size, speed, and bubble size can be measured from the photographs. The growth rate of the bubbles can be measured from the sequence of photographs. The formation of extremely dense fog inside the vessel has prevented photographs of the exit plane to be made at this time. As discussed in the previous section, the fog results from water boiling off the copper wedge. It is conceivable that this problem can be solved by coating the wedge with a non-wetting material or channeling the exhaust water away by some wicking material.

CHAPTER IV

DESCRIPTION OF TEST FACILITY AND TEST PROCEDURES

All test equipment for the transpiration cooling experiment is located in The University of Tennessee Space Institute Heat Transfer Laboratory. Figure 17 shows a schematic of the test equipment and arrangement relative to the laboratory. A movable overhead pulley is used to lift the approximately 200 pound vessel cover for repair or maintenance of the test package. Two operators are required to run the test with one monitoring the test equipment and the other recording data and visual observations. The entire flow loop is displayed schematically on a four by eight foot control console shown in Figure 18. The D.C. power supplies for the heating elements and for the differential pressure transducer are located separately from the console. Both of the power supplies are located on the wall facing the console and the operator simply turns around to operate the controls as shown in Figure 17.

The detailed test procedure is illustrated in Appendix A where the check list followed for all experiments is given. Essentially the procedure was to establish the vessel pressure and heater power setting for a given test. These were then maintained constant with suitable



1) Storage and Degassing Tank
2) High Pressure Pump
3) Accumulator
4) Back Pressure Regulator
5) 5000 psi Rotameter
6) Differential Pressure Transducer
7) Pressure Vessel
8) Vessel Pressure Gage
9) Multipoint Strip Chart Recorder
10) D.C. Power Supply
11) Differential Pressure Transducer
12) Continuous Reading Strip Chart Recorder
13) 6000 Nitrogen Bottle and Regulator
14) Thermostat Control for Heater in Degassing Tank

Figure 17. Test facility layout.

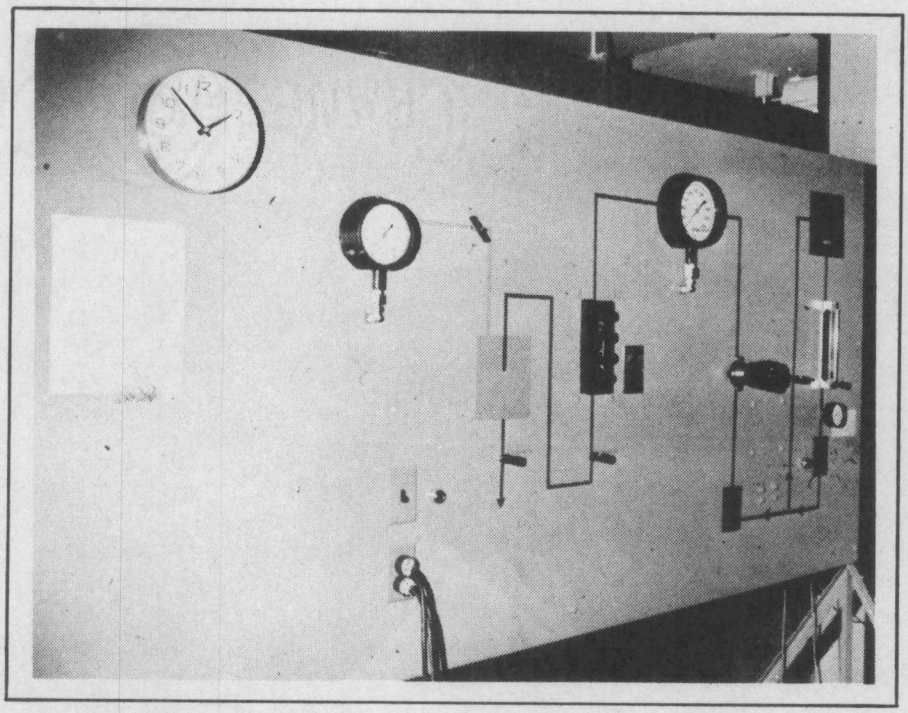


Figure 18. Control panel for TCNT experiment.

adjustments. The pressure tended to creep upward during a run but could be adjusted with a relief valve on the high pressure regulator. Flow was initiated at a low flow rate and increased incrementally to consecutive steady state settings. Steady state was determined when the recorded temperatures showed less than 3 to 4 °F variation over 15 print-out cycles (approximately 2.5 minutes). Times for the system to adjust from one steady state setting to another varied but were on the order of 5 to 10 minutes.

CHAPTER V

RESULTS OF TEST RUNS

Nine runs at pressure levels of 0, 200, 500, 1000, and 2000 psig were carried out. Table I lists the steady state settings during each run. The measured flow rate and heater block temperature are indicated; the latter is a measure of the heat flux level. The data for each steady state setting are tabulated in Tables II through XIV. Runs 9 through 11 were made with the test section suspended in the atmosphere. Runs 12 through 17 were made inside the pressure vessel without removing the test section between runs. Although visual inspection showed water was flowing during these runs it is now apparent that the slots were becoming progressively plugged with each run. Finally, during run 17 the plenum chamber plug blew out resulting in the major overhaul described earlier. Run 18 was made after cleaning the system and replacing the ceramic heater clamping blocks with stainless steel blocks which provided greater clamping pressures and thus reduced heater contact resistance. Additional runs after number 18 were attempted at 3000 and 1000 psig. Plugging occurred within 15 to 20 minutes in all cases.

The plugging is attributed to the formation of an oxide scale on the blocks and around the slots.

TABLE I

TEST MATRIX

0 psig T_{sat} = 212 °F		200 psig T_{sat} = 381 °F		500 psig T_{sat} = 467 °F		1000 psig T_{sat} = 544 °F		2000 psig T_{sat} = 635 °F	
Flow Rate cc/min	Block Temp. °F	Flow Rate cc/min	Block Temp. °F	Flow Rate cc/min	Block Temp. °F	Flow Rate cc/min	Block Temp. °F	Flow Rate cc/min	Block Temp. °F
0.4	786	0.5	924	0.1	909	0.37	1046	0.4	679
0.4	841	0.5	937	0.1	917	0.5	1042	0.5	682
0.4	713	0.6	928	0.21	926	1.0	1040	1.0	672
0.4	610	0.7	947	0.4	936	1.5	1042	1.5	693
0.4	521	0.82	946	0.5	930	2.0	1035	2.0	690
0.4	494	0.9	947	0.6	930	2.5	1040	2.5	675
0.4	828	0.8	937	0.7	926	3.0	1010	3.5	663
0.44	912			0.8	922	3.5	1042	3.5	699
0.44	957			0.8	922	4.0	1034		
0.44	780*			0.9	922	4.5	854		
0.44	710*			1.0	930	4.5	701		
0.44	690			1.0	934	0	931		
0.44	552			1.0	937	0.5	930		
0.44	860			0.24	926	2.0	936		
0.44	780*			0.2	926	3.0	923*		
0.44	379			2.0	406*	3.7	923*		
0.44	344			2.0	550*	4.0	905*		
0.44	296*			2.0	886				
0.44	255*			2.0	885				
2.0	255*			2.0	902				
2.0	964*								
2.0	1040*								
2.0	1040*								

TABLE I (continued)

0 psig T_{sat} = 212 °F		200 psig T_{sat} = 381 °F		500 psig T_{sat} = 467 °F		1000 psig T_{sat} = 544 °F		2000 psig T_{sat} = 635 °F	
Flow Rate cc/min	Block Temp. °F	Flow Rate cc/min	Block Temp. °F	Flow Rate cc/min	Block Temp. °F	Flow Rate cc/min	Block Temp. °F	Flow Rate cc/min	Block Temp. °F
2.0	684*								
2.0	477*								
3.0	361*								
3.0	306*								
4.0	295*								
2.0	296*								
2.0	884*								
2.0	1052*								
2.0	133*								
2.0	924*								
0	846								
0	675								

*Single phase flow conditions.

TABLE II

TEST DATA FROM RUN 9a

Vessel-Pressure: 14.7 psig $h = 1.0\left(\frac{Btu}{hr\text{-}ft^2\text{-}°F}\right)$

T.C.	Run #1 [mV]	Run #1 [°F]	Run #2 [mV]	Run #2 [°F]	Run #3 [mV]	Run #3 [°F]
1	15.2	701	16.72	766	14.63	676
2	15.05	695	16.58	760	14.41	667
3	14.85	686	16.4	752	14.35	665
4	14.75	682	16.22	745	14.27	661
5	14.5	671	16.00	735	14.07	652
6	11.4	537	17.75	595	11.96	561
7	8.18	394	9.40	449	9.26	442
8	1.4	95	1.65	106	2.1	125
9	15.96	735	17.09	781	14.6	652
10	17.20	786	18.45	841	15.48	713
11	17.15	785	18.40	837	15.40	710
ΔP		[psi]		[psi]		[psi]
V	50.0	[volts]	50.00	[volts]	25.0	[volts]
A	5.1	[amps]	5.1	[amps]	2.2	[amps]
P	14.7	[psig]	14.7	[psig]	14.7	[psig]
$\mathring{V}$	0.4	[cm^3/min]	0.4	[cm^3/min]	0.4	[cm^3/min]

T.C.	Run #4 [mV]	Run #4 [°F]	Run #5 [mV]	Run #5 [°F]	Run #6 [mV]	Run #6 [°F]
1	12.53	586	11.02	520	9.99	475
2	12.5	565	11.00	519	9.97	474
3	12.4	580	10.56	513	9.79	466
4	12.78	575	10.83	512	9.75	464
5	12.13	568	10.75	508	9.71	462
6	10.60	501	9.49	453	8.6	413
7	8.55	410	7.8	377	7.25	352
8	2.49	143	2.72	153	2.96	163
9	12.50	585	11.00	519	9.98	474
10	13.10	610	11.5	521	10.43	494
11	13.08	610	11.49	540	10.39	492
ΔP		[psi]		[psi]		[psi]
V	25.0	[volts]	25.0	[volts]	25.0	[volts]
A	2.2	[amps]	2.2	[amps]	2.2	[amps]
P	14.7	[psig]	14.7	[psig]	14.7	[psig]
$\mathring{V}$	0.4	[cm^3/min]	0.4	[cm^3/min]	0.4	[cm^3/min]

TABLE III

TEST DATA FROM RUN 9b

Vessel-Pressure: 14.7 psig

T.C.	[mV]	[°F]	[mV]	[°F]	[mV]	[°F]
	Run #7		Run #8		Run #9	
1	17.45	797	15.03	694	17.75	810
2	17.24	788	14.10	659	17.50	799
3	16.95	775	12.51	585	17.08	781
4	16.69	765	11.10	524	16.77	767
5	16.40	752	9.46	451	16.42	753
6	11.61	546	4.20	216	10.50	497
7	5.11	256	4.15	214	4.85	245
8	2.91	161	3.78	199	4.04	210
9	18.19	828	16.75	767	18.51	842
10	19.52	885	20.18	912	20.27	917
11	19.55	886	21.25	957	21.50	968
ΔP		[psi]		[psi]		[psi]
V	50.0	[volts]	50.0	[volts]	50.0	[volts]
A	5.1	[amps]	5.1	[amps]	5.0	[amps]
P	14.7	[psig]	14.7	[psig]	14.7	[psig]
$\mathring{V}$	0.4	[cm^3/min]	0.44	[cm^3/min]	0.44	[cm^3/min]
	Run #10		Run #11		Run #12	
1	17.4	795	4.03	209	9.5	453
2	17.25	788	9.75	464	11.8	554
3	17.00	778	9.58	457	11.97	561
4	16.79	769	12.00	563	11.97	561
5	16.68	764	11.48	540	11.95	560
6	13.68	635	6.72	328	6.58	322
7	10.45	495	4.75	240	4.20	216
8	4.12	213	4.10	212	4.02	209
9	17.5	799	14.5	671	13.85	643
10	18.46	840	17.07	780	15.46	712
11	18.48	841	16.72	766	15.08	696
ΔP		[psi]		[psi]		[psi]
V	30.0	[volts]	40.0	[volts]	40.0	[volts]
A	2.8	[amps]	3.8	[amps]	3.7	[amps]
P	14.7	[psig]	14.7	[psig]	14.7	[psig]
$\mathring{V}$	0.44	[cm^3/min]	0.44	[cm^3/min]	0.44	[cm^3/min]

TABLE III (continued)

T.C.	[mV]	[°F]	[mV]	[°F]	[mV]	[°F]
		Vessel-Pressure: 14.7 psig				
	Run #13		Run #14			
1	4.00	208	7.76	375		
2	4.12	212	4.95	249		
3	9.05	423	6.02	297		
4	9.06	423	7.39	358		
5	9.52	452	7.55	366		
6	4.77	242	4.20	222		
7	4.13	212	4.05	210		
8	4.00	208	3.91	204		
9	13.49	627	10.30	488		
10	14.90	690	11.75	552		
11	14.42	667	10.95	517		
ΔP		[psi]		[psi]		
V	40.0	[volts]	30.00	[volts]		
A	3.7	[amps]	2.9	[amps]		
P	14.7	[psig]	14.7	[psig]		
$\mathring{V}$	0.44	[cm^3/min]	0.44	[cm^3/min]		

TABLE IV

TEST DATA FROM RUN 9c

Vessel-Pressure: 14.7 psig

T.C.	[mV]	[°F]	[mV]	[°F]	[mV]	[°F]
	Run #15		Run #16		Run #17	
1	6.78	331	4.0	208	7.14	347
2	4.26	219	4.0	208	7.10	345
3	4.26	219	3.99	207	6.92	337
4	6.00	296	4.0	208	6.81	332
5	4.95	245	4.08	208	6.75	330
6	4.03	209	4.06	210	4.78	241
7	4.01	208	4.04	210	4.0	208
8	3.76	197	3.71	195	3.5	186
9	8.01	386	3.85	201	7.35	356
10	10.96	517	9.18	439	7.85	379
11	10.01	475	9.12	436	7.85	379
ΔP		[psi]		[psi		[psi]
V	20.0	[volts]	20.0	[volts]	20.0	[volts]
A	1.7	[amps]	1.7	[amps]	1.7	[amps]
P	14.7	[psig]	14.7	[psig]	14.7	[psig
$\dot{V}$	0.44	[cm^3/min]	0.44	[cm^3/min]	0.44	[cm^3/min]
	Run #18		Run #19		Run #20	
1	6.78	331	4.0	208	4.0	208
2	6.77	330	4.0	208	4.0	208
3	6.73	329	4.0	208	4.0	208
4	6.72	328	4.0	208	4.0	208
5	6.72	328	4.02	209	4.0	208
6	6.05	298	3.95	205	3.75	197
7	5.15	258	3.65	193	3.50	186
8	3.25	175	3.00	165	2.77	155
9	6.90	336	3.98	207	4.0	208
10	7.06	344	6.00	296	5.10	256
11	7.05	343	5.99	295	5.10	256
ΔP		[psi]		[psi]		[psi]
V	20.0	[volts]	10.0	[volts]	10.0	[volts]
A	1.7	[amps]	1.7	[amps]	1.7	[amps
P	14.7	[psig]	14.7	[psig]	14.7	[psig]
$\dot{V}$	0.44	[cm^3/min]	0.44	[cm^3/min]	0.44	[cm^3/min]

TABLE V

TEST DATA FROM RUN 10a

Vessel-Pressure: 14.7 psig

T.C.	[mV]	[°F]	[mV]	[°F]	[mV]	[°F]
	Run #1		Run #2		Run #3	
1	2.7	150	4.07	211	4.23	217
2	2.5	142	4.03	209	4.10	212
3	2.27	132	4.0	207	3.9	203
4	2.23	130	4.0	207	3.8	199
5	2.07	124	4.0	207	3.1	169
6	1.48	97	2.74	153	2.45	140
7	1.40	95	2.4	138	2.3	134
8	1.40	95	2.4	138	2.45	140
9	2.50	142	3.8	199	3.7	195
10	5.07	255	21.4	964	23.2	1040
11	4.40	225	20.15	911	22.2	997
ΔP	0.34	[psi]	0.19	[psi]	0.29	[psi]
V	50.0	[volts]	75.0	[volts]	75.0	[volts]
A	5.1	[amps]	7.6	[amps]	7.7	[amps]
P	14.7	[psig]	14.7	[psig]	14.7	[psig]
$\dot{V}$	7.0	[cm^3/min]	2.0	[cm^3/min]	2.0	[cm^3/min]
	Run #4		Run #5		Run #6	
1	4.2	216	3.95	205	3.5	186
2	4.1	212	3.9	203	3.4	182
3	3.8	199	3.6	190	3.08	168
4	3.7	195	3.5	186	3.00	164
5	3.05	167	3.45	184	2.78	155
6	2.6	148	2.8	156	2.26	133
7	2.5	142	2.75	154	2.20	130
8	2.53	144	2.8	156	2.27	133
9	4.74	240	3.9	203	3.75	197
10	22.50	1010	14.8	684	10.05	477
11	21.75	979	15.4	710	9.8	465
ΔP	0.29	[psi]	0.29	[psi]	0.33	[psi]
V	70.0	[volts]	50.0	[volts]	50.0	[volts]
A	7.1	[amps]	5.2	[amps]	5.0	[amps]
P	14.7	[psig]	14.7	[psig]	14.7	[psig]
$\dot{V}$	2.0	[cm^3/min]	2.0	[cm^3/min]	2.0	[cm^3/min]

TABLE VI

TEST DATA FROM RUN 10b

Vessel-Pressure: 14.7

T.C.	[mV]	[°F]	[mV]	[°F]	[mV]	[°F]
	Run #7		Run #8		Run #9	
1	3.2	173	3.0	165	2.8	156
2	3.05	167	2.9	160	2.7	151
3	2.8	156	2.61	148	2.51	143
4	2.65	150	2.58	146	2.49	142
5	2.55	146	2.50	142	2.41	140
6	2.05	123	2.03	122	1.92	118
7	2.04	122	2.45	162	2.4	139
8	2.05	123	2.03	122	2.0	120
9	3.48	185	3.09	168	2.75	154
10	7.45	361	6.25	306	6.00	295
11	6.00	296	4.43	226	4.41	225
ΔP	0.46	[psi]	0.46	[psi]	0.52	[psi]
V	50.0	[volts]	50.0	[volts]	50.0	[volts]
A	5.0	[amps]	5.0	[amps]	5.0	[amps]
P	14.7	[psig]	14.7	[psig]	14.7	[psig]
$\dot{V}$	3.0	[cm^3/min]	3.0	[cm^3/min]	4.0	[cm^3/min]
	Run #10		Run #11			
1	3.0	164	4.0	207		
2	2.97	163	4.0	207		
3	2.66	155	3.91	203		
4	2.53	144	3.88	202		
5	2.45	140	3.75	177		
6	1.90	117	2.9	160		
7	1.70	108	2.61	148		
8	1.91	117	2.6	148		
9	3.00	164	3.71	195		
10	6.00	796	19.5	884		
11	--		--			
ΔP	0.36	[psi]	0.34	[psi]		
V	50.0	[volts]	75.0	[volts]		
A	5.2	[amps]	7.8	[amps		
P	14.7	[psig]	14.7	[psig]		
$\dot{V}$	2.0	[cm^3/min]	2.0	[cm^3/min]		

TABLE VII

TEST DATA FROM RUN 11

T.C.	[mV]	[°F]	[mV]	[°F]	[mV]	[°F]
	Vessel-Pressure: 14.7 psig					
	Run #12		Run #13		Run #14	
1	4.01	207	4.1	212	4.1	212
2	4.01	207	4.1	212	4.1	212
3	4.0	207	4.02	208	4.06	210
4	4.0	207	2.0	207	4.05	207
5	4.0	207	4.0	207	4.02	208
6	3.56	188	3.45	184	3.5	186
7	3.1	169	3.11	170	3.45	184
8	3.04	166	3.09	169	3.2	193
9	3.9	203	3.95	205	3.95	205
10	23.5	1052	25.40	1133	20.45	924
11	--		--		--	
ΔP	0.33	[psi]	0.34	[psi]	0.34	[psi]
V	75.0	[volts]	75.0	[volts]	60.0	[volts]
A	7.8	[amps]	7.75	[amps]	6.0	[amps]
P	14.7	[psig]	14.7	[psig]	14.7	[psig]
$\dot{V}$	2.0	[cm^3/min]	2.0	[cm^3/min]	2.0	[cm^3/min]
	Run #15		Run #16			
1	18.6	846	14.61	675		
2	18.55	845	14.59	675		
3	18.41	837	14.48	670		
4	18.26	831	14.41	668		
5	18.15	826	14.4	668		
6	15.6	718	12.91	603		
7	12.75	595	11.05	521		
8	4.6	234	5.0	251		
9	19.1	866	14.74	681		
10	20.26	915	15.49	713		
11	--		--			
ΔP	0	[psi]	0	[psi]		
V	43.0	[volts]	30.0	[volts]		
A	4.1	[amps]	2.9	[amps]		
P	14.7	[psig]	14.7	[psig]		
$\dot{V}$	0	[cm^3/min]	0	[cm^3/min]		

TABLE VIII

TEST DATA FROM RUN 13a

T.C.	[mV]	[°F]	[mV]	[°F]	[mV]	[°F]
	Vessel-Pressure: 500 psig					
	Run #1		Run #2		Run #3	
1	17.3	790	17.6	803	17.85	814
2	17.15	784	17.5	799	17.75	810
3	16.85	769	16.7	765	17.5	799
4	16.75	766	16.6	760	16.9	773
5	16.5	756	16.4	752	16.65	763
6	13.3	619	13.25	617	14.15	655
7	10.8	510	11.35	535	11.75	551
8	6.65	325	7.2	350	7.5	364
9	17.1	781	17.8	812	17.8	812
10	20.1	909	20.3	917	20.5	926
11	19.35	877	19.6	888	19.8	896
ΔP	0.25	[psi]	0.19	[psi]	0	[psi]
V	77.5	[volts]	78.0	[volts]	78.0	[volts]
A	8.0	[amps]	7.95	[amps]	7.8	[amps
P	525.0	[psig]	510.0	[psig]	500.0	[psig]
$\dot{V}$	0.1	[cm^3/min]	0.1	[cm^3/min]	0.21	[cm^3/min]
	Run #4		Run #5		Run #6	
1	18.1	825	10.25	486	10.05	477
2	18.0	820	10.05	477	9.95	473
3	17.75	810	9.9	471	9.85	469
4	17.65	805	9.9	471	9.95	473
5	16.95	775	10.0	475	10.05	477
6	14.5	671	9.5	454	9.5	454
7	12.0	563	9.0	431	9.0	431
8	7.75	375	7.8	377	7.85	379
9	18.15	827	14.9	688	13.9	645
10	10.7	936	20.6	930	20.6	930
11	20.0	905	19.95	903	19.9	900
ΔP	0	[psi]	-0.023	[psi]	-0.027	[psi]
V	77.5	[volts]	76.0	[volts]	76.0	[volts]
A	7.8	[amps]	7.6	[amps]	7.6	[amps]
P	475.0	[psig]	475.0	[psig]	475.0	[psig]
$\dot{V}$	0.4	[cm^3/min]	0.5	[cm^3/min]	0.6	[cm^3/min]

TABLE VIII (continued)

T.C.	[mV]	[°F]	[mV]	[°F]	[mV]	[°F]
	Vessel-Pressure: 500 psig					
	Run #7		Run #8			
1	10.0	475	10.0	475		
2	9.9	471	9.95	473		
3	9.8	466	9.8	466		
4	9.9	471	9.9	471		
5	10.0	475	10.0	475		
6	9.4	449	9.2	440		
7	8.8	422	8.65	415		
8	7.75	375	7.65	370		
9	13.2	615	13.2	615		
10	20.5	926	20.4	922		
11	19.8	896	19.75	894		
ΔP	-0.088	[psi]	-0.088	[psi]		
V	75.5	[volts]	76.0	[volts]		
A	7.6	[amps]	7.6	[amps]		
P	475.0	[psig]	475.0	[psig]		
$\dot{V}$	0.7	[cm^3/min]	0.8	[cm^3/min]		

TABLE IX

TEST DATA FROM RUN 13b

Vessel-Pressure: 500 psig

T.C.	[mV]	[°F]	[mV]	[°F]	[mV]	[°F]
	Run #9		Run #10		Run #11	
1	10.0	475	10.05	477	10.10	480
2	9.9	471	9.9	471	10.05	477
3	9.8	466	9.8	466	10.02	476
4	9.85	469	9.85	469	10.03	476
5	9.9	471	9.9	471	10.04	477
6	9.2	440	9.1	435	9.0	431
7	8.6	413	8.5	409	8.49	408
8	7.6	368	7.6	368	7.45	361
9	13.4	623	8.75	-	13.73	-
10	20.4	922	20.4	922	20.6	930
11	19.7	-	19.75	-	19.99	-
ΔP	-0.027	[psi]	-0.026	[psi]	-0.018	[psi]
V	77.0	[volts]	77.0	[volts]	76.5	[volts]
A	7.6	[amps]	7.65	[amps]	7.7	[amps]
P	475.0	[psig]	490.0	[psig]	475.0	[psig]
$\dot{V}$	0.8	[cm^3/min]	0.9	[cm^3/min]	1.0	[cm^3/min]
	Run #12		Run #13		Run #14	
1	11.79	554	12.95	604	17.02	778
2	11.32	534	11.77	553	16.27	746
3	11.24	530	11.28	531	15.76	725
4	11.50	541	11.60	545	15.75	725
5	11.51	541	11.60	545	15.50	714
6	9.0	431	9.15	438	11.21	531
7	7.82	378	7.88	380	9.55	455
8	6.5	319	6.42	315	6.55	321
9	16.22	-	16.55	758	16.55	756
10	20.68	934	20.77	937	20.50	926
11	19.8	-	19.99	904	19.74	893
ΔP	0.35	[psi]	0.35	[psi]	0.031	[psi]
V	83.0	[volts]	82.5	[volts]	80.0	[volts]
A	8.3	[amps]	8.15	[amps]	8.15	[amps]
P	525.0	[psig]	475.0	[psig]	-	[psig]
$\dot{V}$	1.0	[cm^3/min]	1.0	[cm^3/min]	0.24	[cm^3/min]

TABLE IX (continued)

T.C.	[mV]	[°F]	[mV]	[°F]	[mV]	[°F]
	Vessel-Pressure: 500 psig					
	Run #15		Run #16			
1	14.82	685	10.65	547		
2	14.26	660	10.51	541		
3	13.75	639	9.73	463		
4	14.25	660	9.5	454		
5	14.00	649	8.73	419		
6	10.55	499	7.65	370		
7	9.05	433	5.03	253		
8	6.68	326	4.92	248		
9	16.58	760	9.75	464		
10	20.50	926	20.55	928		
11	19.74	894	18.27	831		
ΔP	0.75	[psi]	-	[psi]		
V	80.0	[volts]	90.0	[volts]		
A	7.95	[amps]	8.45	[amps]		
P	475.0	[psig]	510.0	[psig]		
$\dot{V}$	0.20	[cm^3/min]	2.0	[cm^3/min]		

TABLE X

TEST DATA FROM RUN 14

Vessel-Pressure: 500 psig

T.C.	[mV]	[°F]	[mV]	[°F]	[mV]	[°F]
	Run #1		Run #2		Run #3	
1	6.99	340	7.55	365	9.87	470
2	7.01	341	8.17	393	10.10	480
3	5.97	295	6.84	333	9.22	440
4	6.0	296	6.83	333	9.00	431
5	6.15	303	6.55	320	8.75	420
6	3.95	205	3.8	200	6.00	296
7	2.83	157	3.22	173	5.08	255
8	1.9	116	2.50	142	4.49	229
9	7.5	364	9.20	440	12.00	563
10	8.45	406	11.69	550	19.55	886
11	8.05	388	9.55	455	17.20	786
ΔP	0.68	[psi]	0.9	[psi]	1.015	[psi]
V	50.0	[volts]	75.0	[volts]	90.0	[volts]
A	5.2	[amps]	7.8	[amps]	9.4	[amps]
P	500.0	[psig]	550.0	[psig]	600.0	[psig]
$\dot{V}$	2.0	[cm^3/min]	2.0	[cm^3/min]	2.0	[cm^3/min]
	Run #4		Run #5			
1	10.70	505	11.49	540		
2	9.51	453	9.0	431		
3	9.49	452	9.77	465		
4	9.55	455	9.76	465		
5	9.51	453	9.76	465		
6	6.35	312	6.51	319		
7	5.52	275	6.35	312		
8	4.51	230	4.51	230		
9	13.59	632	14.01	650		
10	19.99	885	19.95	902		
11	17.5	798	17.57	802		
ΔP	1.015	[psi]	0.56	[psi]		
V	9.0	[volts]	9.0	[volts]		
A	9.4	[amps]	9.4	[amps]		
P	500.0	[psig]	500.0	[psig]		
$\dot{V}$	2.0	[cm^3/min]	2.0	[cm^3/min]		

TABLE XI

TEST DATA FROM RUN 15

Vessel-Pressure: 200 psig

T.C.	[mV]	[°F]	[mV]	[°F]	[mV]	[°F]
	Run #1		Run #2		Run #3	
1	14.07	652	14.15	656	13.75	639
2	14.10	653	14.10	653	14.10	653
3	13.00	607	13.00	607	12.60	588
4	12.90	602	12.98	605	12.50	585
5	12.55	587	12.6	590	12.15	569
6	9.00	431	9.00	431	8.75	420
7	7.70	373	7.90	381	7.95	384
8	5.26	268	5.95	293	6.20	305
9	16.85	772	16.62	761	15.65	720
10	20.95	924	20.77	937	20.55	928
11	19.55	886	19.98	904	19.70	892
ΔP	0.03	[psi]	0.04	[psi]	0.04	[psi]
V	70.00	[volts]	70.00	[volts]	69.00	[volts]
A	6.55	[amps]	7.60	[amps]	6.85	[amps]
P	195.0	[psig]	200.0	[psig]	196.0	[psig]
$\dot{V}$	0.5	[cm^3/min]	0.5	[cm^3/min]	0.6	[cm^3/min]
	Run #4		Run #5		Run #6	
1	14.00	649	14.10	654	14.26	660
2	13.45	625	13.60	632	13.75	638
3	12.78	597	13.00	606	13.18	614
4	12.80	598	12.76	596	12.95	604
5	12.25	576	12.47	583	12.50	585
6	8.78	421	8.92	427	8.97	430
7	7.95	384	8.00	386	7.97	385
8	6.15	303	6.35	312	6.48	318
9	16.75	754	16.20	744	16.25	746
10	21.00	947	20.98	946	20.99	947
11	20.07	908	20.03	906	20.04	907
ΔP	0.07	[psi]	0	[psi]	0.295	[psi]
V	72.00	[volts]	70.0	[volts]	70.0	[volts]
A	7.2	[amps]	7.0	[amps]	6.95	[amps]
P	200.0	[psig]	199.0	[psig]	195.0	[psig]
$\dot{V}$	0.7	[cm^3/min]	0.82	[cm^3/min]	0.9	[cm^3/min]

TABLE XI (continued)

T.C.	[mV]	[°F]	[mV]	[°F]	[mV]	[°F]
	Vessel-Pressure: 200 psig					
	Run #7		Run #8			
1	14.25	660	14.75	682		
2	13.75	639	14.27	661		
3	13.18	614	13.7	636		
4	12.98	605	13.48	627		
5	12.51	585	12.99	606		
6	8.85	424	8.62	414		
7	8.10	390	8.18	394		
8	6.50	319	6.58	322		
9	16.18	742	16.02	736		
10	20.77	937	21.05	949		
11	20.00	905	0.7	0		
ΔP	1.015	[psi]		[psi]		
V	69.5	[volts]	70.0	[volts]		
A	7.0	[amps]	7.0	[amps]		
P	219.0	[psig]	199.0	[psig]		
$\dot{V}$	0.80	[cm^3/min]	0.85	[cm^3/min]		

TABLE XII

TEST DATA FROM RUN 16a

T.C.	[mV]	[°F]	[mV]	[°F]	[mV]	[°F]
	Vessel-Pressure: 2000 psig					
	Run #1		Run #2		Run #3	
1	11.27	531	11.32	533	11.15	526
2	11.25	530	11.24	530	10.95	517
3	10.77	509	10.85	513	10.60	501
4	10.60	502	10.75	508	10.58	500
5	10.45	495	10.50	497	10.25	487
6	7.10	345	7.19	350	6.95	338
7	5.12	257	5.20	260	5.03	253
8	3.52	187	3.55	188	3.55	188
9	11.10	524	11.05	522	10.62	502
10	14.68	679	14.76	682	14.51	672
ΔP	-0.04	[psi]	-0.04	[psi]	0.025	[psi]
V	95.0	[volts]	95.00	[volts]	96.0	[volts]
A	9.9	[amps]	9.9	[amps]	10.0	[amps]
P	1990.0	[psig]	1975.0	[psig]	2030.0	[psig]
$\dot{V}$	0.4	[cm^3/min]	0.5	[cm^3/min]	1.0	[cm^3/min]
	Run #4		Run #5			
1	11.50	541	11.08	523		
2	11.25	530	10.30	510		
3	10.99	-	10.50	-		
4	10.80	-	10.21	-		
5	10.55	499	9.65	460		
6	7.05	343	6.25	307		
7	5.18	259	4.70	238		
8	3.58	190	3.60	190		
9	11.23	-	10.32	-		
10	15.02	693	14.95	690		
ΔP	0.033	[psi]	0.673	[psi]		
V	97.0	[volts]	98.0	[volts]		
A	10.0	[amps]	10.0	[amps]		
P	2025.0	[psig]	2000.0	[psig]		
$\dot{V}$	1.5	[cm^3/min]	2.0	[cm^3/min]		

TABLE XIII

TEST DATA FROM RUN 16b

T.C.	[mV]	[°F]	[mV]	[°F]	[mV]	[°F]
	Vessel-Pressure 2000 psig					
	Run #6		Run #7		Run #8	
1	10.99	519	10.25	486	10.72	507
2	10.80	510	10.18	483	10.67	505
3	10.50	-	9.80	-	10.25	487
4	10.25	-	9.55	-	10.02	476
5	9.95	473	9.15	437	9.59	457
6	6.50	319	6.32	310	6.65	325
7	5.03	251	5.15	257	5.25	262
8	3.62	191	3.59	190	3.69	195
9	8.77	-	7.10	-	7.40	359
10	14.60	675	14.32	663	15.15	698
ΔP	0.453	[psi]	0.823	[psi]	0.825	[psi]
V	97.0	[volts]	96.0	[volts]	100.0	[volts]
A	10.0	[amps]	10.0	[amps]	10.04	[amps]
P	2010.0	[psig]	2020.0	[psig]	2020.0	[psig]
$\dot{V}$	2.5	[cm^3/min]	3.45	[cm^3/min]	3.5	[cm^3/min]
	Run #9		Run #10			
1	10.32	489	9.85	468		
2	10.27	487	9.89	470		
3	10.00	475	9.49	453		
4	9.72	463	9.25	442		
5	9.01	431	8.72	418		
6	6.18	304	5.79	286		
7	4.60	234	4.47	228		
8	3.61	191	3.55	188		
9	7.20	350	6.70	327		
10	15.03	694	14.52	672		
ΔP	0.849	[psi]	0.859	[psi]		
V	100.0	[volts]	100.0	[volts]		
A	10.4	[amps]	10.4	[amps]		
P	2025.0	[psig]	2020.0	[psig]		
$\dot{V}$	4.0	[cm^3/min]	4.5	[cm^3/min]		

TABLE XIV

TEST DATA FROM RUN 18

T.C.	[mV]	[°F]	[mV]	[°F]	[mV]	[°F]
	Vessel-Pressure: 1000 psig					
	Run #1		Run #2		Run #3	
1	20.05	901	19.5	885	19.9	900
2	19.55	886	18.55	843	-	-
3	19.0	863	17.90	815	18.4	837
4	18.5	841	17.45	796	18.0	820
5	17.7	808	16.55	758	17.2	785
6	10.45	495	9.55	455	10.0	475
7	7.50	364	7.00	340	7.10	345
8	5.75	285	5.50	274	5.50	274
9	-	-	-	-	-	-
10	-	-	-	-	-	-
11	20.75	936	20.70	930	20.75	936
ΔP		[psi]		[psi]		[psi]
V	223.0	[volts]	227.0	[volts]	227.0	[volts]
A	6.0	[amps]	6.2	[amps]	6.2	[amps]
P	980.0	[psig]	1050.0	[psig]	1030.0	[psig]
$\dot{V}$	0	[cm^3/min]	0.5	[cm^3/min]	2.0	[cm^3/min]
	Run #4		Run #5		Run #6	
1	11.4	536	11.3	533	10.5	476
2	-	-	-	-	-	-
3	11.1	523	10.5	498	9.5	452
4	11.0	520	10.0	475	8.6	412
5	10.55	500	9.0	431	7.6	367
6	5.9	290	5.7	282	5.7	282
7	5.5	274	5.3	265	5.4	269
8	5.45	271	5.2	260	5.2	260
9	-	-	-	-	-	-
10	-	-	-	-	-	-
11	20.55	928	20.55	928	20.0	905
ΔP		[psi]	0.22	[psi]	.335	[psi]
V	228.0	[volts]	228.0	[volts]	223.0	[volts]
A	6.2	[amps]	6.2	[amps]	6.0	[amps]
P	1030.0	[psig]	1030.0	[psig]	1030.0	[psig]
$\dot{V}$	3.0	[cm^3/min]	3.7	[cm^3/min]	4.0	[cm^3/min]

Spectroscopic analysis of scale taken from the heater block after the 1000 psig run indicated 99 per cent copper oxide with traces of Mg, Si, and Zn oxides. If indeed the plugging is due to oxide formation, the rate of plugging will be a function of temperature and prssure. Reference (1)[5] shows that when copper is heated to various temperatures in air or oxygen, supplied by water vapor in this case, changes of color occur that indicate the presence of oxide films, each color being related to the temperature of the film. Color characteristics of the particular temperature are grange blue at 392 °F, rose red at 482 °F, violet at 572 °F, steel blue at 662 °F, brass yellow at 725 °F, red (cuprous oxide) at 842 °F, greenish gray at 932 °F, gray at 1022 °F, and black (cupric oxide) at 1112 °F. Practically all these colors were observed on the block or on the plate at various run conditions.

When copper is used at high temperature in air or oxygen, scaling results. At low temperatures (up to 212 °F) the oxide film increases in thickness linearly with the logarithm of time. There is an irregular increase of scaling rate with increases of temperature and a rapid increase with pressure up to 12 mm Hg. Above 150 mm Hg the rate of increase is steady.

The rate of growth of oxide film beyond the temper

---

[5]Numbers in parentheses refer to similarly numbered references in the bibliography.

thickness is approximately defined by: $W^2 = kt$.

W = weight increase or equivalent film thickness

t = time

k = constant (P,T)

This suggests that plugging will occur more rapidly at the higher pressure levels and this effect was observed. The temperature level of the block was normally within a value of 800-1100 °F for all runs.

Due to plugging of the slots during the experiment the measured mass flow through the instrumented slot was not accurately known. The most reliable data from the experiment was therefore the temperature distribution along the land. The data for the single phase flow (i.e., where liquid flows from the slot exit) was used to compute the mass flux analytically employing the theory of Appendix B and iterating on mass flow until the calculated and measured temperatures were in agreement. Figures 19 through 32 show the measured temperatures and the computed curve fit. The assumption that the fluid temperature and solid temperature are equal is made in the theoretical calculation. The measured and calculated mass flux, the calculated heat flux, and the measured pressure are also recorded on the figures. The heat transfer coefficients for the single phase flow were calculated with the theory of Appendix C and are plotted on the figures as a function of position. Since the system was plugging as time progressed a plot of the ratio of calculated flow rate to measured flow rate for the single phase flow

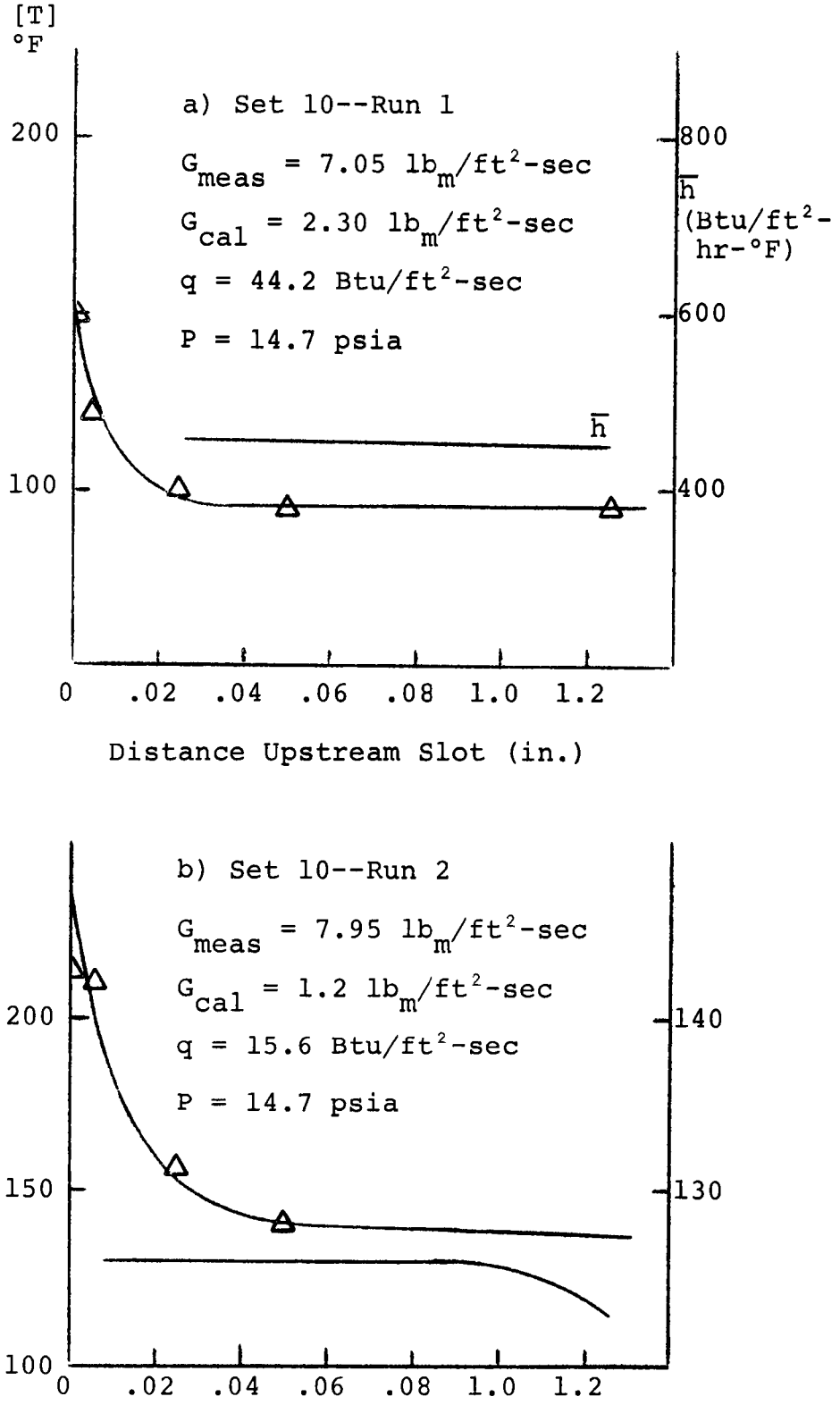


Figure 19. Single phase data, set 10--runs 1 and 2.

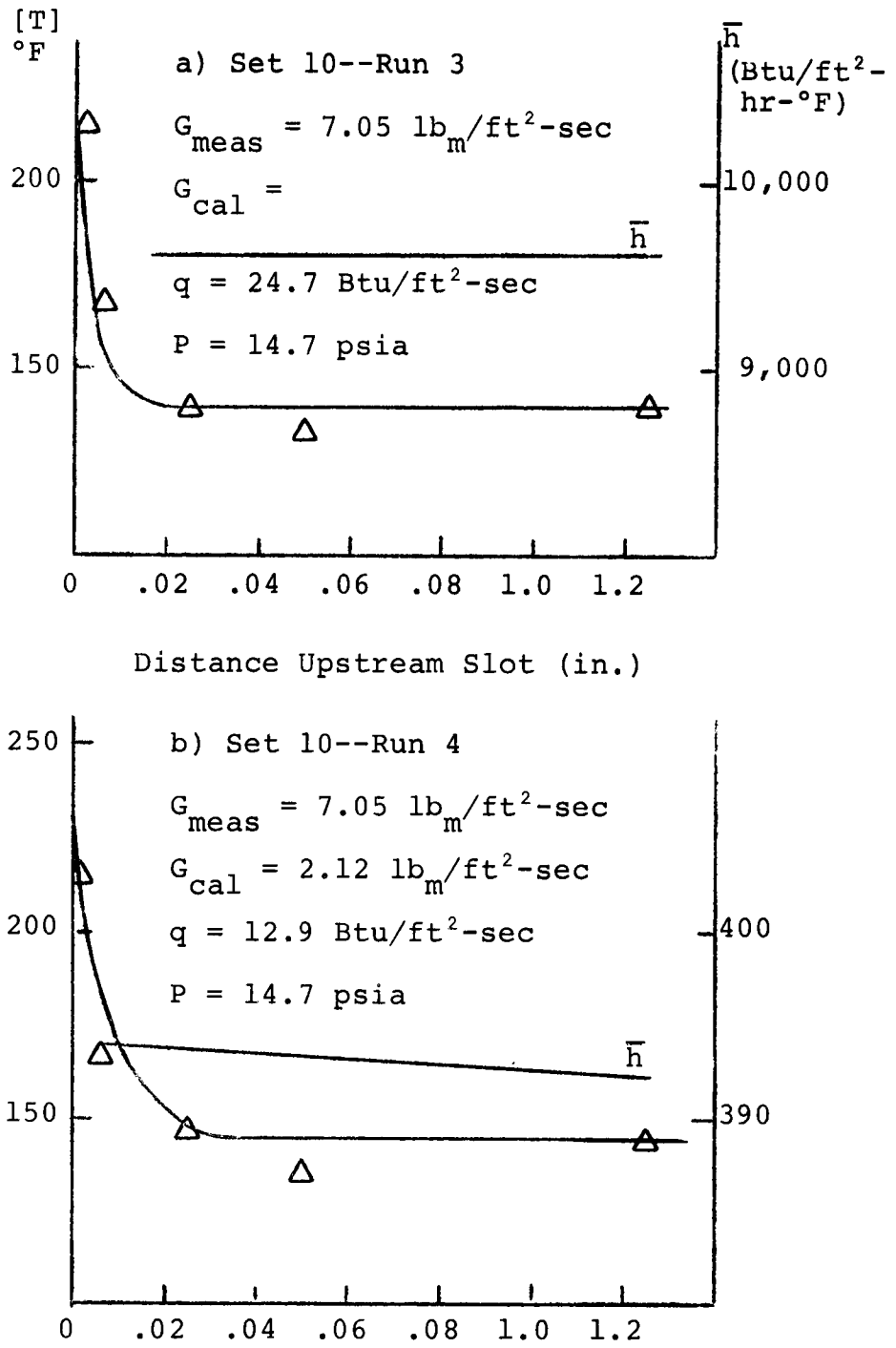
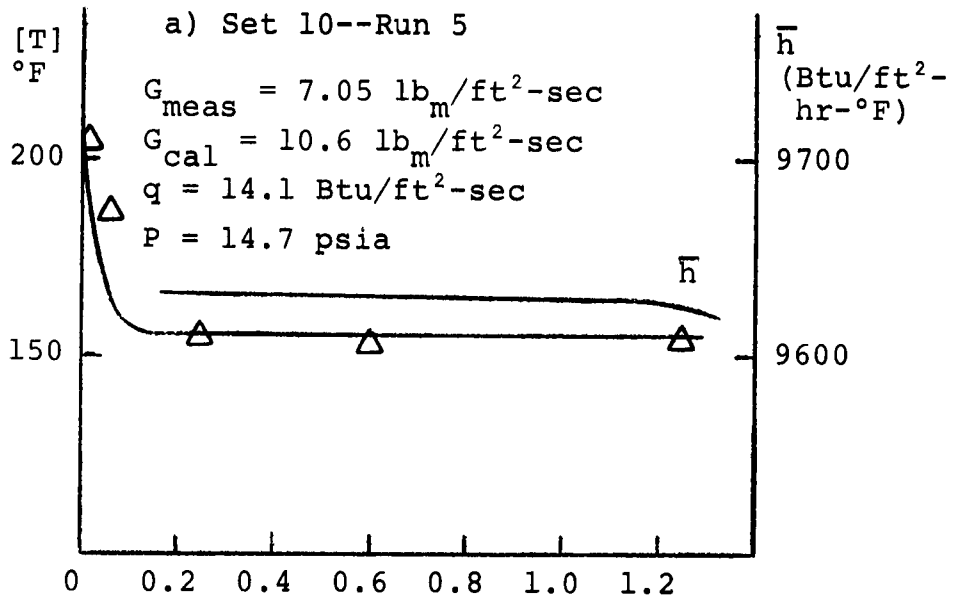


Figure 20. Single phase data, set 10--runs 3 and 4.



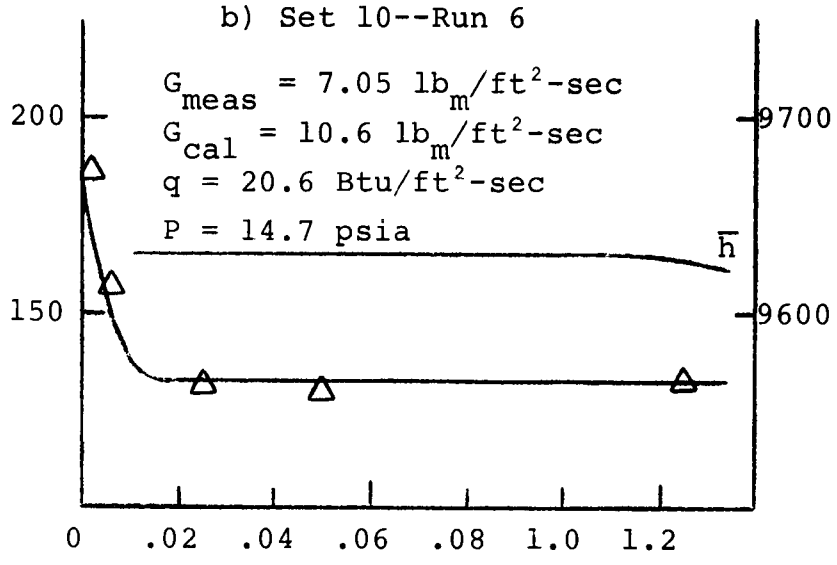


Figure 21. Single phase data, set 10--runs 5 and 6.

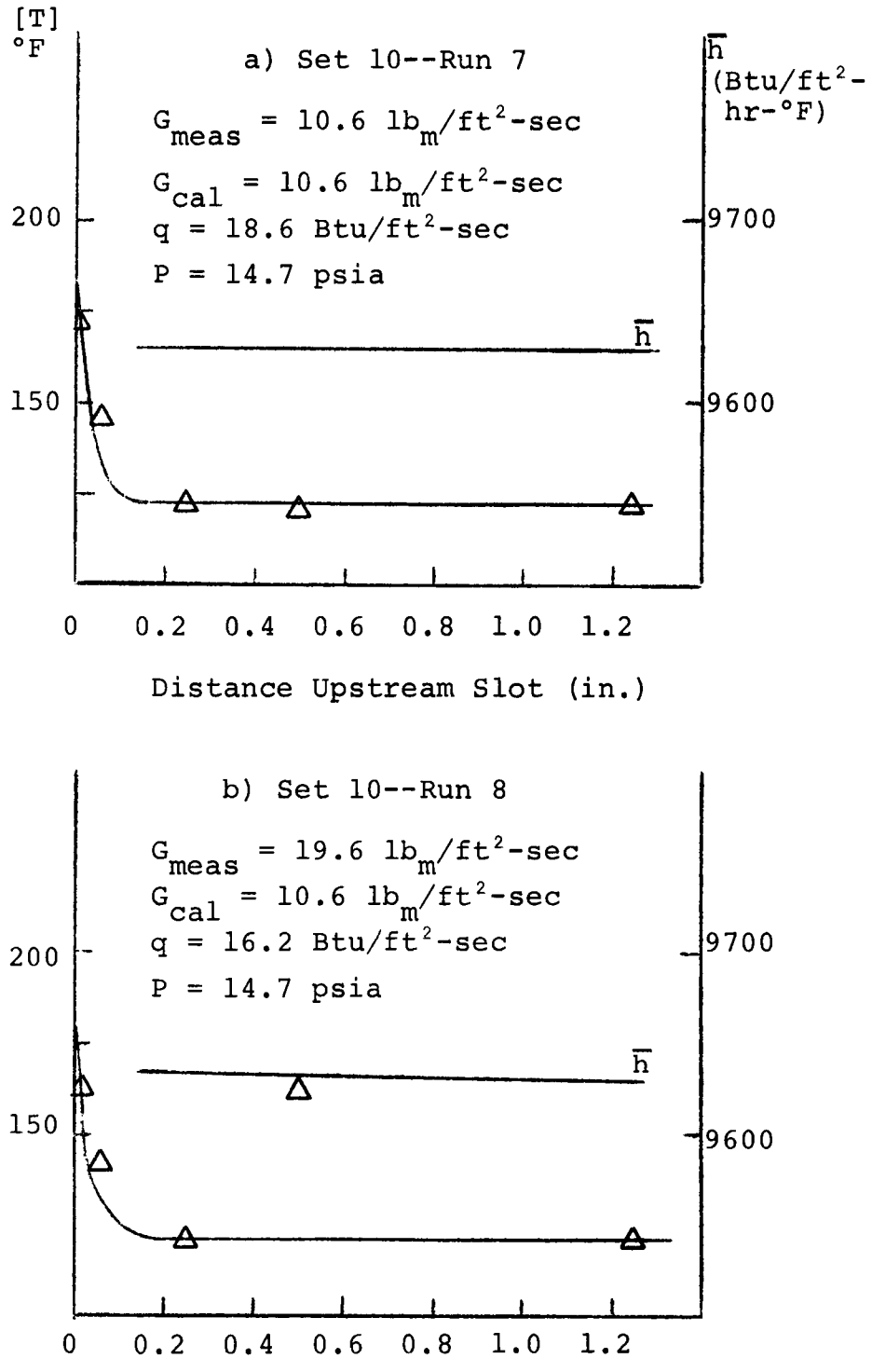


Figure 22. Single phase data, set 10--runs 7 and 8.

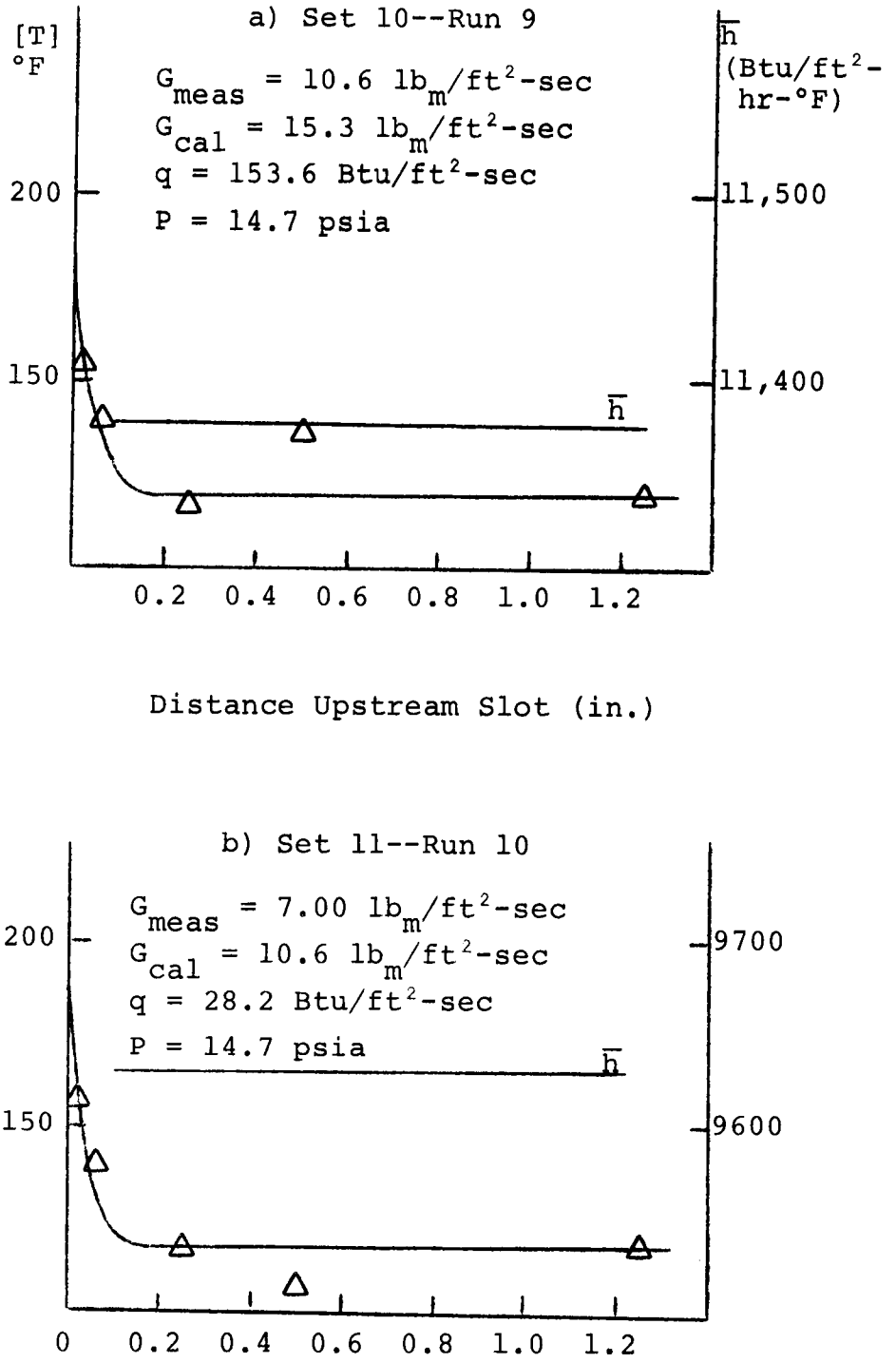
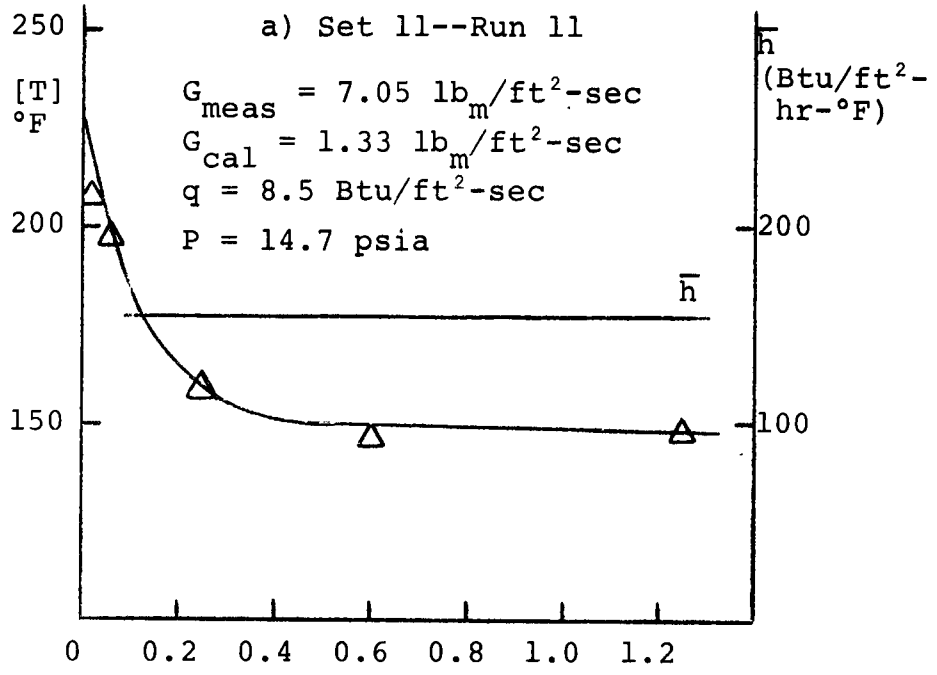


Figure 23. Single phase data, set 10--run 9, and set 11--run 10.



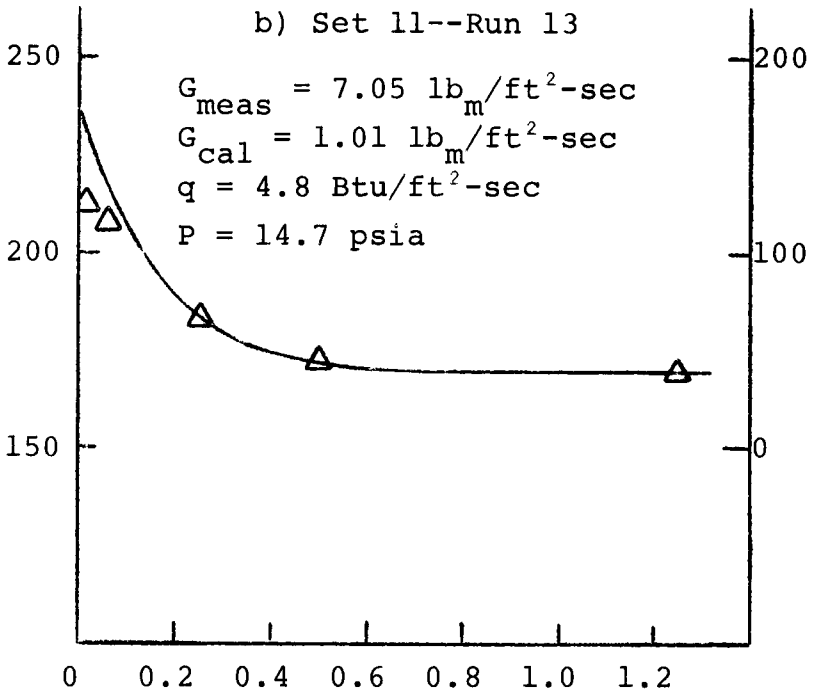


Figure 24. Single phase data, Set 11--Runs 11 and 13.

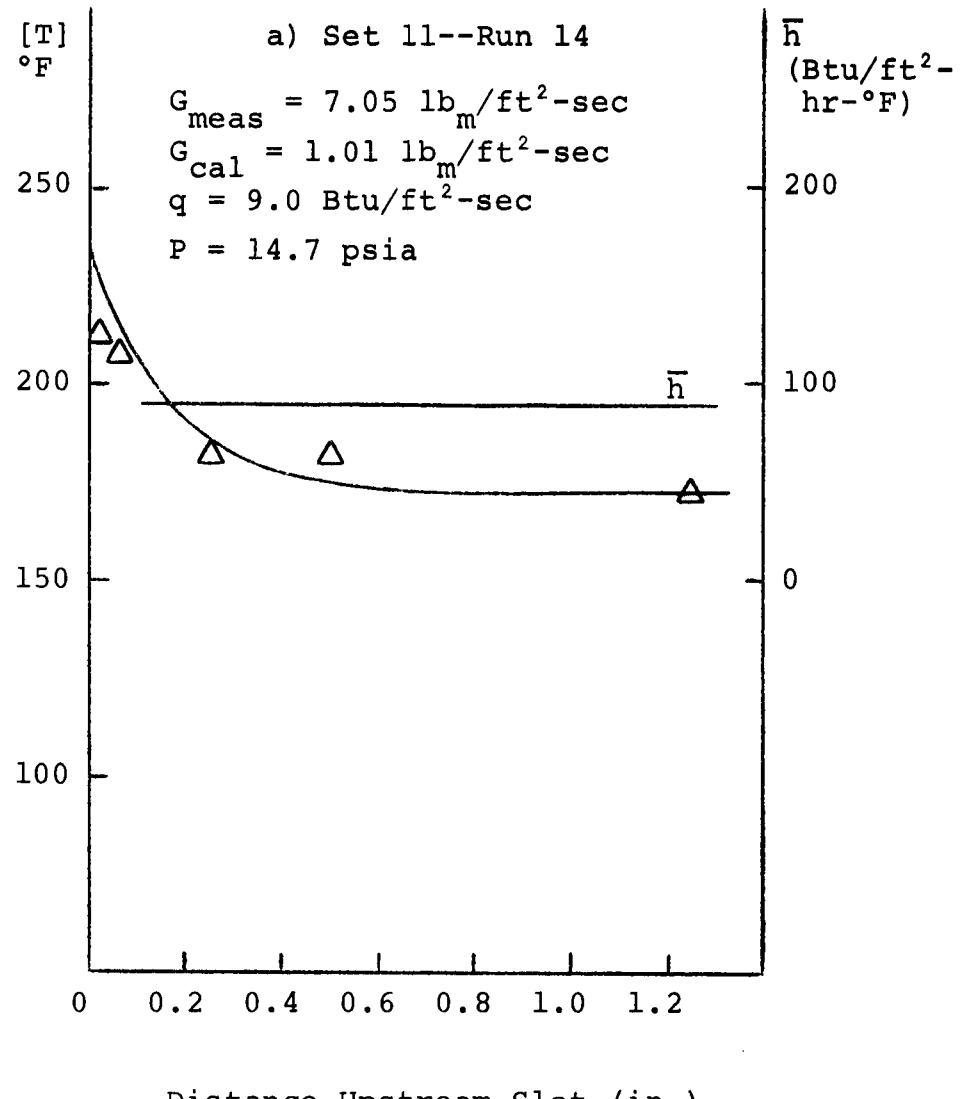


Figure 25. Single phase data, set 11--run 14.

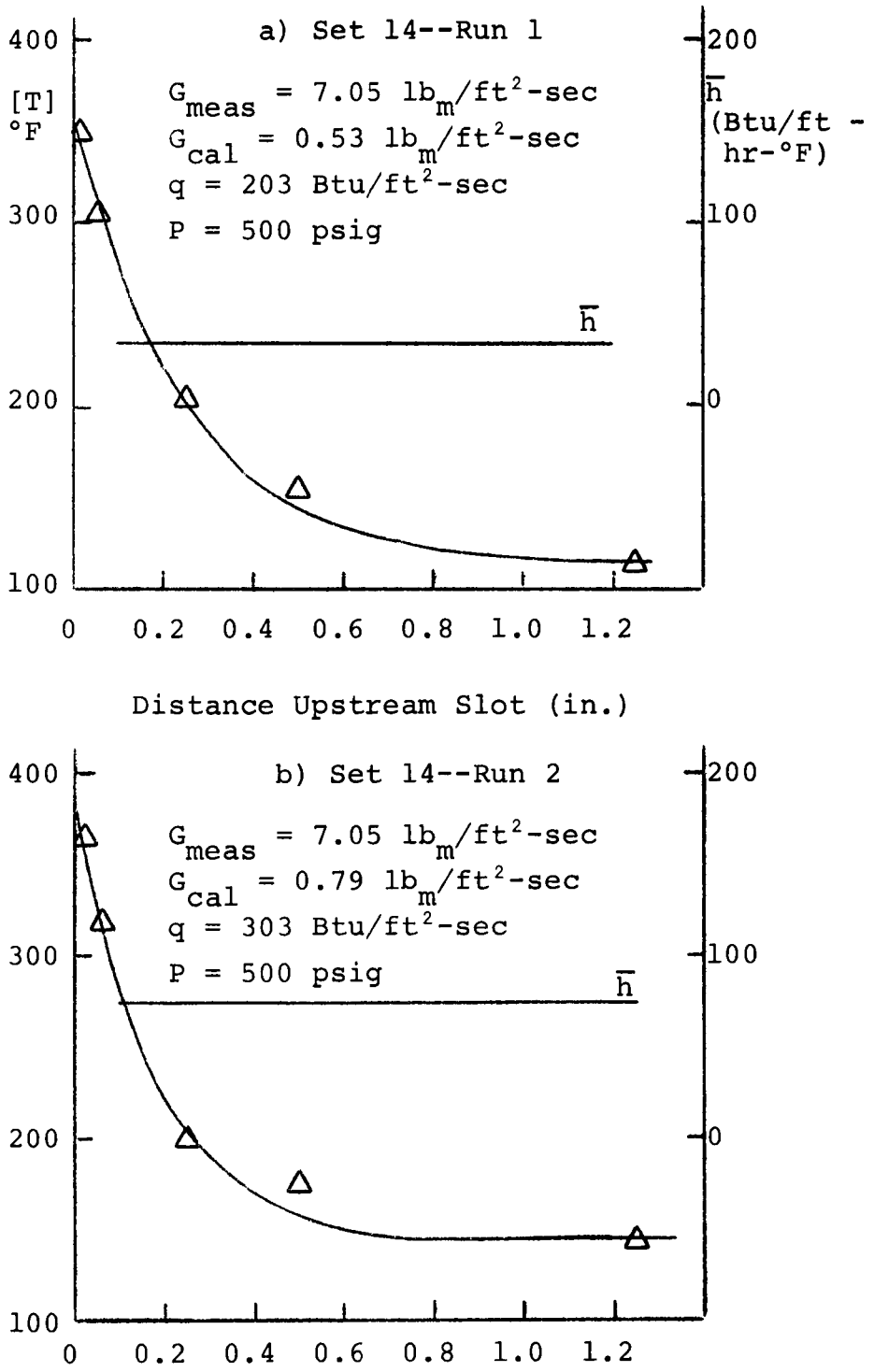


Figure 26. Single phase data, set 14--runs 1 and 2.

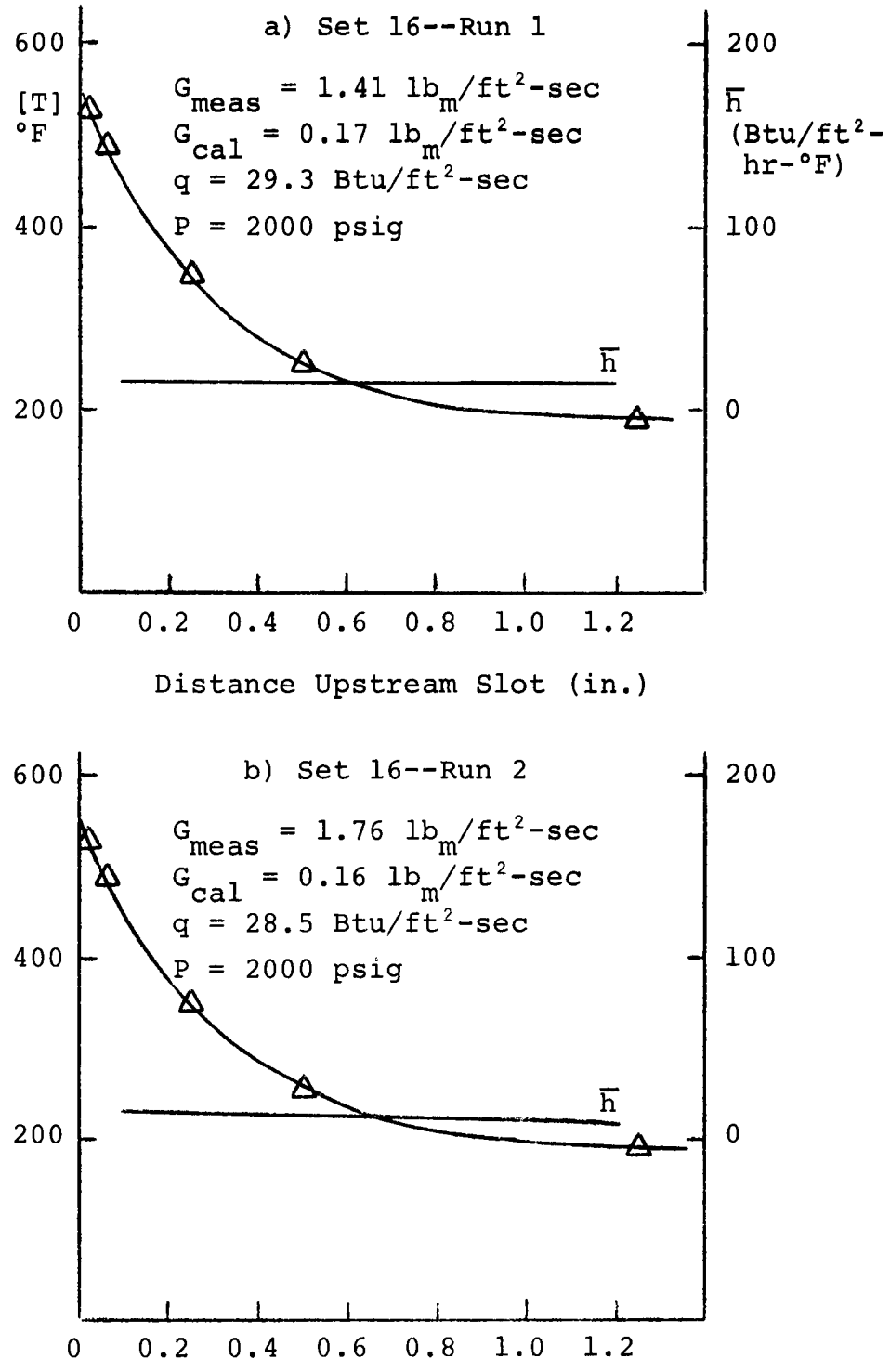


Figure 27. Single phase data, set 16--runs 1 and 2.

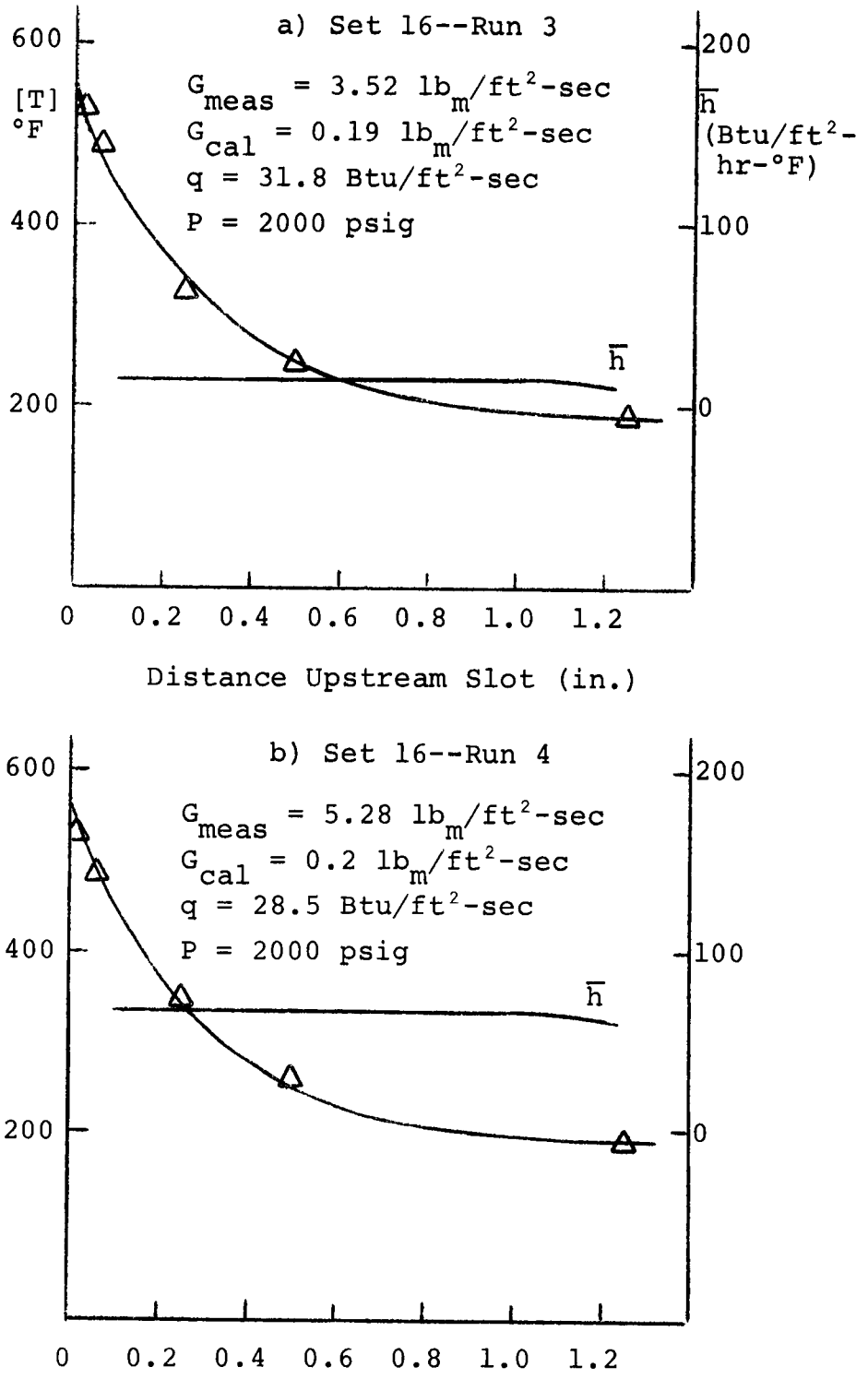


Figure 28. Single phase data, set 16--runs 3 and 4.

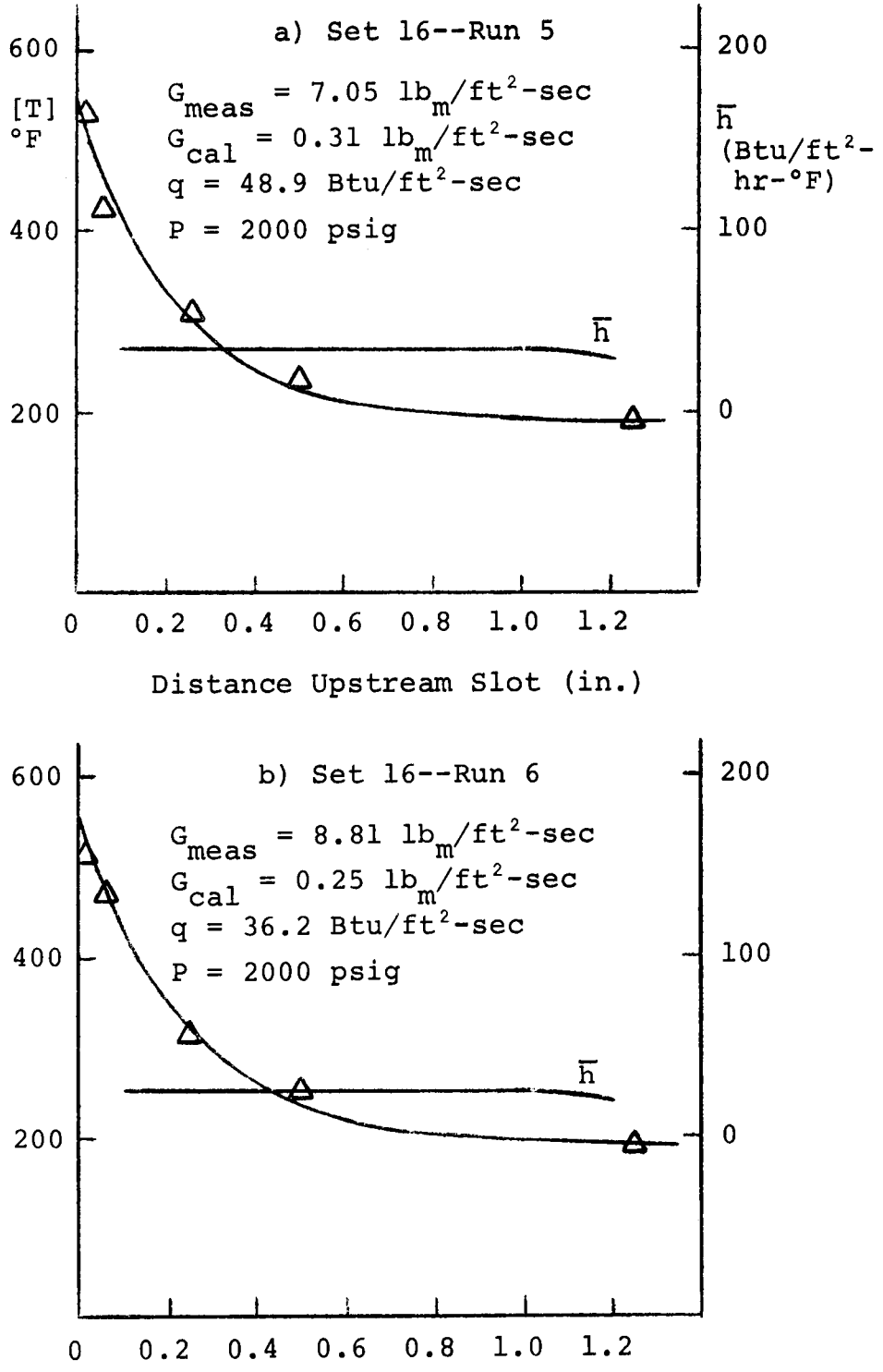


Figure 29. Single phase data, set 16--runs 5 and 6.

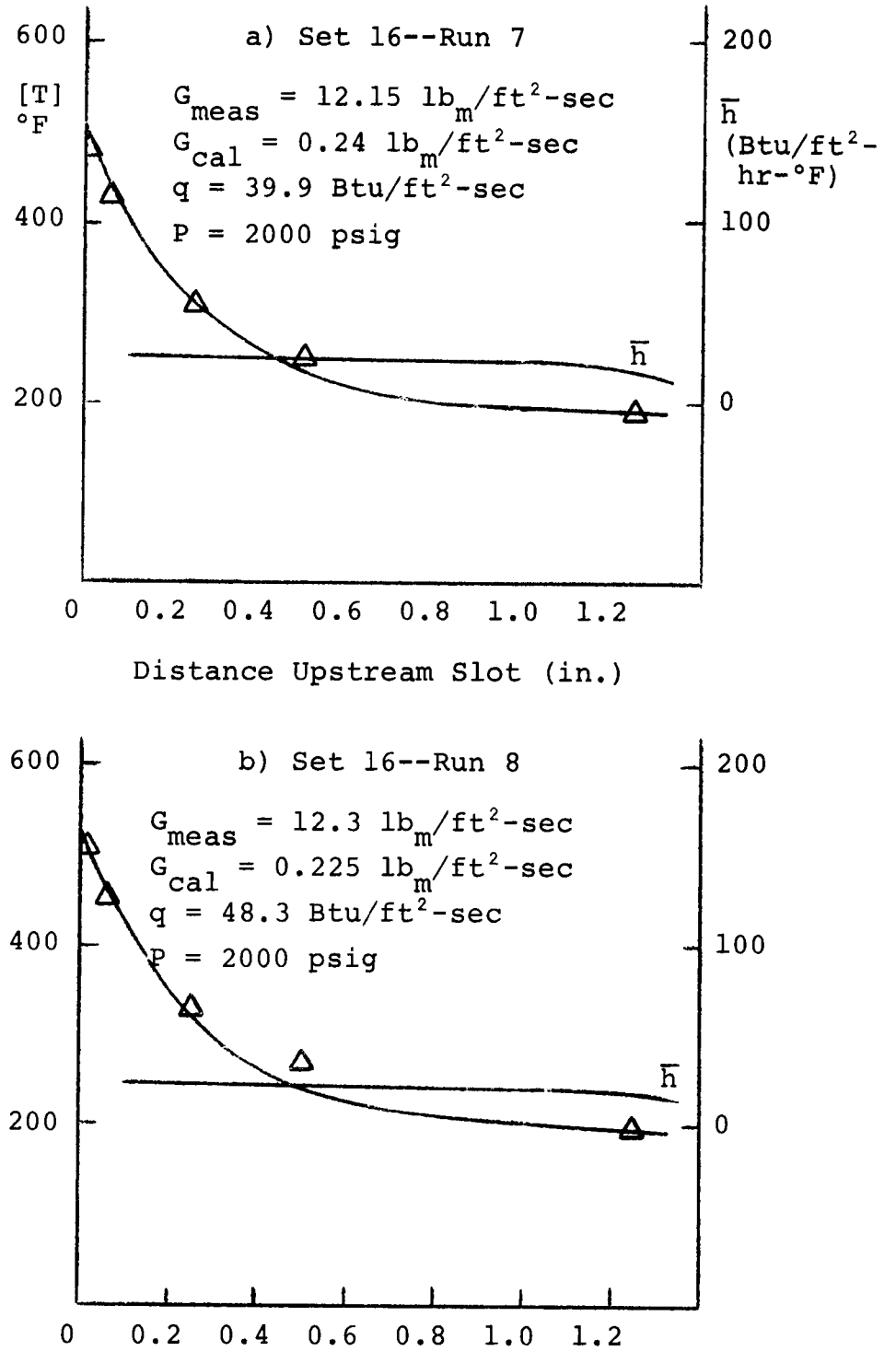


Figure 30. Single phase data, set 16--runs 7 and 8.

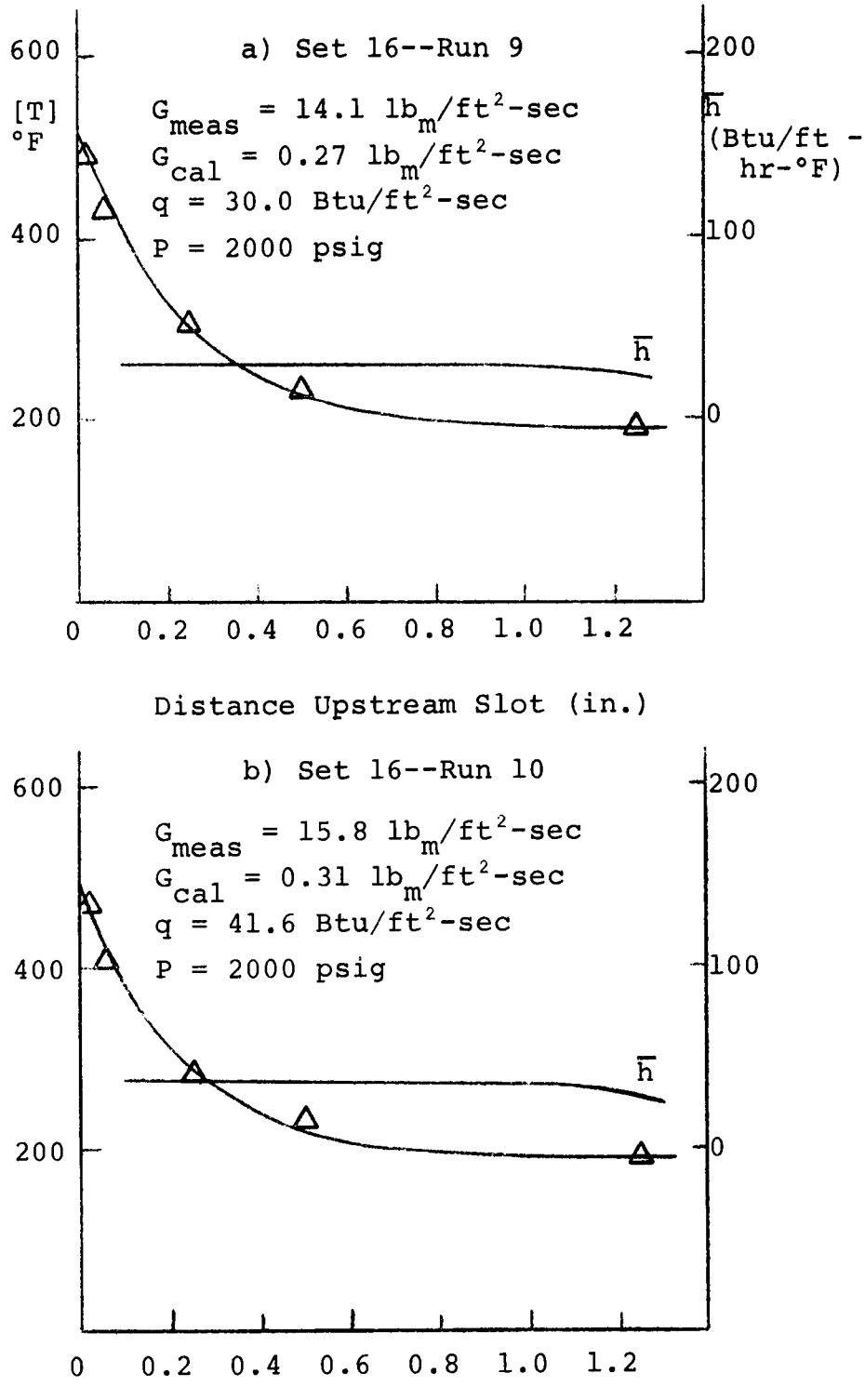


Figure 31. Single phase data, set 16--runs 9 and 10.

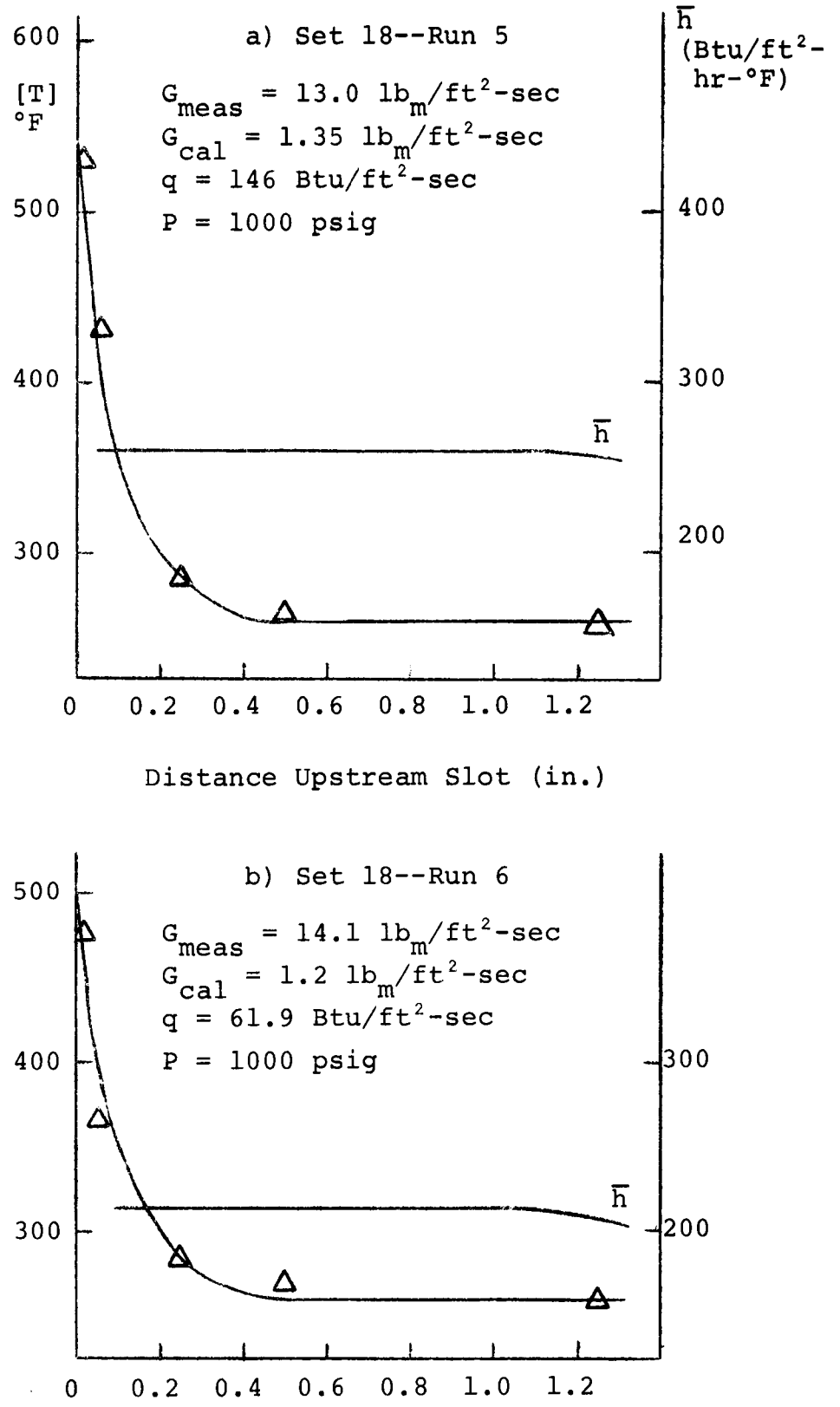


Figure 32. Single phase data, set 18--runs 5 and 6.

regime is plotted in Figure 33. The data shows a generally decreasing value of the ratio. The data for run 18 represent runs after the system was disassembled and cleaned. The two data points for this run demonstrate that the system apparently never returned to the original unplugged condition (i.e., G_{cal}/G_{meas} did not become unity). Measured pressure drops at the corresponding run numbers are also plotted in Figure 33. A rough correlation is evident in that the higher pressure drops are recorded when plugging is most severe. Difficulty with a broken wire was responsible for the zero pressure drop data shown.

Temperature profiles for the two phase flow data are shown in Figures 34 through 42. Data for the case of liquid-vapor mixture at the exit and of superheated vapor at the exit are clearly evident. The data for which the liquid-vapor mixture occur at the exit have essentially a constant temperature (approximately saturation temperature) along the first 0.6 inches from the surface; see for example Figure 37, run 12, and Figure 39, runs 9 and 10. The constant temperature results from the high heat transfer coefficient in the two-phase regime coupled with a heat leak from the copper block through the ceramic insulator behind the upper 1/8 inch of the plate. The land very near the surface thus behaves as a constant heated duct which in two-phase flow generally takes on a temperature near the saturated temperature of the fluid. The fact that the temperature profile becomes constant at the surface makes it impossible to

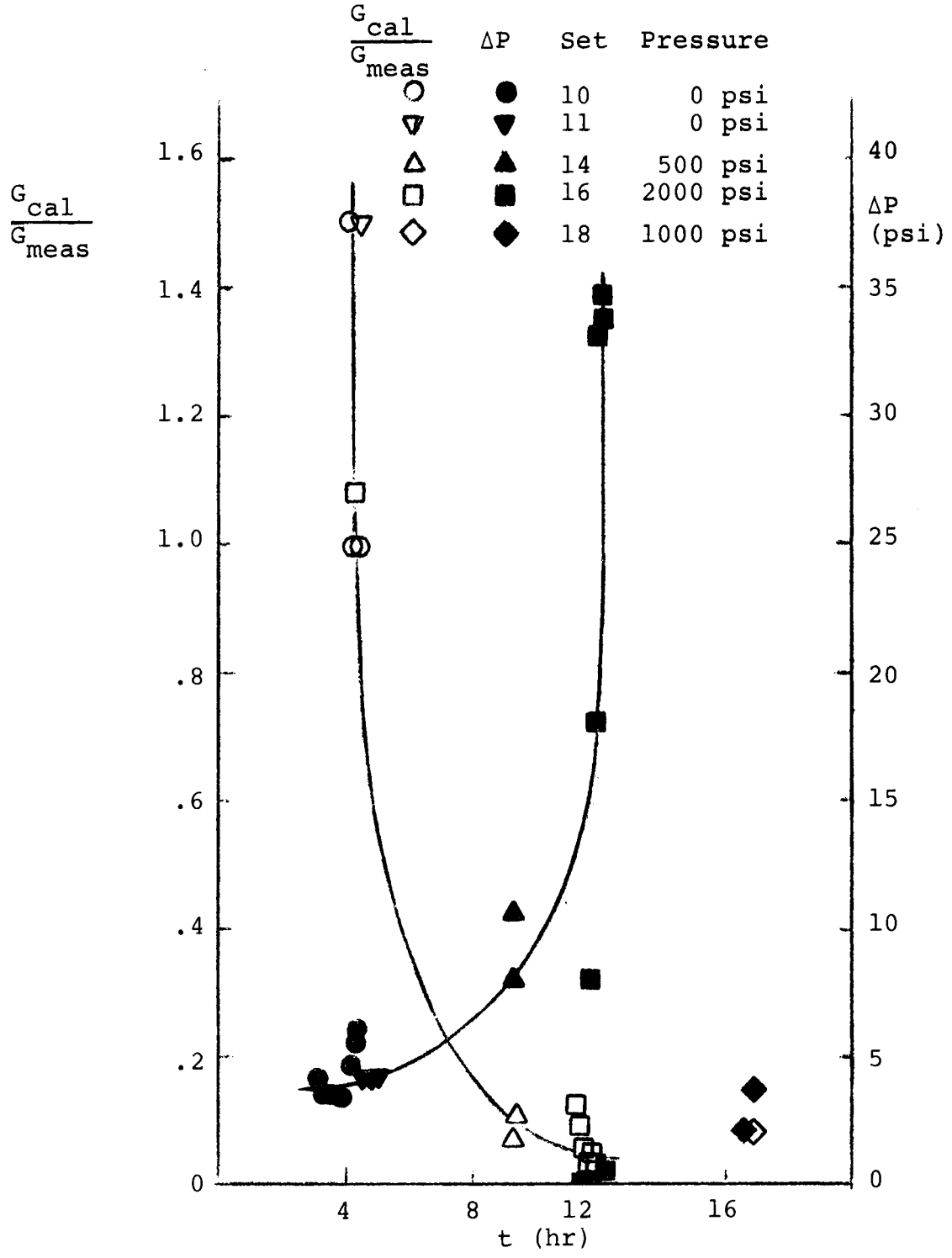


Figure 33. Pressure drop and ratio of calculated to measured mass flux versus elapsed run time.

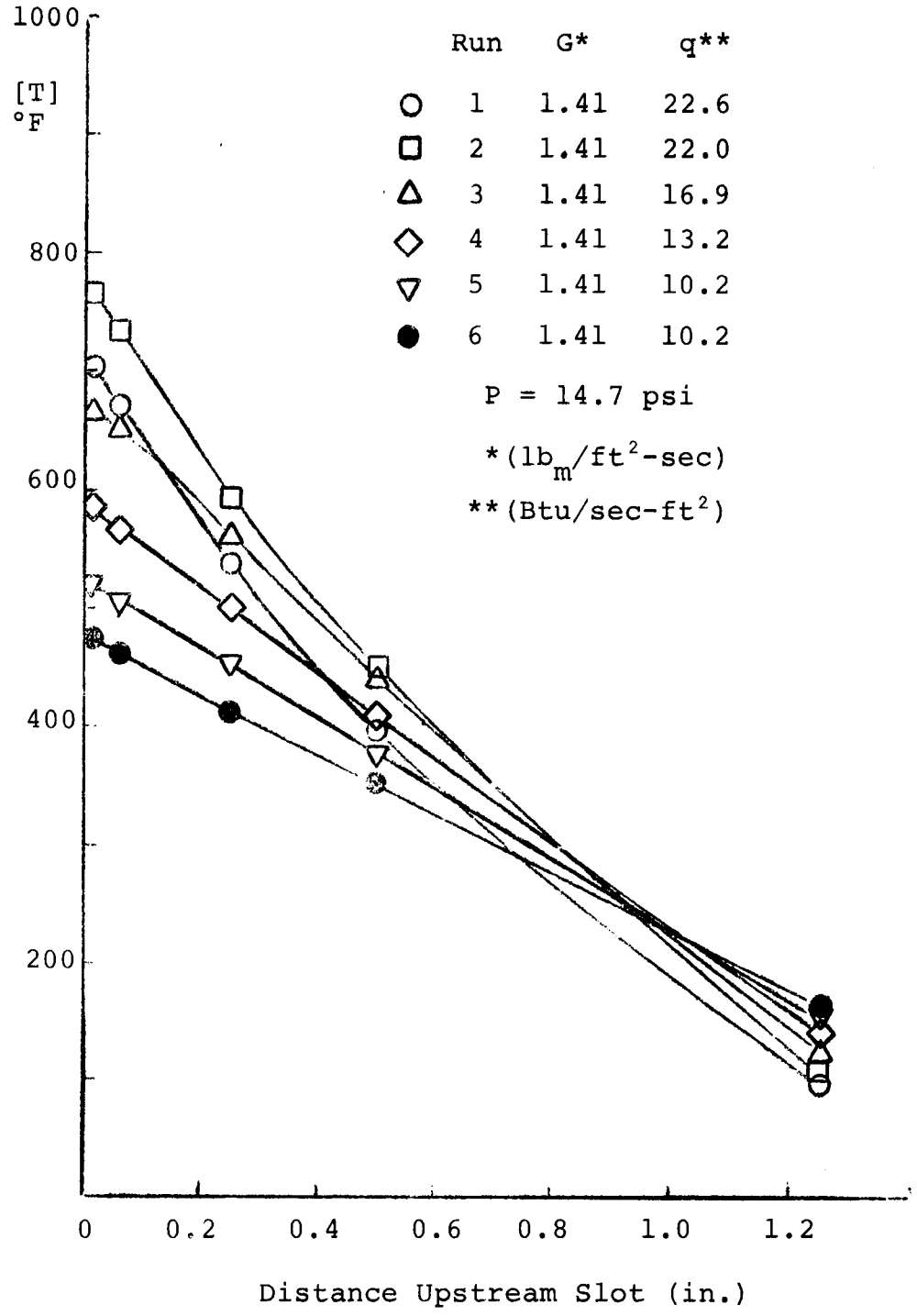


Figure 34. Temperature distribution, test 9--runs 1-6.

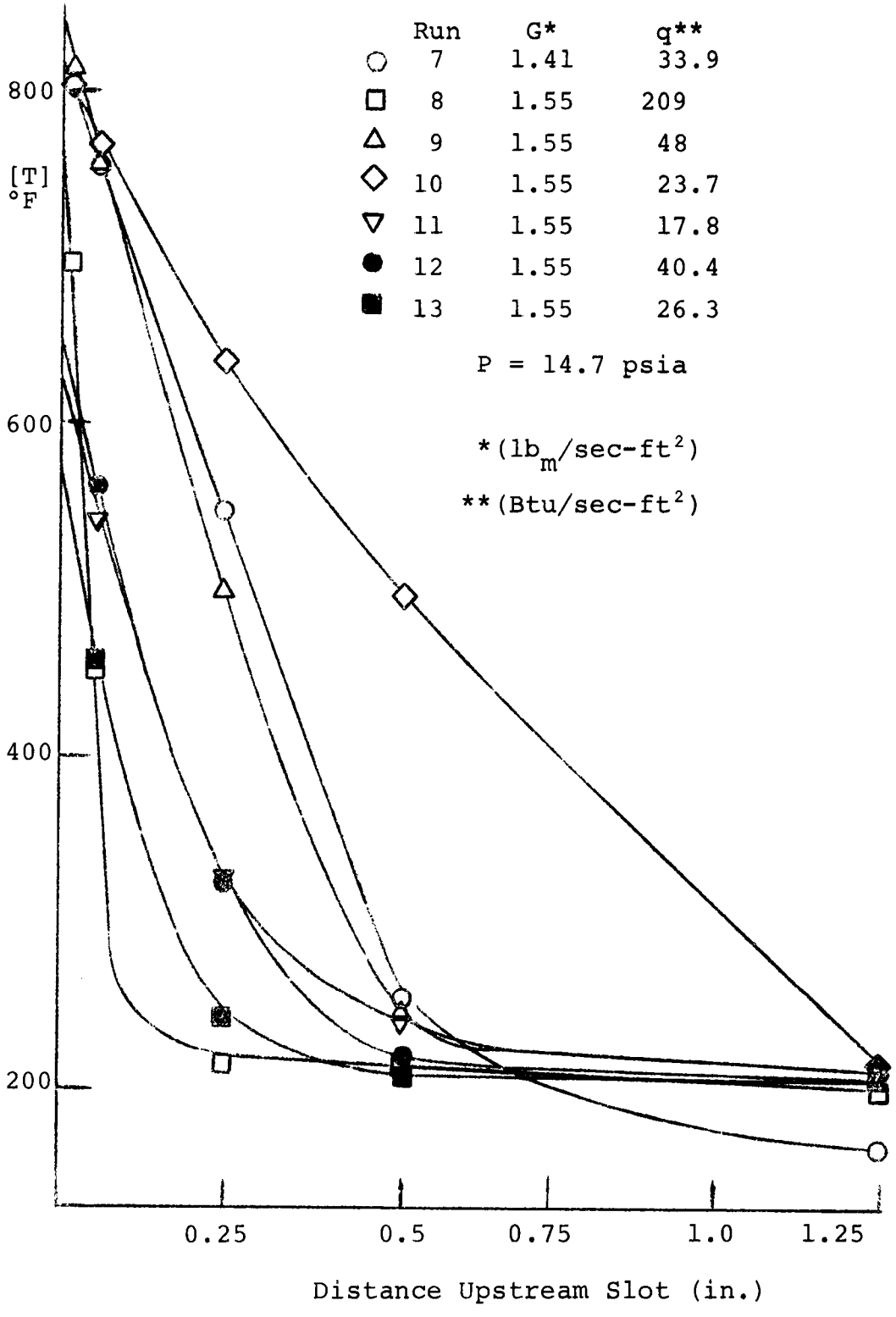


Figure 35. Temperature distribution, test 9--runs 7-13.

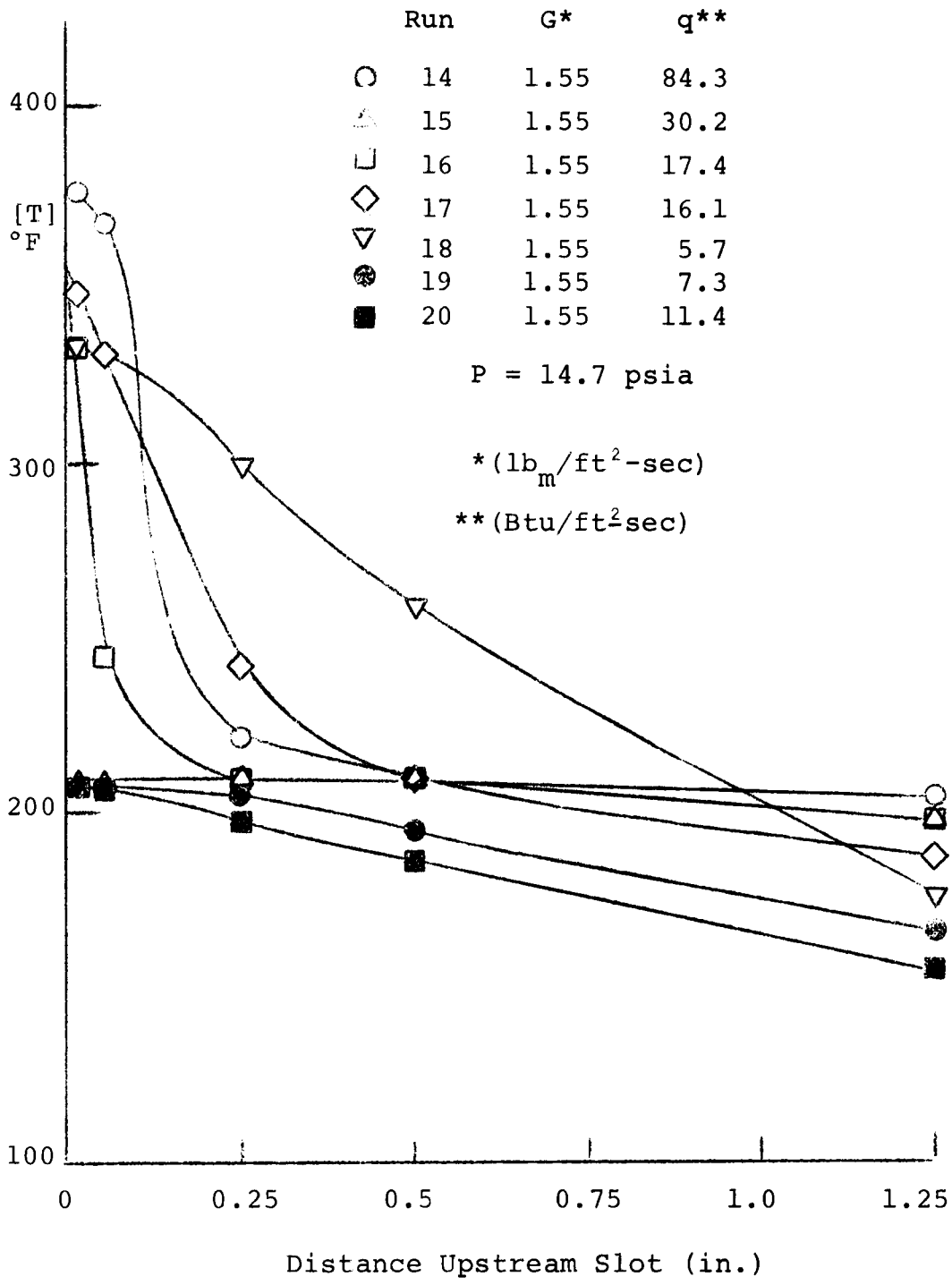


Figure 36. Temperature distribution, test 9--runs 14-20.

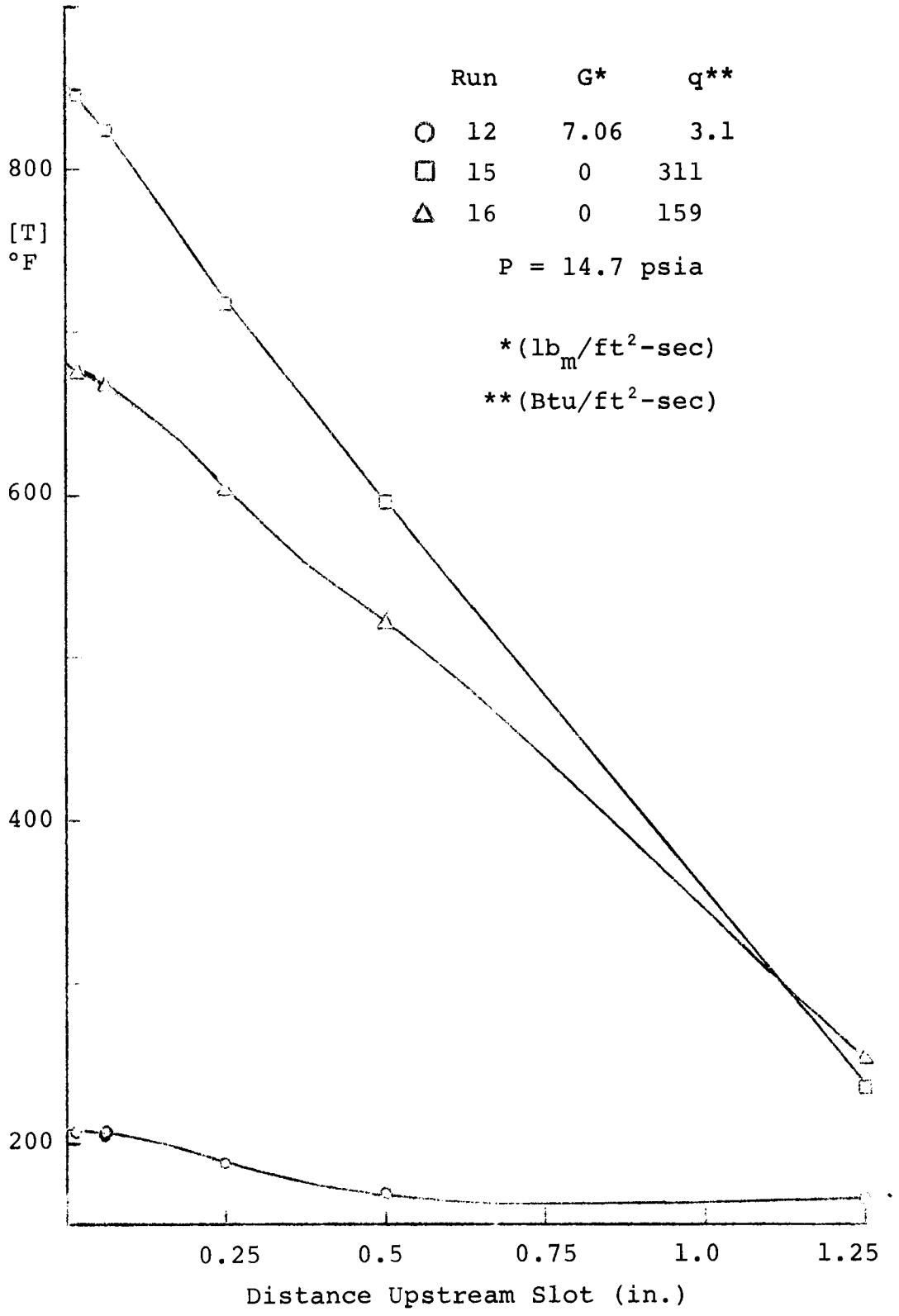


Figure 37. Temperature distribution, test 11--runs 12, 15, and 16.

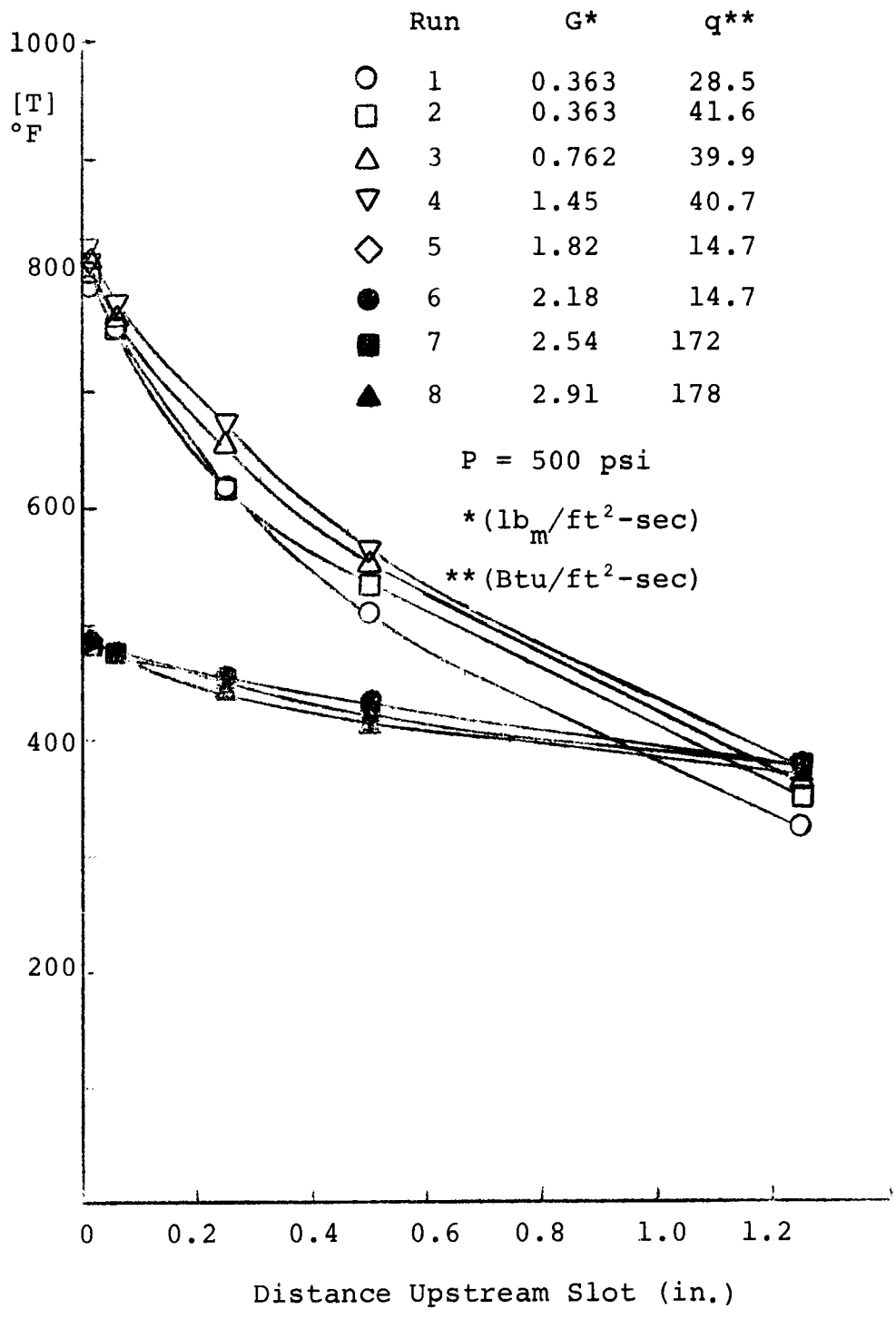


Figure 38. Temperature distribution, test 13a--runs 1-8.

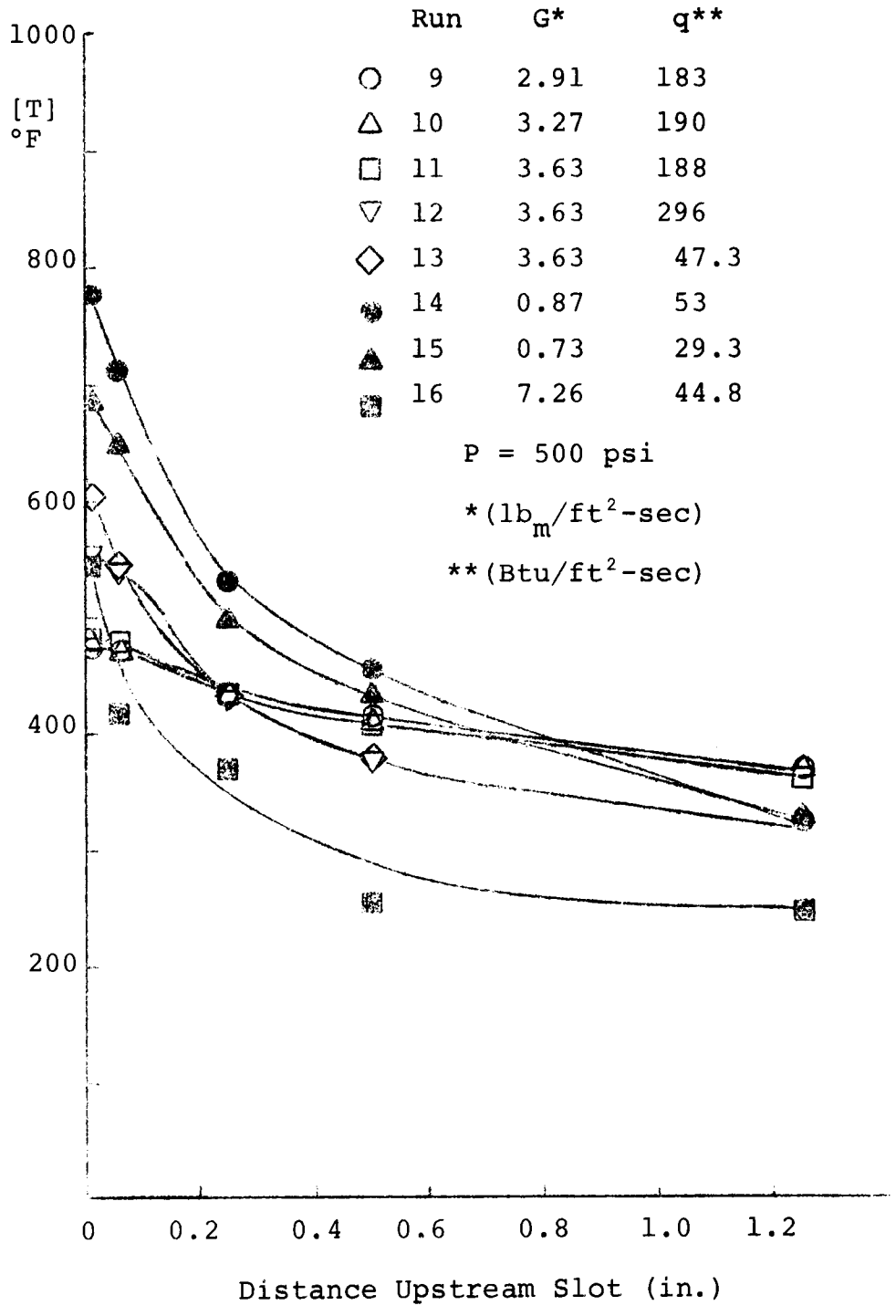


Figure 39. Temperature distribution, test 13b--runs 9-16.

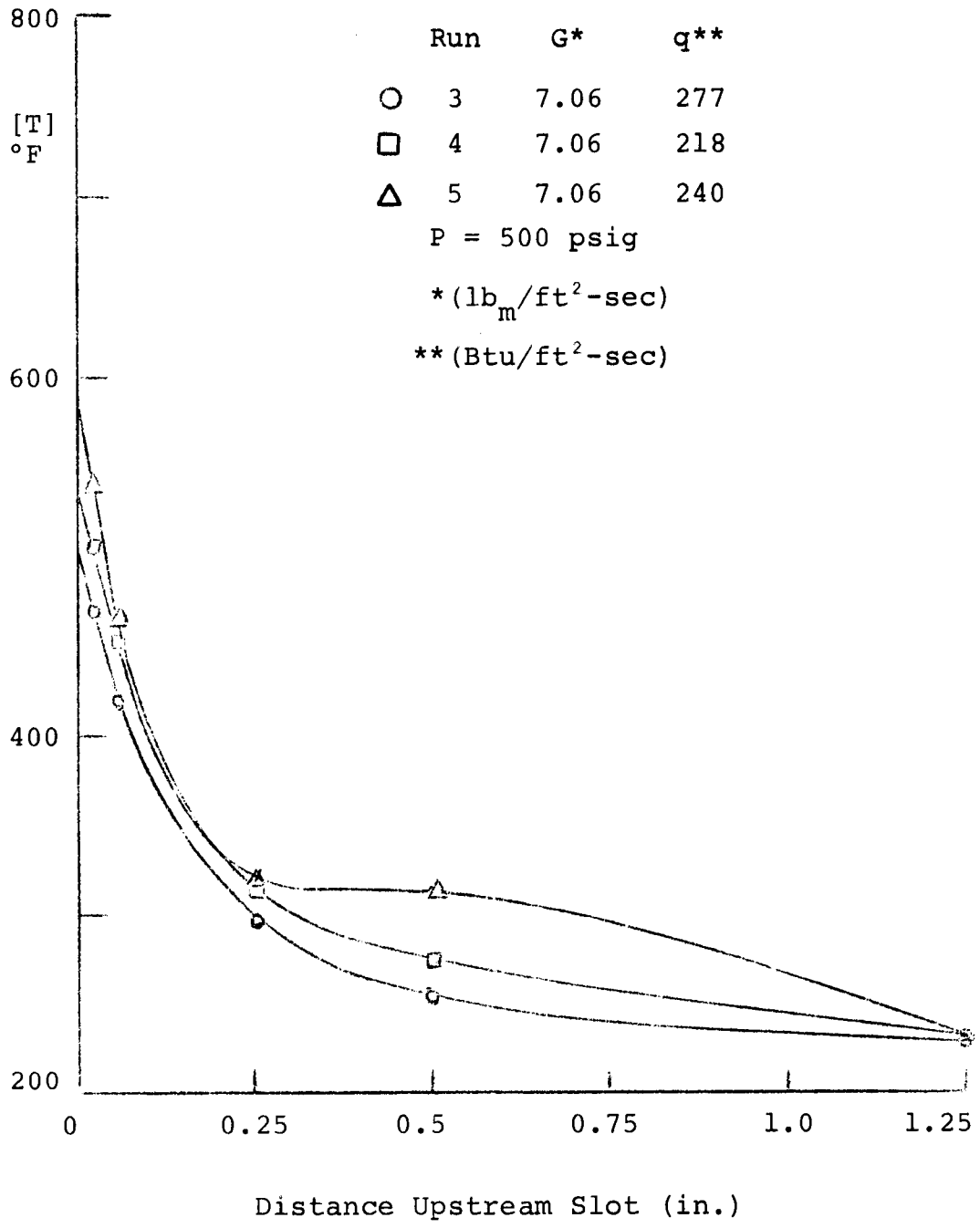


Figure 40. Temperature distribution, test 14--runs 3, 4, and 5.

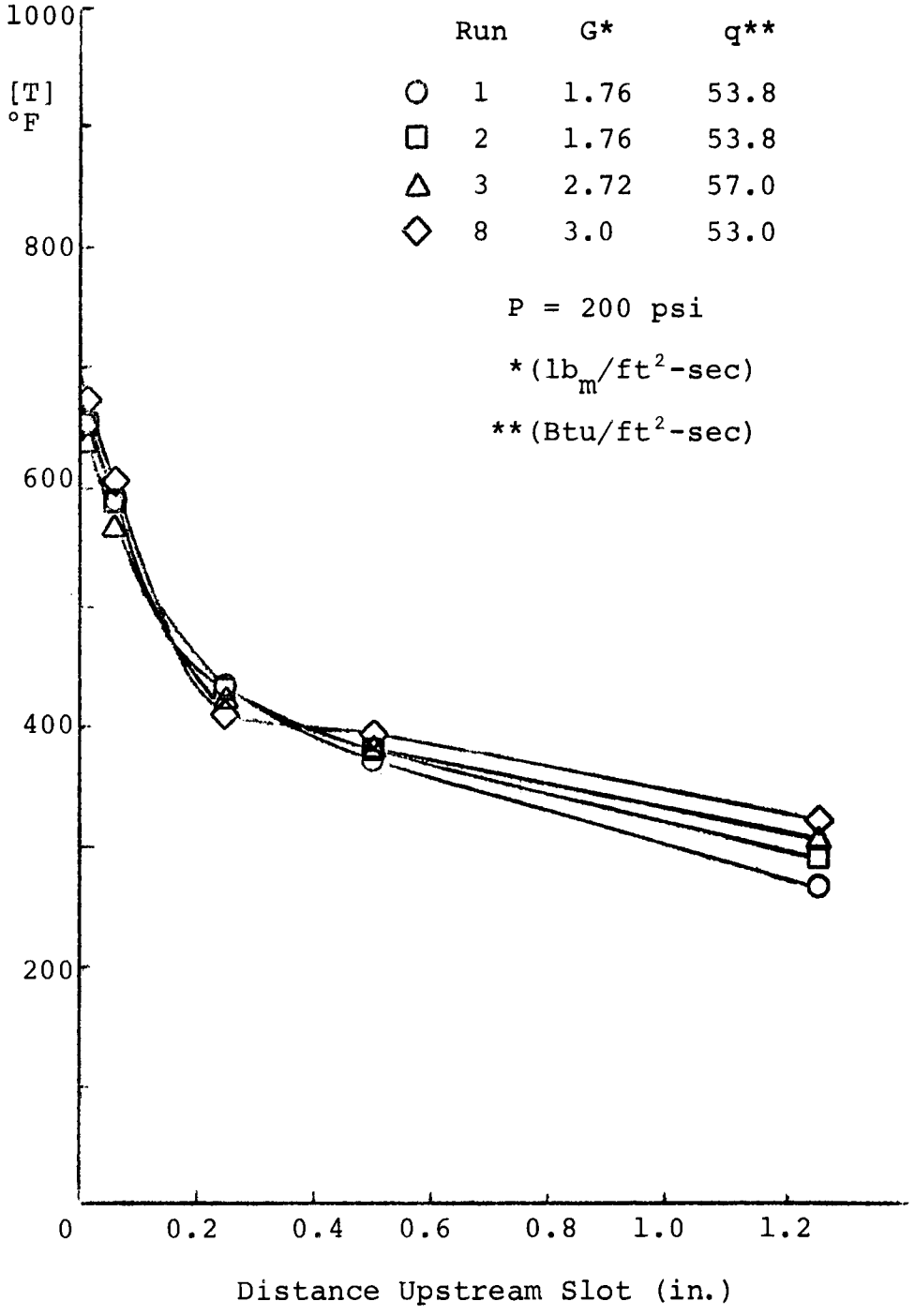


Figure 41. Temperature distribution, test 15--runs 1, 2, 3, and 8.

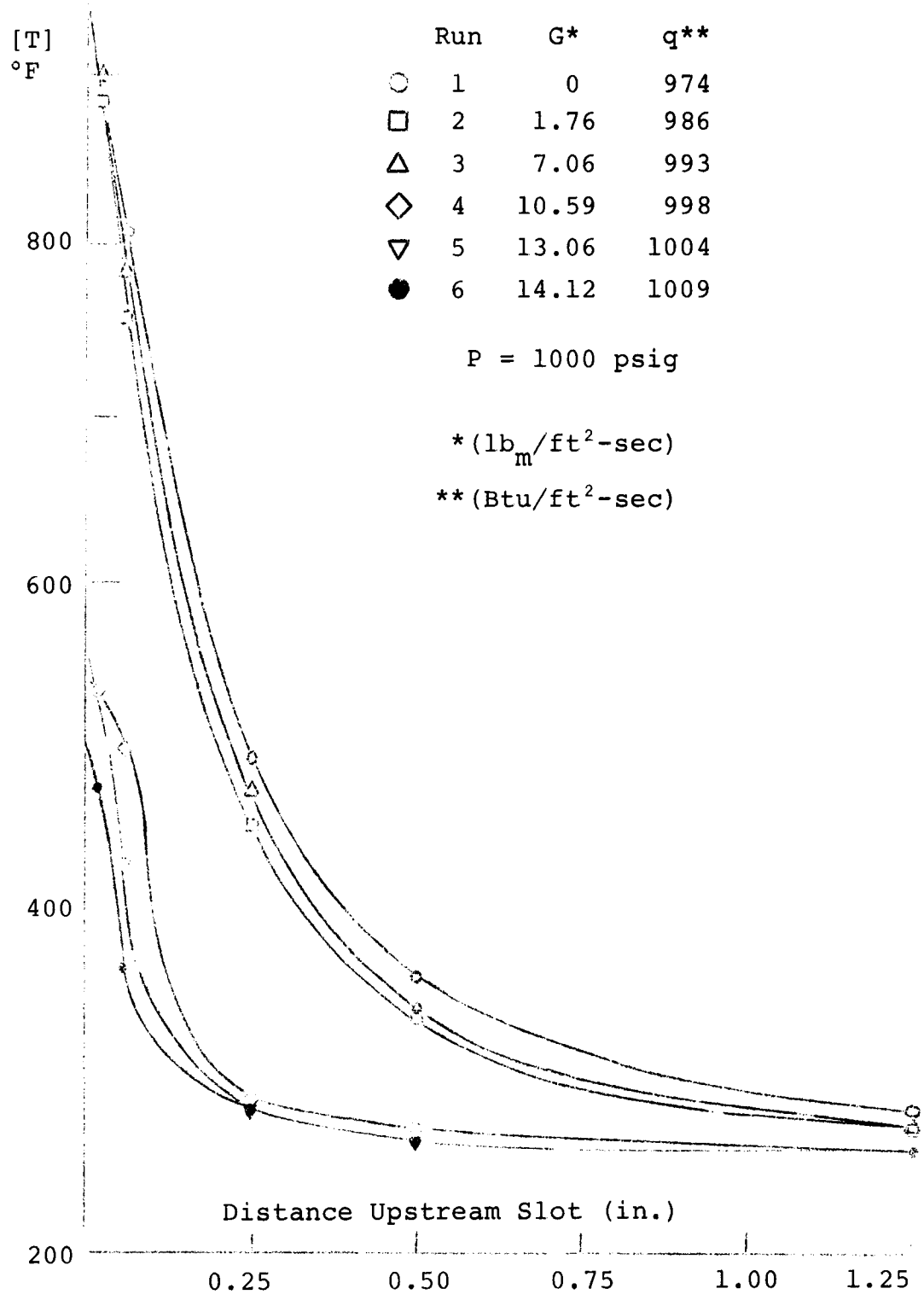


Figure 42. Temperature distribution, test 18--runs 1-6.

evaluate the surface heat flux from the measured temperature profile. Consequently the ratio of computed heat flux in the single phase region to power setting P was plotted (Figure 43) versus the ratio of land surface temperature minus chamber temperature to block temperature minus chamber temperature, divided by the approximate coefficient in the chamber, h_e. The analysis of Appendix D shows that the P and h_e are the parameters governing the heat transfer from the blocks. The correlation is not particularly good but shows a rapid increase in q with θ. The data is for the case of water running over the heater block and the value of h_e may be significantly different from that used to plot Figure 43. Figure 43 will be used for estimating the heat flux in the two phase flow regimes where the temperature gradient is not well defined.

For super-heated vapor flow at the exit the temperature profiles are essentially linear from the surface to approximately saturation temperature then become uniform at the saturation value over a short length dropping finally to the inlet temperature. This profile is most evident in Figure 41 (200 psig data) and not readily as apparent in Figure 39 (runs 1 through 5) where it is anticipated that the uniform portion of the temperature profile occurred between temperature recording stations.

Under certain conditions of two-phase flow a steady-state setting was not possible due to oscillations of the flow. This was primarily encountered for the zero psig runs

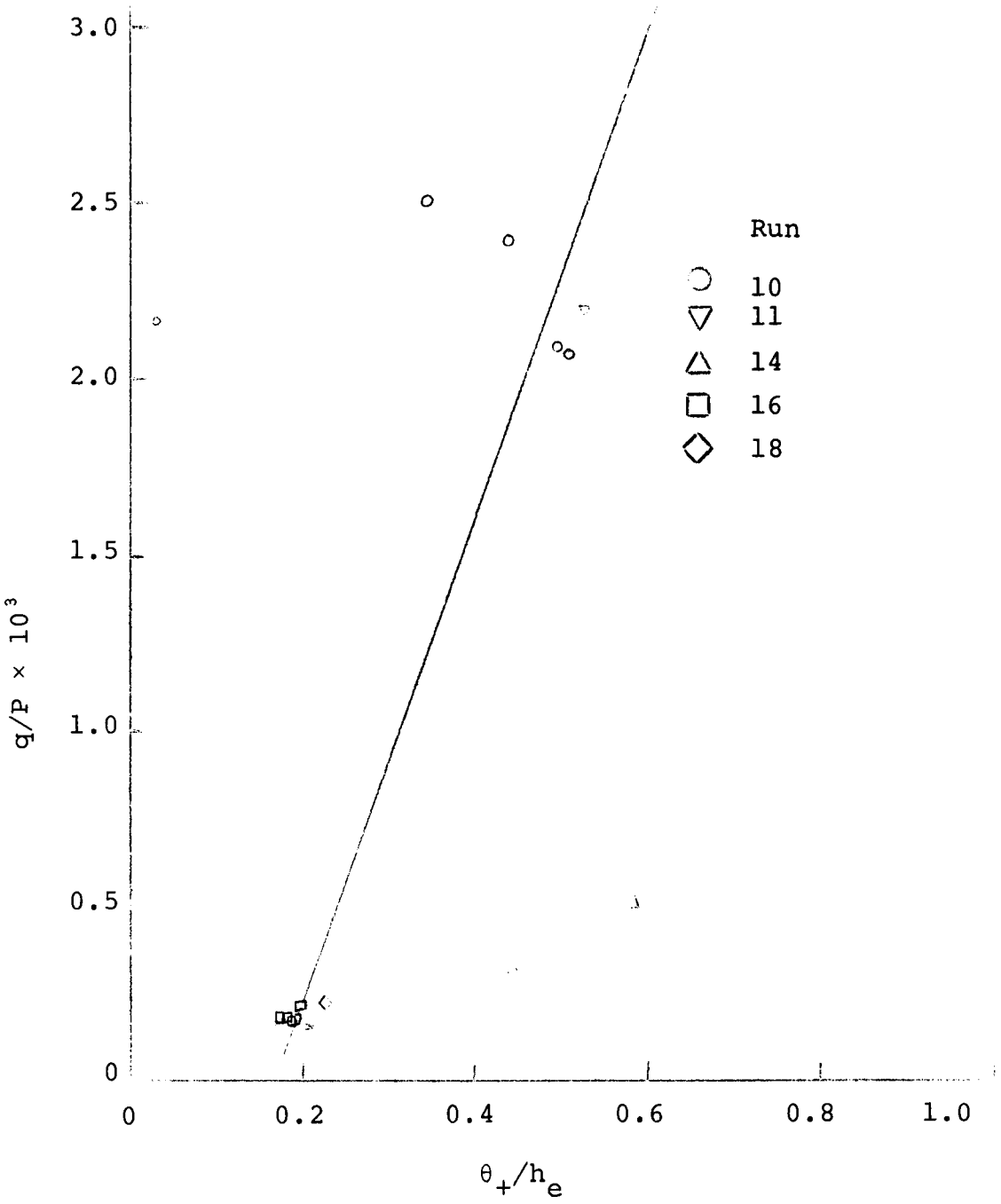


Figure 43. Correlation of heat flux with heater power, temperatures of heater block--slot exit and vessel atmosphere and heat transfer coefficient to chamber atmosphere.

when the fluid inlet temperature was close to the saturation value. Figure 44 shows temperature profiles obtained from consecutive recorder print-outs during oscillating flow. Continuous monitoring of the temperature was not possible, but a plot of the temperature measured by the surface thermocouple as a function of time based on the period of recorder print-out cycle is shown in Figure 45.

Sudden excursion in the temperature profiles were also observed. Figure 46 shows consecutive temperature profiles which illustrate a steady profile with a sudden excursion to a lower temperature profile without any change in setting of the system controls. This type of temperature excursion is believed to be associated with a change from film boiling to nucleate boiling commonly encountered in two phase flow heat transfer but not necessarily expected in the thin slots of the discrete injector nosetip.

Further evidence of different two phase flow patterns occurring in the slots is given by photographs taken of the slot exit during various flow conditions (Figures 47, 48, and 49). In Figure 47 liquid water is emerging from the slots (only four slots are unplugged in these photographs). During photographing of these pictures the test apparatus was positioned on its side and the water is exiting horizontally. The water formed a free surface due to surface tension with ripples directly over the open slots and extending down over a fraction of the lower block where it evaporates. The temperature of the plate is below the

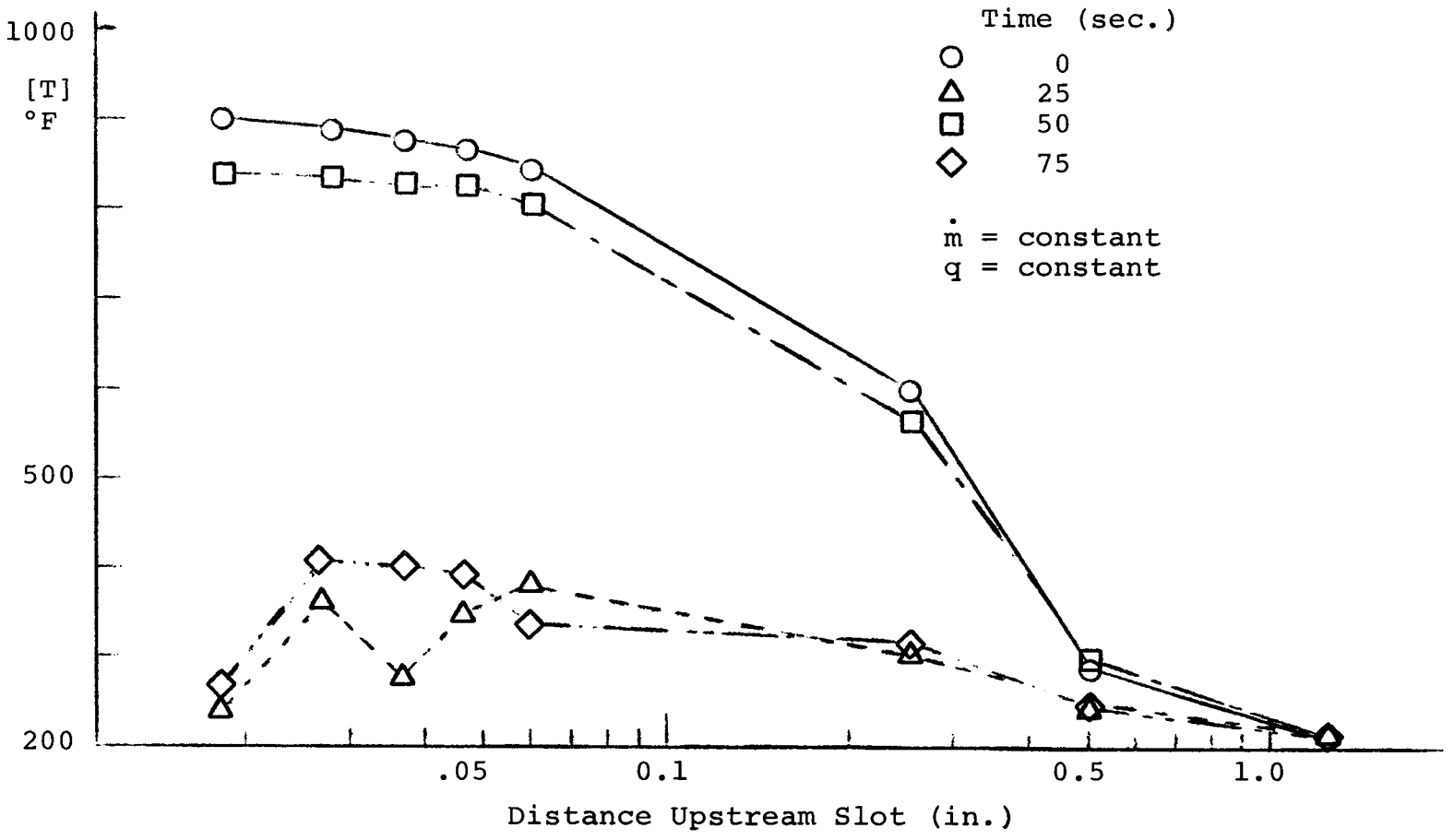


Figure 44. Consecutive temperature profiles during oscillating flow.

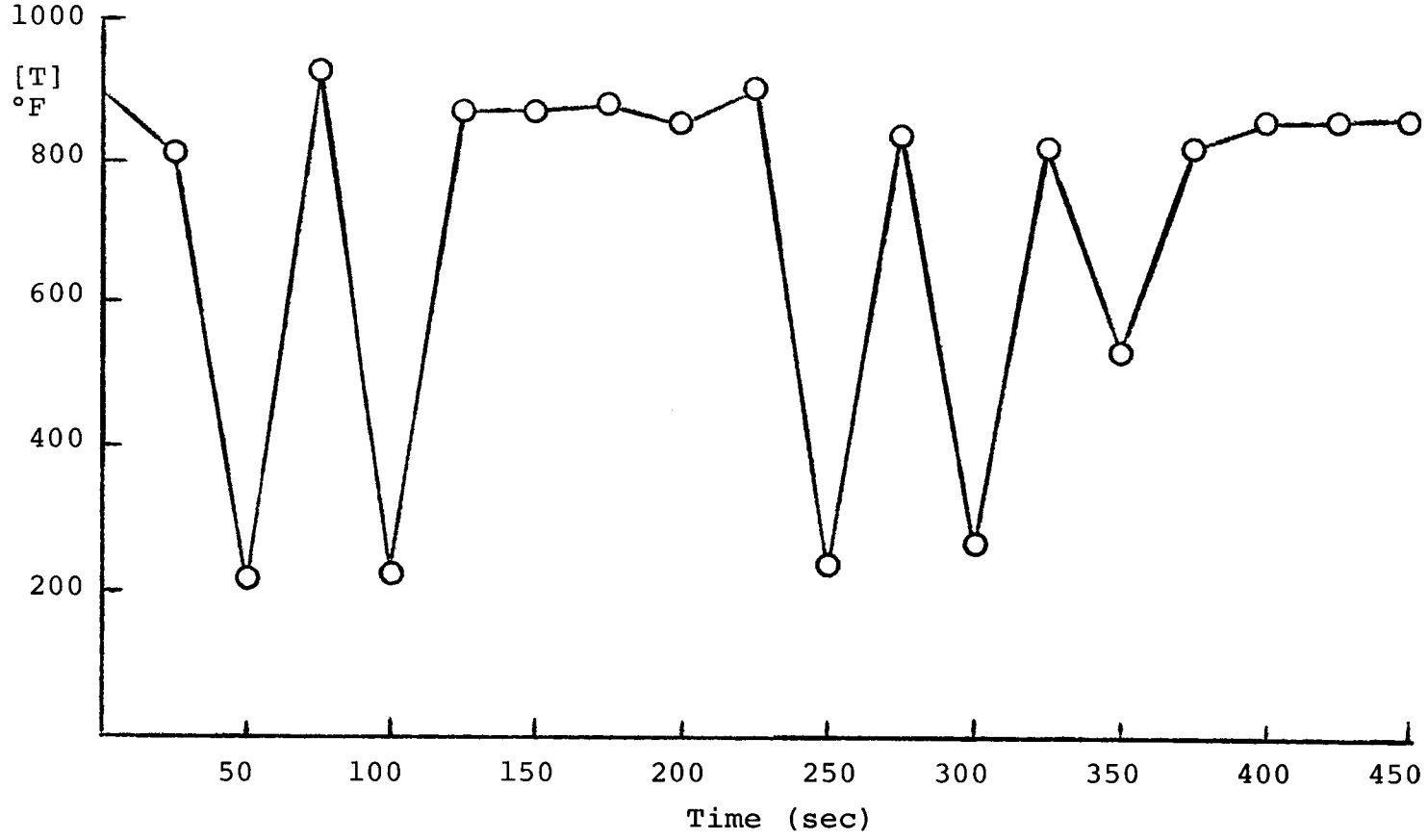


Figure 45. Temperature at station 1 versus time for oscillating flow.

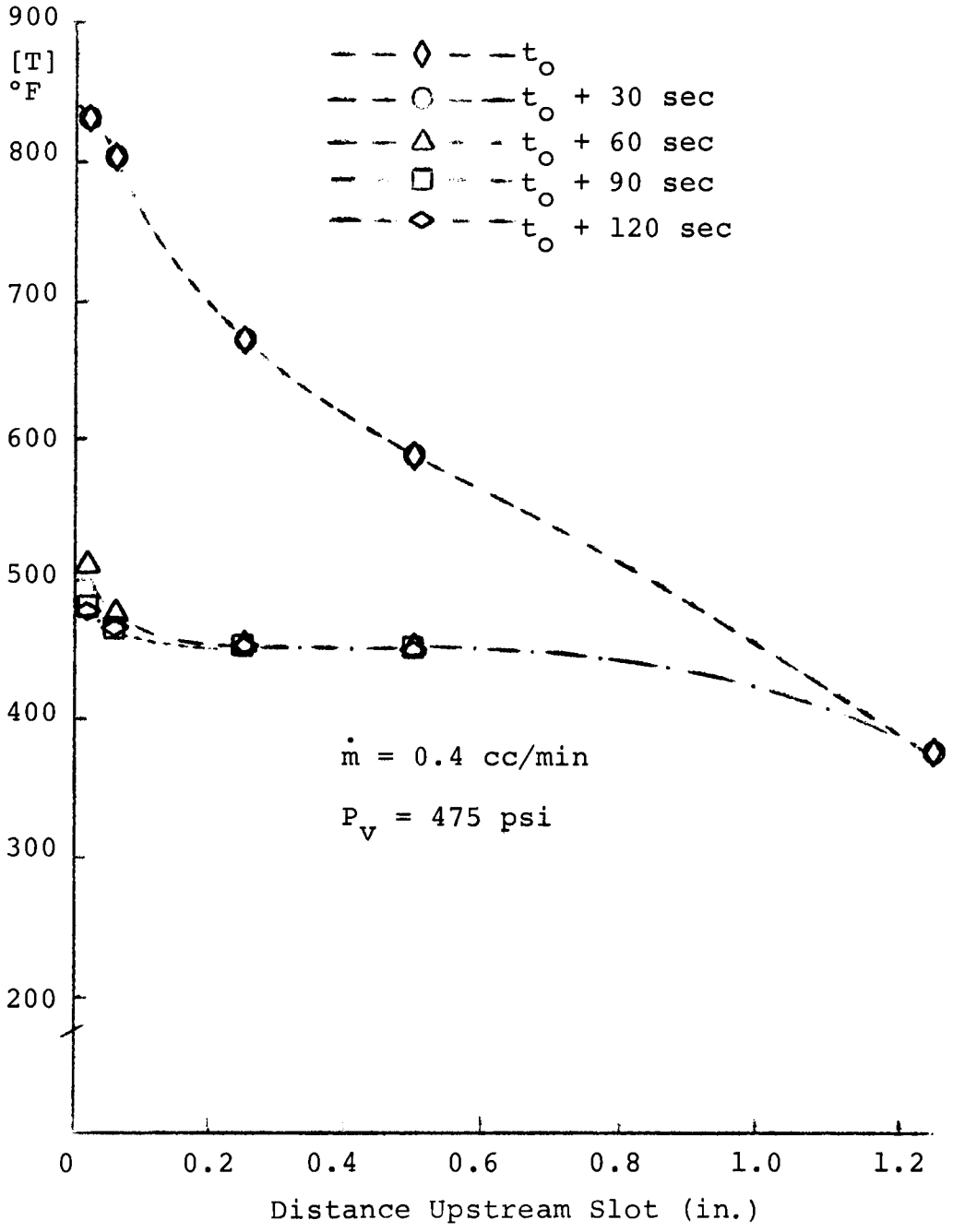


Figure 46. Temperature profile excursion.



Figure 47. Single-phase flow.

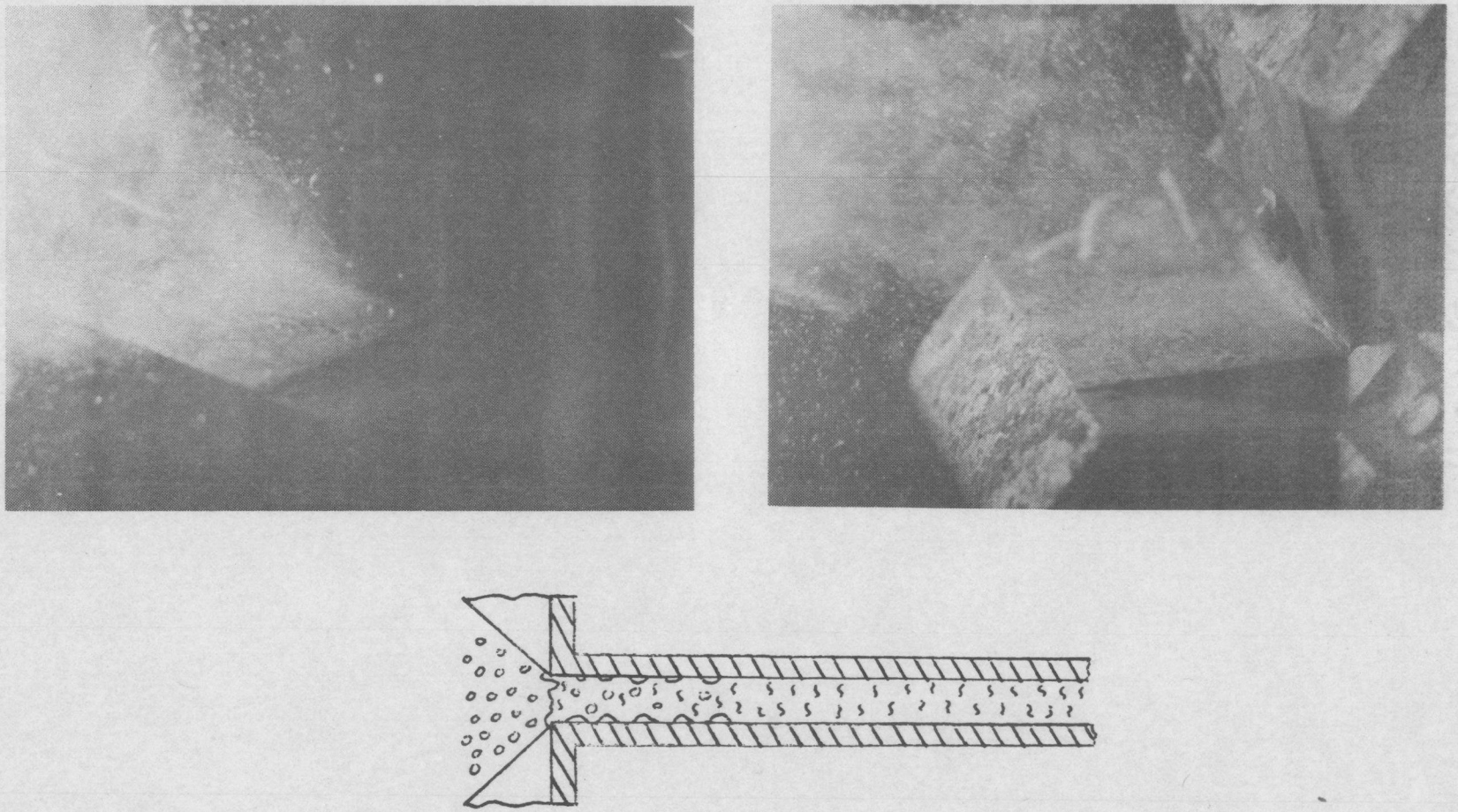


Figure 48. Two-phase dispersed flow.

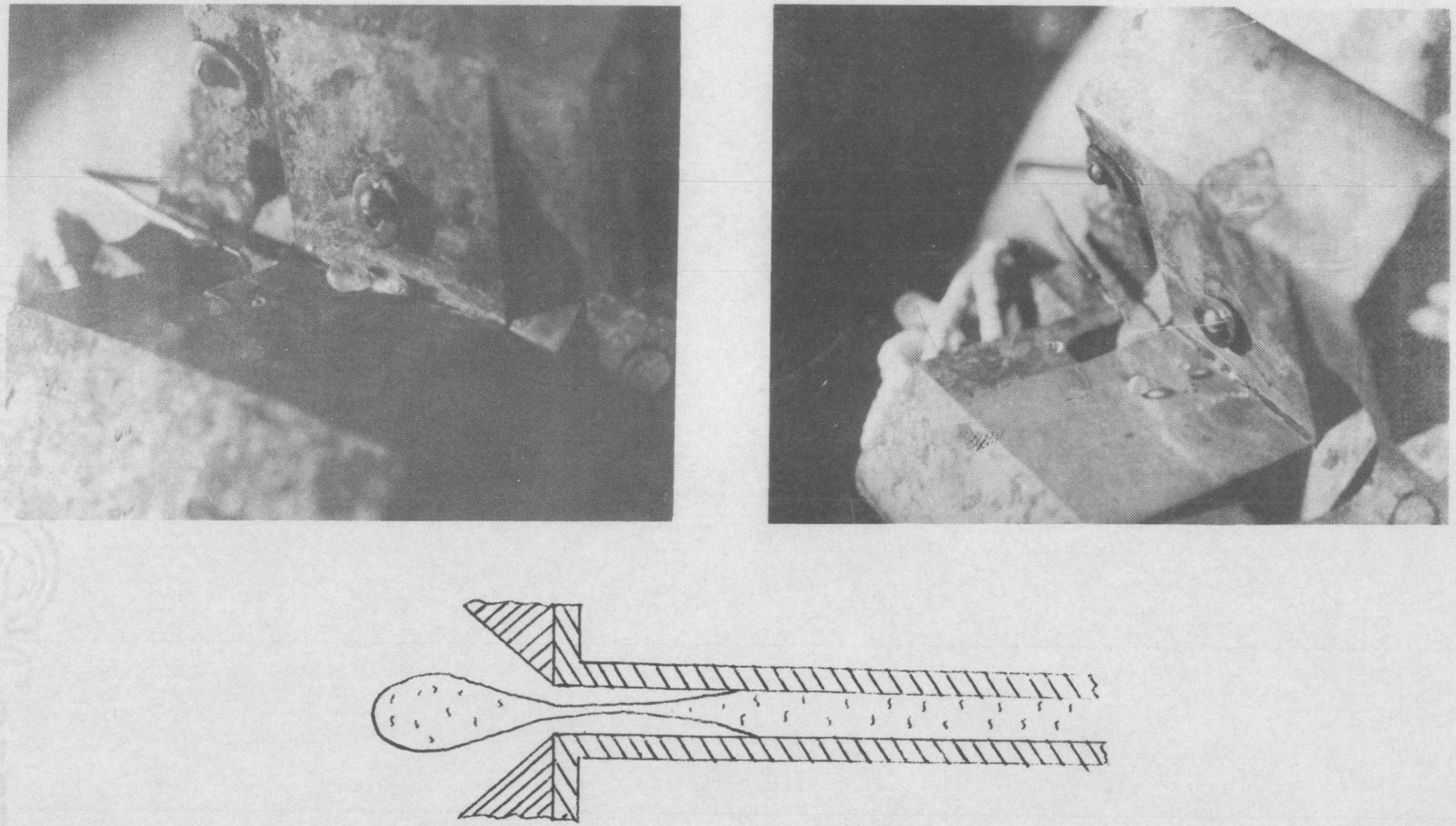


Figure 49. Two-phase globule flow.

saturation value. In Figure 48 the flow rate has been reduced and two phase flow occurs directly at the exit. The fluid is effected in a highly dispersed pattern, which will be referred to as mist flow, and the land temperature is approximately equal to the saturation value. It is evident from this picture that complete evaporation does not occur and the latent heat of evaporation is not available for cooling the plate. In Figure 49 a further reduction in flow has resulted in a globule flow pattern where the water is ejected in globules. The temperature of the plate is very high (on the order of 800-900 °F). This flow regime is similar to the film boiling phenomenon in pools where the water is separated from the heated surface by a film of vapor. It is also familiar to those who have observed a drop of water on a red hot stove. The water does not wet the surface but dances around as a little sphere. This type of behavior is called the spheriodial state.

The sensitivity of the temperature profiles to small changes in mass flux is demonstrated in Figures 50 and 51. Although the absolute value of the mass flux is not accurately known, the incremental change in mass flux is meaningful. The surface temperature for the 500 psig run shows a 10 per cent variation corresponding to a 40 per cent variation in mass flux whereas the 1000 psig run the temperature variation is less pronounced.

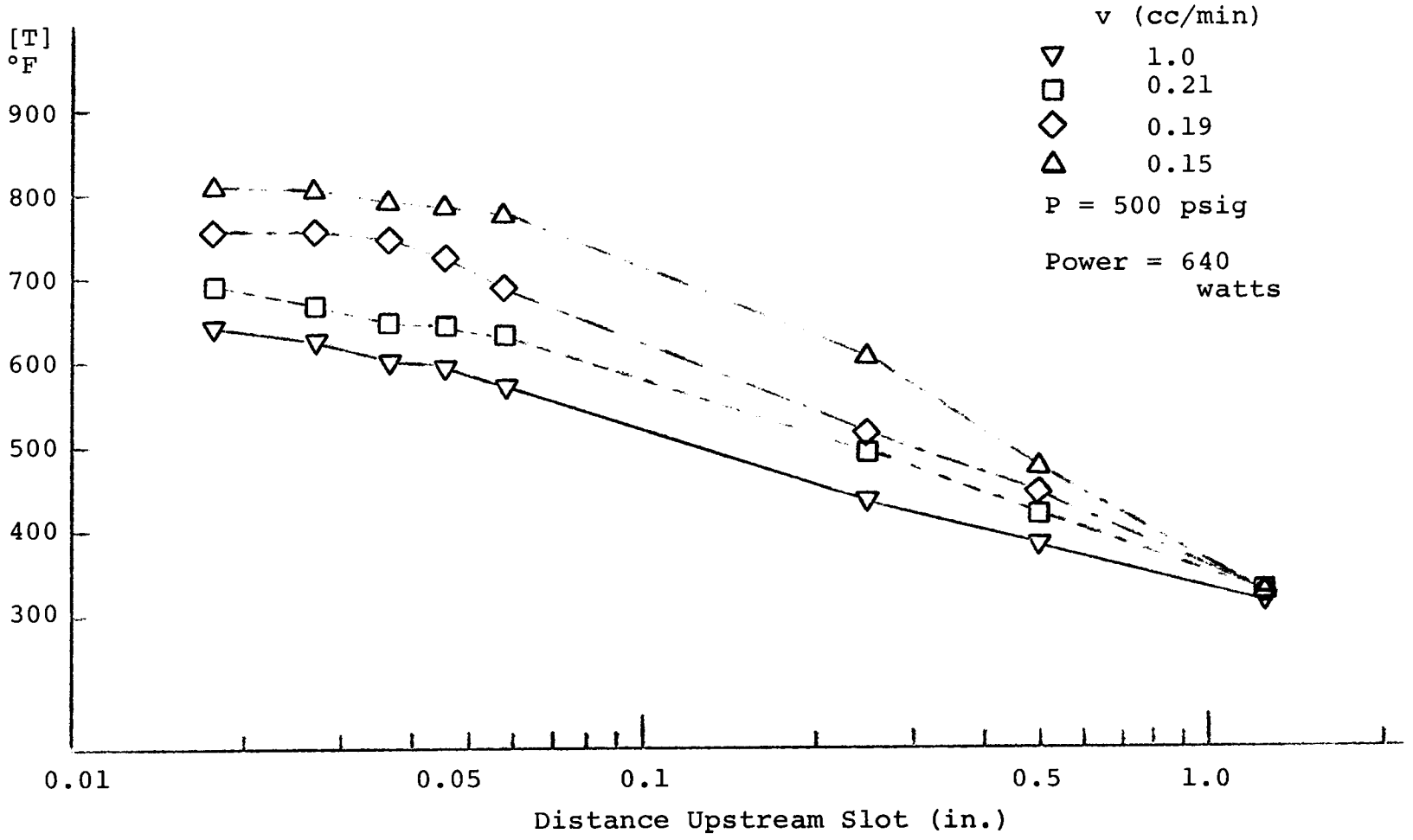


Figure 50. Sensitivity to change in mass flux at pressure = 500 psig, power = 640 watts.

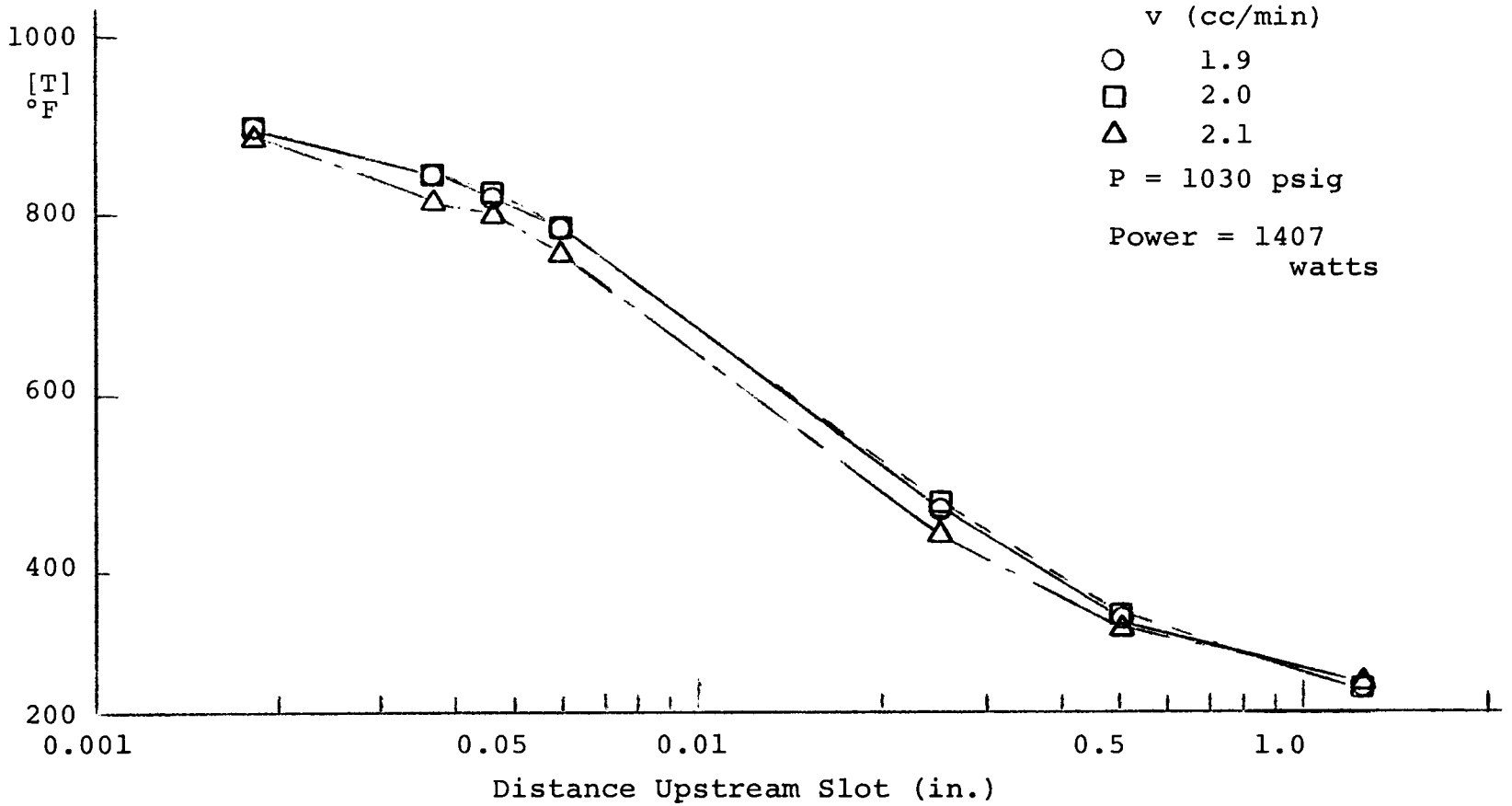


Figure 51. Sensitivity to change in mass flux at pressure = 1030 psig, power = 1407 watts.

CHAPTER VI

DISCUSSION OF RESULTS

Single Phase Flow

The temperature distribution in the land correlates very well with the theory of Appendix B. Thus, the assumptions that the fluid temperature T_F is equal to the solid temperature T_S and that the thermal properties may be treated as a constant frequently used in design analysis appears justified, for the low range of mass fluxes considered in this investigation. The method of solution avoids the problem of evaluating the heat transfer coefficient, h, since h factors out of the equations.

Values of Nu based on h computed from the data by the method of Appendix C correlate with the Peclet number, Pe = RePr, as shown in Figure 52. This value of the heat transfer coefficient, which will be designated h_L, does not necessarily represent the actual value of h in the slot flow passage but rather the value of h above which any larger value of h would not contribute to the heat transfer process. Expressed differently, this implies that the thermal energy capacity of the mass is so small that its temperature adjusts almost instantaneously to that of the solid. The heat transfer coefficient controls the rate at which energy flows from the wall to the mass. Adding energy at a rate higher than h_L only decreases the time required for T_F to

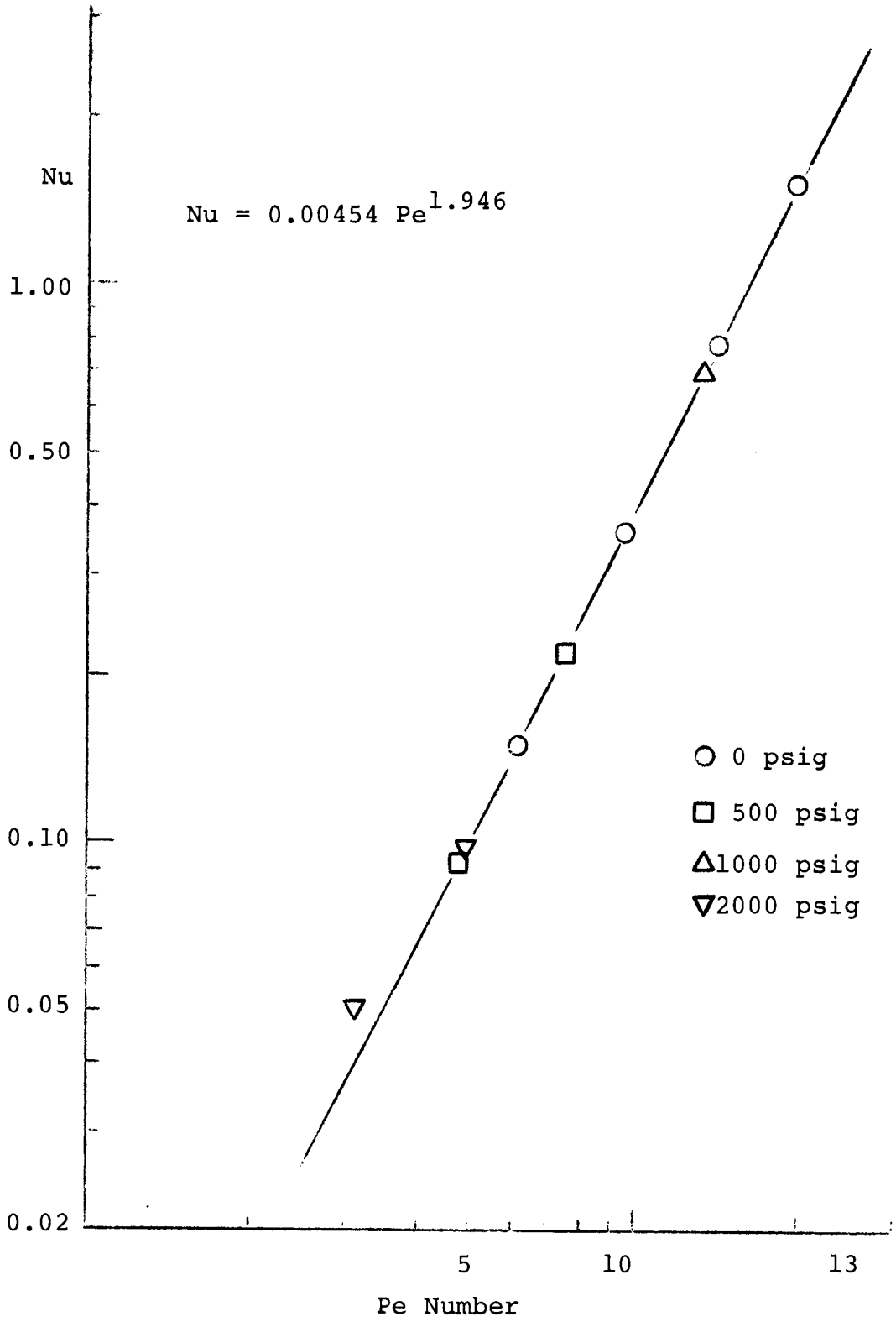


Figure 52. Correlation of heat transfer coefficient for liquid water.

adjust to T_s, which is already too small to be detected. Hence, the correlation given on Figure 52, i.e., Nu = $0.00454\ Pe^{1.946}$, predicts the limiting value of h. If h in the minute channel is larger than this value, which the data indicates is the case, the single phase heat transfer may be predicted without knowledge of h.

Thompson (2) has solved the one-dimensional governing equation without the assumption $T_F = T_s$, however, his method requires knowing both h and $\dot{m}$ in advance. He derives the equation Nu = $0.00454\ Pe^{1.946}$ analytically beginning with Equation E-9 of Appendix E. These authors have been unable to derive Equation E-9, however, Thompson shows Nu = $C_f(T_f)Pe^{1/2}$.

Unfortunately, Thompson's method fails to have a closed form solution when the heat leak from the back side of the plate is introduced into the governing equations in terms of measured heat transfer coefficient h_e (Appendix B). The heat leak can be significant fraction of the heat transfer, hence, Thompson's solution does not show as good a correlation of the temperature profiles as the method of Appendix B.

The pressure drop in the single phase region is compared with the Aerojet design correlation (6) in Figure 53.

$$\dot{m} = A\left[\left(\frac{2g}{144}\ \rho\Delta p\right)/K_c + K_e + f\frac{L}{D}\right]^{1/2}$$

K_c = contraction coefficient

K_e = expansion coefficient

f = friction factor

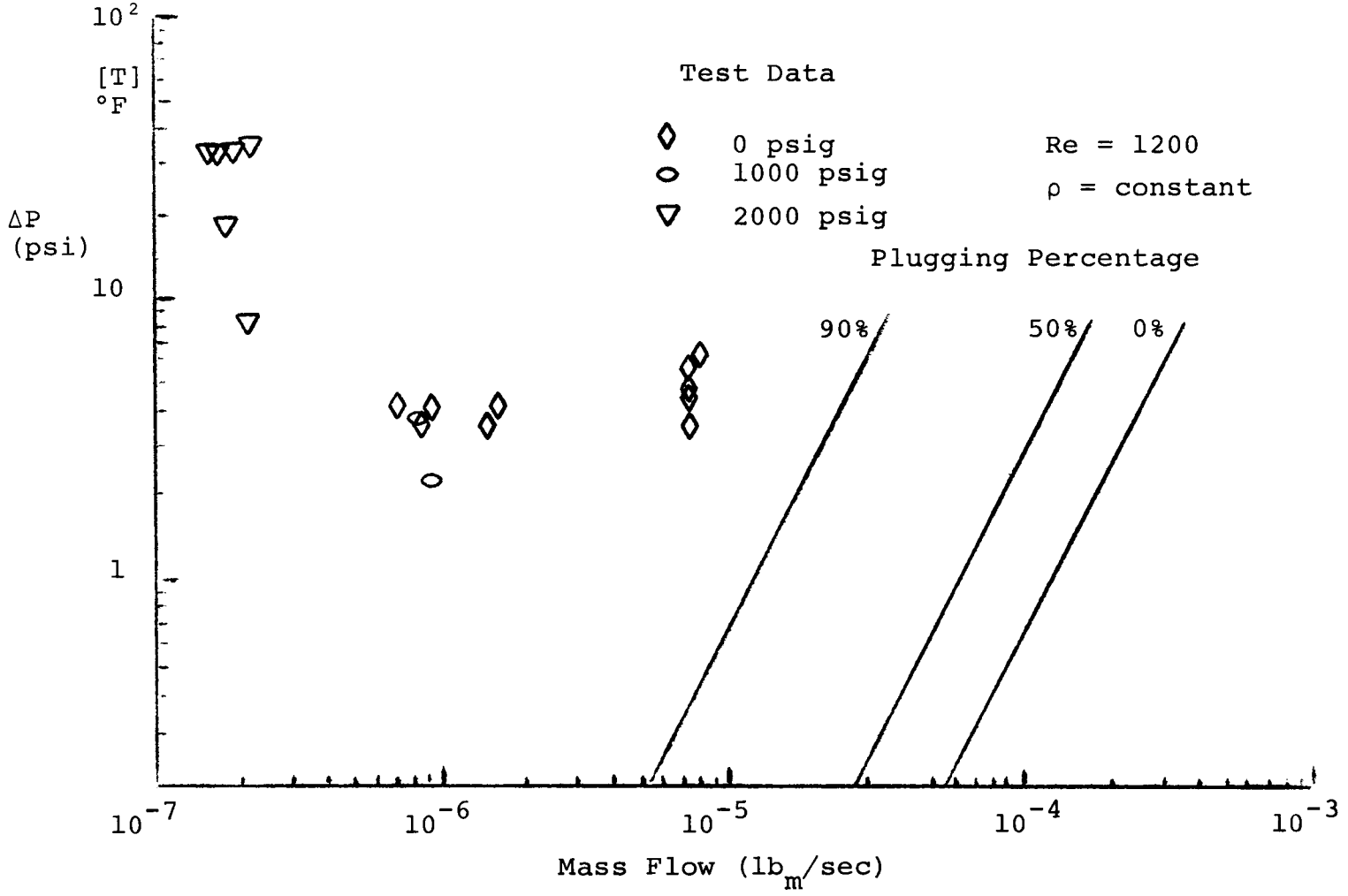


Figure 53. Comparison of single phase pressure drop with aerojet design correlation.

Curves for 0 to 90 per cent reduction in channel area are plotted to assess the effect of plugging. All measured pressure drops are considerably higher than the theoretical values. No explanation of these discrepancies is presently available.

Two Phase Flow

Correlation of the two phase flow data has been carried out with The University of Tennessee Space Institute computer code (5). The two phase flow region was analyzed from the governing equations:

$$\frac{d^2T_s}{dx^2} = \frac{h\ P(T_s - T_f)}{K_s\ A_c} \tag{6-1}$$

$$\frac{dH}{dx} = \frac{h\ P(T_s - T_f)}{\dot{m}} \tag{6-2}$$

where

P = periphery of slot

A_c = cross-sectional area of solid

$\dot{m}$ = mass flow rate of fluid per unit area of plate (lbm/ft^2-sec)

In the two phase region, the quality ($\bar{x}$) is introduced and an additional equation is required. An energy balance equation on a volume fluid element can be written in terms of a variable, η. η is defined as the fraction of the total amount of thermal energy used for evaporation in an element of mixture of thickness dx. Thus the equation is:

$$\frac{d\bar{x}}{dx} = \eta \frac{P}{\dot{m}} \frac{h(T_s - T_f)}{H_{\ell g}} \qquad (6\text{-}3)$$

η is a parameter which accounts for the departure from thermodynamic equilibrium. The limiting case, $\eta = 1.0$, means all the energy transferred to an element of mixture causes evaporation of the liquid and not superheating of the vapor; a constant vapor temperature also results. If $\eta = 0$, the quality would be constant and all heat transferred to the mixture would be used to superheat the vapor.

One parameter which is input to the analysis is the heat transfer coefficient. Precise relations for the coefficient are not available. For the forced convection region the heat transfer coefficient used is that for laminar fully developed flow in circular tubes:

$$h_c = Ek \frac{\alpha}{\beta}$$

where

k = fluid thermal conductivity

α = viscous resistance coefficient

β = inertial resistance coefficient

An average value for the constant E in the relation for the Nusselt number for constant heat flux and constant wall temperature was used.

The forced convection nucleate boiling heat transfer coefficient is estimated by superposition of forced convection and nucleate pool boiling coefficients.

$$h = h_{\text{forced convection}} + h_{\text{pool boiling}}$$

$$h = \frac{Nu\ k_\ell}{D_H} + \frac{k_\ell^3}{B^3 \mu_\ell^2 H_{\ell g}^2}\left(\frac{1}{\sigma}\left(\frac{1}{V_\ell} - \frac{1}{V_g}\right)^{1/2}\right)\frac{(T_s - T_\ell)^3}{T_s - T_f}$$

where B equals 0.013 to account for the water and stainless steel liquid-solid surface interaction. σ is the surface tension and the subscript ℓ denotes values at saturated conditions. V is the specific volume.

A criterion for the value $(T_s - T_\ell)$ above which the transition to film boiling occurs is given by:

$$(T_s - T_\ell)^3_{crit} = \frac{0.397\ B^3 H_{\ell g}}{V_g F_\ell}\left(\frac{V_g}{V_\ell} - 1\right)^{0.6}$$

$$F_\ell = \frac{k_\ell^3}{\mu_\ell^2 H_{\ell g}^2}\left(\frac{1}{\sigma_\ell}\left(\frac{1}{V_\ell} - \frac{1}{V_g}\right)\right)^{1/2}$$

H = fluid enthalpy

A closed form solution of the governing equations is not possible since they form a system of nonhomogeneous nonlinear differential equations. They can be solved using a Runge-Kutta numerical scheme. The experimental data provides the initial values to start the integration of the equations.

Difficulty was experienced in applying the theory since there are three unknown parameters which are required for input to the program. Unknown is the mass flux, G,

(due to the inaccuracy resulting in the measurement) the heat transfer coefficient, h, and the non-equilibrium thermodynamic parameter, η, which is defined as the fraction of heat transfer which contributes to phase change of the liquid.

Figure 54 shows a comparison of the data for Test 15--Run 1 with the computed curve for a number of combinations of the parameters, h, η, and G. For mass fluxes on the order of measured values, conventional boiling heat transfer coefficient and $\eta = 1$ (i.e., thermodynamic equilibrium) the correlation immediately departs from the two-phase flow data. By assuming a constant heat transfer coefficient and reducing its magnitude, the theoretical curve approach experimental values but only for ridiculously low values of h. Finally, the theoretical curve can be made comparable to the measured data for reduced values of η.

This suggests incomplete vaporization of the fluid in the channel which is a reasonable conclusion in view of the flow pattern shown in Figure 48, page 93. Figure 48 shows numerous unevaporated liquid droplets being expelled with the vapor. The latent energy content of these droplets is a very large fraction of the latent heat content of the complete mass flow.

With respect to the design of discrete injector nose-tips, this is a significant observation since a value of $\eta = 0.5$ represents a substantial reduction in the design heat flux calculated on the basis of thermodynamic

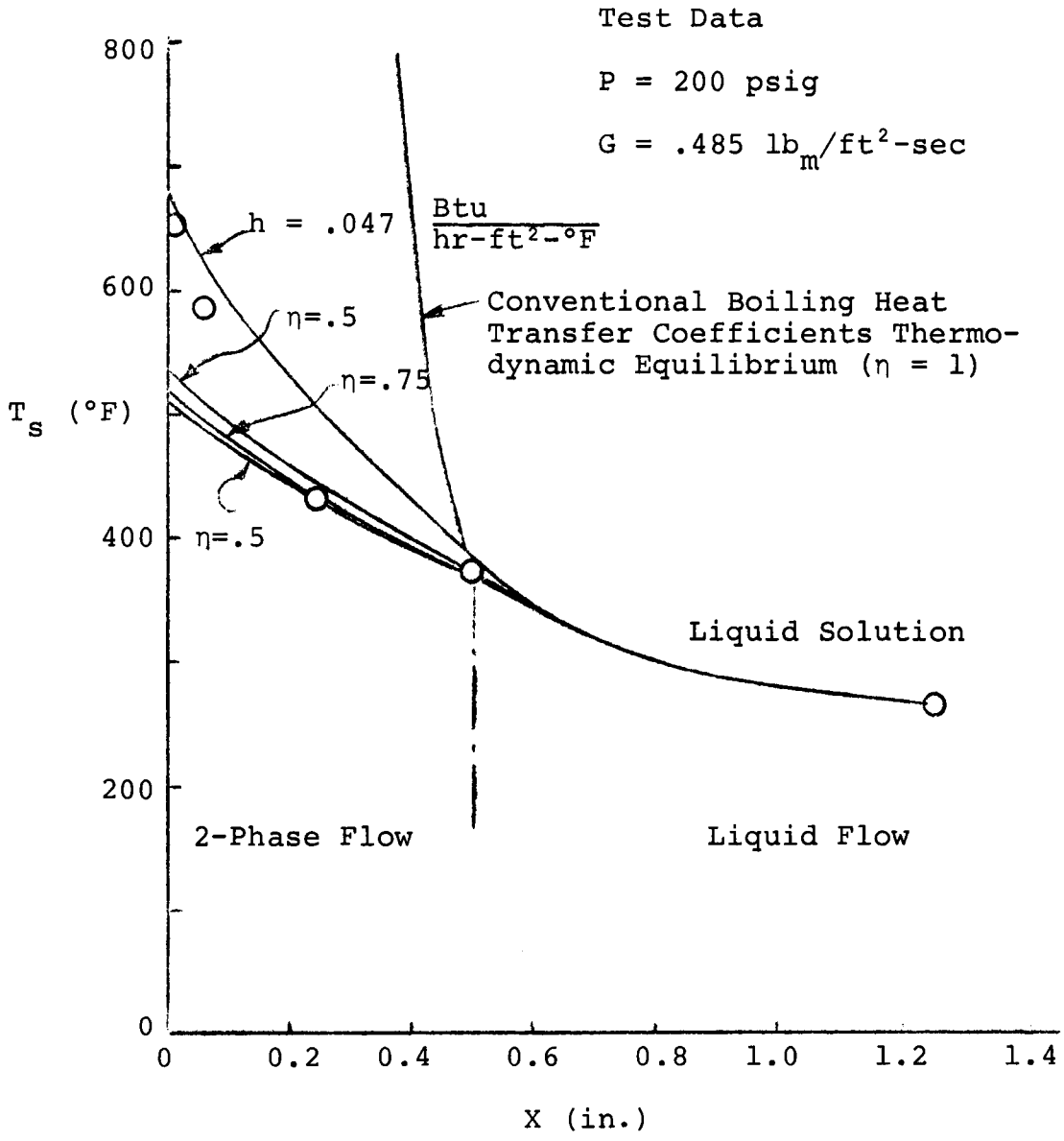


Figure 54. Comparison of The University of Tennessee Space Institute computer code solutions with data from test 15, run 1.

equilibrium. The calculated quality change of the fluid for the curve of Figure 54 is 24 per cent. The surface temperature of the land is considerably in excess of the saturation value. The computed solution indicates the liquid droplets are slightly superheated and the vapor temperature is near that of the wall. The magnitude of the quality change is greater, the further down the channel phase change occurs. The beginning of phase change is near the location where the solid temperature exceeds the saturated value of the fluid. In Figure 54 this is approximately 0.42 inches from the surface.

The two phase flow data shows two characteristic profiles:

1. A temperature profile having a uniform portion close to the surface with a value near saturation.

2. A temperature profile having a linear portion near the surface crossing the saturation value in-depth in the slot.

The first temperature profiles suggest that two phase flow occurs immediately at the exit and that the surface temperature can be maintained near the saturation temperature for a fairly significant variation in mass flux. Consider, for example, Test 13a where T_1 has a value between 486 °F and 475 °F corresponding to changes in measured mass flux from 1.76 $lb_m/sec\text{-}ft^2$ to 2.82 $lb_m/sec\text{-}ft^2$ (computed values are 0.28 $lb_m/sec\text{-}ft^2$ and 0.45 $lb_m/sec\text{-}ft^2$ respectively). The heat flux from Figure 43, page 87, is

approximately 165 Btu/sec-ft^2.

The transition to a high surface temperature with a linear profile and phase change in-depth occurs over a relatively narrow range of flow rate, evidenced again by the data of Test 13a--Runs 4 and 5. Note the surface temperature goes from 825 °F to 486 °F between the incremental change in mass flux of 0.1 cc/min. A similar effect is shown by the data of Test 18--Runs 3 and 4. The incremental change in mass flux employed with this test was larger, however, 1.0 cc/min and the transition region cannot be as carefully defined. This transition is believed to be associated with the transition from mist flow to the globule flow clearly evident in Figures 48 and 49, pages 93 and 94.

The general nature of the observed flow is not unlike the flow associated with the boiling crisis encountered in high heat flux nuclear reactor cooling systems. The boiling crisis is an instability phenomenon that is triggered when a critical condition in the heat transfer process is reached. A slight increase in heat flux or a decrease in mass flow at this critical condition will result in a rapid excursion in wall temperature from a nominal value to a value well in excess of the common melting temperature of metals. If during intense heating of the nosetip, one slot was to undergo this transition to the high temperature regime the resulting localized heating would trip the neighboring slots and melting would rapidly propagate over the surface.

MacBeth (3) has correlated the "world's data" on

burnout for low velocity water flowing in uniformly heated round tubes. The correlation for the pressure range of 15-2000 psia is

$$q \times 10^{-6} = \frac{(G \times 10^{-6})(h_{fg} + \Delta h)}{158d^{-0.1}(6 \times 10^{-6})^{0.49} + 4L/d}$$

q = heat flux, Btu/hr-ft^2

G = mass flux, lb_m/hr-ft^2

d = diameter, in.

L = length of channel, in.

For Test 13 this predicts a burnout heat flux of approximately 2 Btu/sec-ft^2 suggesting that correlation for the uniformly heated conventional dimensional ducts do not predict the transition in non-uniformly heated narrow passages. Tong (4) observes that the magnitude of the critical heat flux depends upon the length of hot patch. Shorter hot patch gives higher critical heat flux. The shorter hot patch is applicable to this study, however, Tong does not show a hundred fold increase as required for the theory to match the measured fluxes in this case. Therefore, method of predicting the expected transition from mist flow to globule flow in narrow slots heated on the end is apparently not presently available.

The mechanism envisioned for the change from mist flow to globule flow is illustrated in Figure 55. Consider Figure 55(a), the flow is mist flow and the surface is

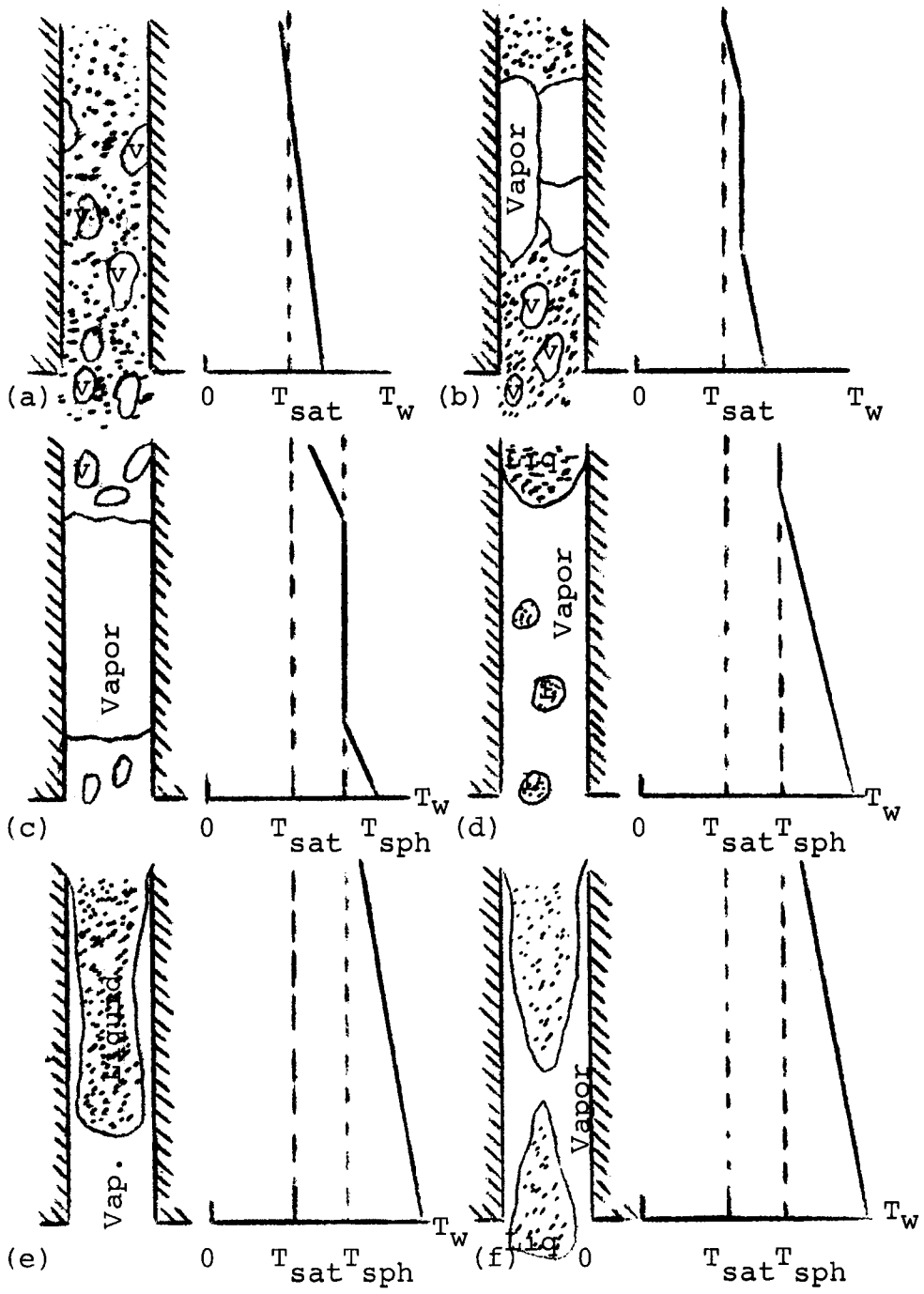


Figure 55. Transition from mist flow to globule flow.

cooled by the fluid. In (b) large vapor formation has insulated the surface causing a region of temperature rise.

The coolant is blocked by the vapor formation which grows toward the exit. At the same time the temperature rises near the surface since heating is from that direction and the cooling path is blocked by the vapor. In (d) the vapor formation is finally expelled, however, the wall temperature has exceeded the spheroidal temperature and the fluid returning to the wall can no longer wet the surface. Hence, a film is formed between the wall and the liquid and the globule flow pattern begins.

The development of a mathematical model of the described phenomenon subsequently verified with experiment may shed light upon the transition from mist flow to globule flow. It is noted that the change in flow pattern with the sudden excursion to high temperatures encountered in this study would be disastrous at the much higher heat fluxes experienced during reentry. For the present study the maximum temperature the land could assume is on the order of 1000 °F (controlled limit due to melting temperature of the block heater). In flight this temperature is unrestricted and the land temperature would change from the saturated value to a value well in excess of melting.

In-Depth Cooling

The important question of the internal cooling study is how much cooling is achieved in-depth. Figure 56 shows a

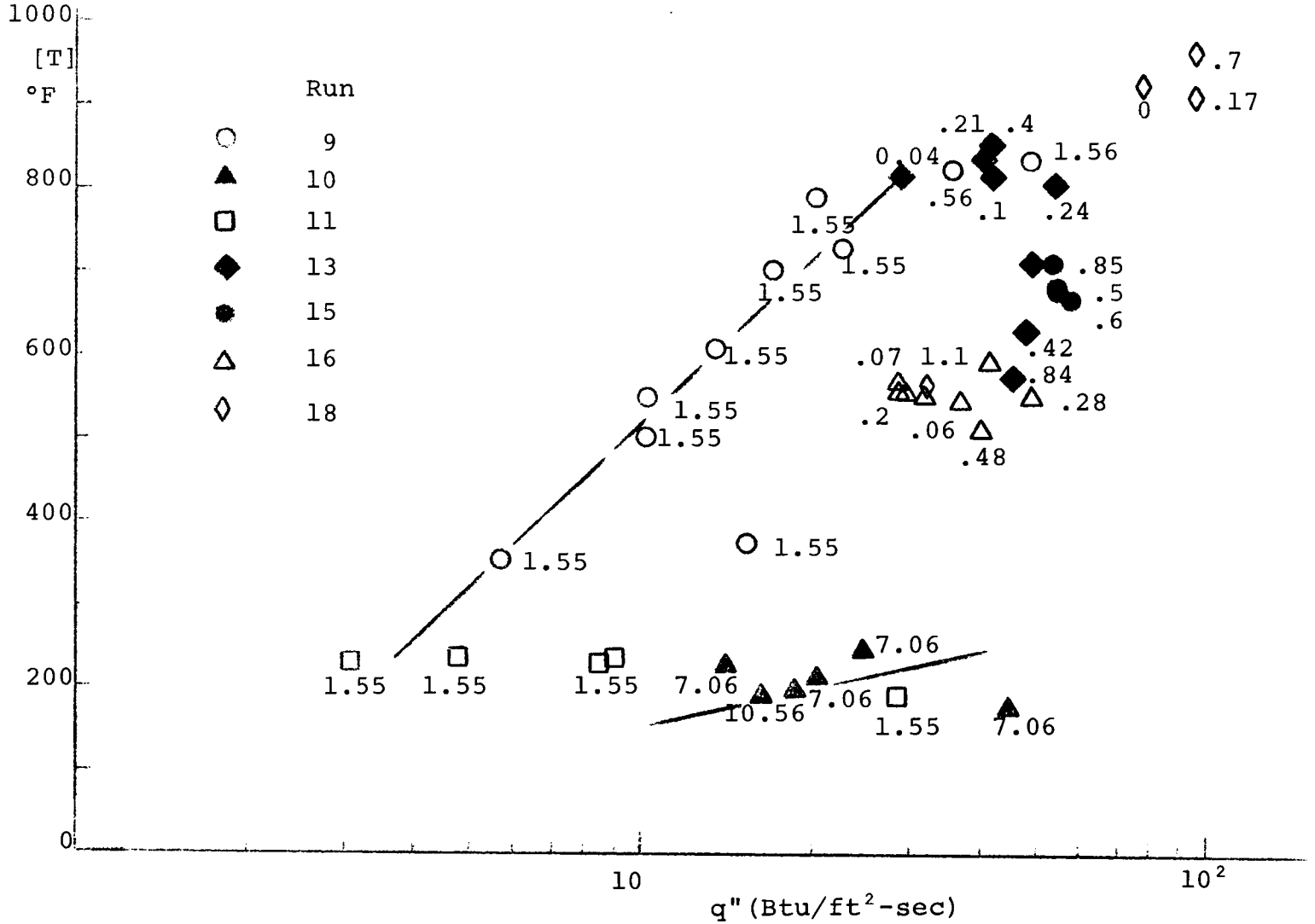


Figure 56. Surface temperature versus heat flux for stable flow.

plot of surface temperature versus heat flux for stable flow. The scatter in the data is rather large; however, one observes that the maximum operating temperature of the system is reached at heat fluxes very low relative to in-flight values for mass fluxes on the order of 0-1.5 lbm/sec-ft^2. The upper limits of these mass flux values are 50 per cent larger than typical values used in designing nose-tips for in-flight operation where heat fluxes on the order of 2000-5000 Btu/sec-ft^2 are encountered. At very large mass fluxes 7-10 lb_m/sec-ft^2, the surface is maintained at reasonable temperatures for the highest heat fluxes achieved in the present experiment.

Despite the uncertainty in the data of Figure 56, it is evident that in-depth cooling will not provide the necessary thermal capacity required for in-flight operation. In view of the fact the TCNTs have been flown with relative success, one therefore concludes that significant cooling due to discrete injection must occur externally in the boundary layer. Although this suggests that knowledge of in-depth heat transfer and fluid flow is unimportant to design, it is conjectured that the blockage cooling effect in the boundary layer may well be independent upon the pattern of the liquid ejected from the slots which is controlled by the flow and heat transfer mechanism in the slots. For example, the finely atomized flow pattern Figure 48, page 93, will result in the liquid being well dispersed throughout the boundary layer, whereas, for the globule flow

pattern of Figure 49, page 94, the water will be expelled in large drops which will not wet the surface and in high velocity flow would likely be carried downstream. It is intuitively evident that the dispersed liquid pattern provides greater local external boundary layer cooling than the globules. Since at certain critical conditions, this change in flow pattern can occur very suddenly for minor changes in heat flux or mass flux the in-depth problem is concerned with designing to avoid these critical conditions from occurring in the slots under in-flight operation.

CHAPTER VII

CONCLUSIONS

The results of the investigation lead to the following conclusions:

1. In-depth cooling at acceptable mass fluxes (approximately 1 $lb_m/sec\text{-}ft^2$) will not in itself provide thermal protection of TCNTs during in-flight operation.

2. Full vaporization in the slots is generally not realized and under two-phase flow conditions the fluid exits in a mist or in a globule flow pattern.

3. The transition from one flow pattern to the other is accompanied with temperature excursion which is conjectured to represent a situation which could result in melting of the nosetip.

4. The two-phase flow heat transfer is reasonably well correlated with The University of Tennessee Space Institute computer code employing conventional boiling heat transfer coefficients and pressure drop correlations providing the appropriate thermodynamic non-equilibrium factor, η, can be estimated.

5. The single phase flow heat transfer is correlated with conventional prediction methods employing the assumption of constant properties and that the solid temperature and fluid temperature are equal. This alleviates the

problem of determining the heat transfer coefficients.

6. The pressure drop in the single phase flow does not correlate the data and no explanation of this is presently available.

BIBLIOGRAPHY

BIBLIOGRAPHY

1. Metals Handbook. Eighth edition. Vol. 1. Metals Park, Ohio: American Society for Metals, 1961.

2. Thompson, J. Private communication. Aerotherm, Inc., Mountain View, California, November, 1972.

3. MacBeth, Robert V. "The Burn-Out Phenomenon in Forced Convection Boiling," Advances in Chemical Engineering, T. B. Drew, G. R. Cokelet, J. W. Hoopes, Jr., and T. Vermeulen, editors. Vol. 7. New York: Academic Press, 1968. Pp. 207-293.

4. Tong, L. S. Boiling Heat Transfer and Two-Phase Flow. New York: John Wiley and Sons, Inc., 1965.

5. VonReth, Rolf D. "An Experimental and Analytical Investigation of One-Dimensional Two-Phase Flow Transpiration Cooling Through Porous Metals." Ph.D. dissertation, The University of Tennessee, Knoxville, 1971.

6. Anderson, L. Private communication. Aerotherm, Inc., Mountain View, California, December, 1972.

APPENDIXES

APPENDIX A

EXPERIMENT PROCEDURE

The equipment items referred to in the following are listed in Figure 2, page 6.

Check List

1. Set regulator on 3000 psi nitrogen bottle to about 25 psi. Check the filter to make sure it is clean. Operate with a pump inlet pressure between 10 and 15 psi as shown by pump inlet pressure gage on control console. NEVER ALLOW PRESSURE TO BE 5 PSI OR LESS!!!

2. Before opening the regulator shut-off valve, fill storage and de-gassing tank with distilled water. Open shut-off valve.

3. Turn on the electrical heater in the tank and set thermostat control to about 180 °F.

4. Open discharge, bleed and priming valves on pump.

5. Close discharge, bleed and priming valves after liquid water flow is achieved.

6. Charge accumulator to 90 per cent of test feed-line pressure using nitrogen bottle at 3000 psi or 6000 psi depending on test pressure desired. If high pressure bottle is used, follow the procedure below. If the 3000 psi bottle is used this operation must be done before steps 1 through 5 are done. 6000 psi bottle: Close shut-off valve on

regulator and disconnect plug on "T" fitting. Connect line from that fitting to accumulator and open accumulator valve. Disconnect line from regulator to pressure vessel and plug that end of the "T" fitting. Set regulator to 90 per cent of desired feed line pressure and open shut-off valve to charge accumulator. Close valve on accumulator and regulator shut-off valve after charging. Reconnect as before this operation. 3000 psi bottle: Disconnect pressure line from regulator shut-off valve and storage and de-gassing tank at the fitting on the tank. Reconnect that end to the accumulator. Close shut-off valve on regulator and set regulator to 90 per cent of desired feed line pressure. Open accumulator valve and regulator shut-off valve to charge accumulator. Close valve on accumulator and regulator shut-off valve after charging. Reconnect as before this operation.

7. Adjust back-pressure regulator to desired line pressure. This can be done only approximately since there is no scale on the regulator.

8. Turn on pump and let run for at least an hour to reach a stable operating flow rate and to completely prime the pump. Adjust the pump for the maximum stroke with the control on the pump.

9. Close inlet feed valve and open by-pass valve after turning on pump.

10. Steps 10 through 14 are necessary only to establish an inert atmosphere in the vessel after the vessel has been open to the room atmosphere. Close the pressure

gage shut-off valve.

11. Connect vacuum pump at the drain line "T" fitting. Disconnect line to drain and plug that end of "T" fitting.

12. Close shut-off valve on 6000 psi regulator.

13. Open outlet feed valve and turn on vacuum pump. Leave the pump on for about 30 minutes.

14. Disconnect the vacuum pump and reconnect as before this operation.

15. Set the regulator on the 6000 psi nitrogen bottle to slightly above the desired pressure. Open shut-off valve on the regulator and charge vessel. Close valve on regulator after charging.

16. Open pressure gage shut-off valve.

17. Adjust vessel pressure with the outlet feed valve by bleeding excess nitrogen.

18. Turn on multi-point strip chart recorder and continuous reading strip chart recorder. Turn on differential pressure transducer power supply and set for one volt.

19. Turn on cooling coils and finned heat exchanger by opening water valve.

20. Turn on D.C. power supply and adjust to desired power setting. It is advised to monitor the copper block temperature on the recorder to see that it does not exceed about 1200 °F.

21. Close by-pass valve and keep inlet feed line valve closed. Allow the inlet feed line to come to a

pressure above the vessel pressure before proceeding to next step.

22. Open inlet feed line valve to a digital setting of about 20. Also open the by-pass valve slightly to a setting of around 5.

23. Reduce the pump stroke setting from full to about 75 per cent of maximum stroke.

24. The flow rate is now controlled by adjusting the by-pass valve and the pump stroke control. It will be necessary to alternately adjust the two controls to obtain the desired flow rate. The rotameter will show when the desired flow rate has been achieved.

25. Run test.

Shut-Down Procedure

1. Close inlet feed line valve.

2. Turn off pump and close by-pass valve.

3. Turn off D.C. power supply and differential pressure transducer power supply and continuous reading recorder.

4. Close shut-off valve on 3000 psi nitrogen regulator and open vent valve on storage and de-gassing tank.

5. Turn off heater coil inside storage and de-gassing tank.

6. Turn off multi-point strip chart recorder.

7. De-pressurize vessel if desired using 6000 psi nitrogen regulator. Open shut-off valve on regulator and

close valve on the bottle of nitrogen. Turn the knob on the regulator to reduce the pressure until the desired pressure is reached.

8. If a long down time is anticipated it is a good idea to turn off power to the control console.

Emergency Procedures

Clogged Inlet Filter: Inlet pump pressure gage will approach 0 psi reading. Immediately shut off pump before 0 psi reading is reached.

Water Line Rupture (Including Components):

1. Pull emergency switch. This will simultaneously turn off pump and heater elements in copper wedge.

2. Follow standard shut-down procedure. Beware of high velocity blow-down jets.

Pressure Vessel Rupture:

1. Pull emergency switch.

2. Close shut-off valve on 6000 psi nitrogen regulator being cautious of any high pressure nitrogen jets.

3. Follow standard shut-down procedure.

Vessel Over Pressurization:

1. Open outlet feed valve.

2. Close shut-off valve on 6000 psi nitrogen regulator.

3. Proceed to standard shut-down procedure.

APPENDIX B

SINGLE PHASE FLOW DATA ANALYSIS

Correlation of data for the cases where liquid flow was achieved throughout the entire length of the slots have been carried out. The most reliable data for these runs are the temperature distribution along the solid plate. Mass flux was unknown since due to plugging it was not certain whether the flow through a given slot was more or less than measured. This posed the problem that both h and $\dot{m}$ need be determined from the raw data. To circumvent this difficulty the data was analyzed assuming that the fluid temperature was equal to the solid temperature. The heat transfer coefficient can then be eliminated from the governing equations and the mass flux found by trial and error which gives a computed temperature distribution in agreement with the experiment.

The analysis is as follows for the iterative solution for $\dot{m}$:

Energy balance on solid:

$$kA_s \frac{d^2T_s}{dx^2} - 2wh_E[T_s - T_e] = hP[T_s - T_f] \qquad \text{(B-1)}$$

Energy balance on the coolant:

$$\dot{m} \frac{dH}{dx} = -hP[T_s - T_f] \qquad \text{(B-2)}$$

For water it can be assumed:

$$\frac{dH}{dx} = c\,\frac{dT}{dx} \tag{B-3}$$

with

$$\theta(x) = T_s(x) - T_e \tag{B-4}$$

This leads to a governing differential equation:

$$\frac{d^2\theta}{dx^2} + \frac{\dot{m}c}{kA_s}\,\frac{d\theta}{dx} - \frac{2h_E w}{kA_s} = 0 \tag{B-5}$$

which has a general solution of the form:

$$\theta(x) = a_1 e^{\lambda_1 x} + a_2 e^{\lambda_2 x} \tag{B-6}$$

with

$$\lambda_{1/2} = \frac{1}{2}[-A^* \pm \sqrt{(A^*)^2 + 4B^*}] \tag{B-7}$$

where

$$A^* = \frac{\dot{m}c}{kA_s} \text{ and } B^* = \frac{h_E w}{kA_s} \tag{B-8}$$

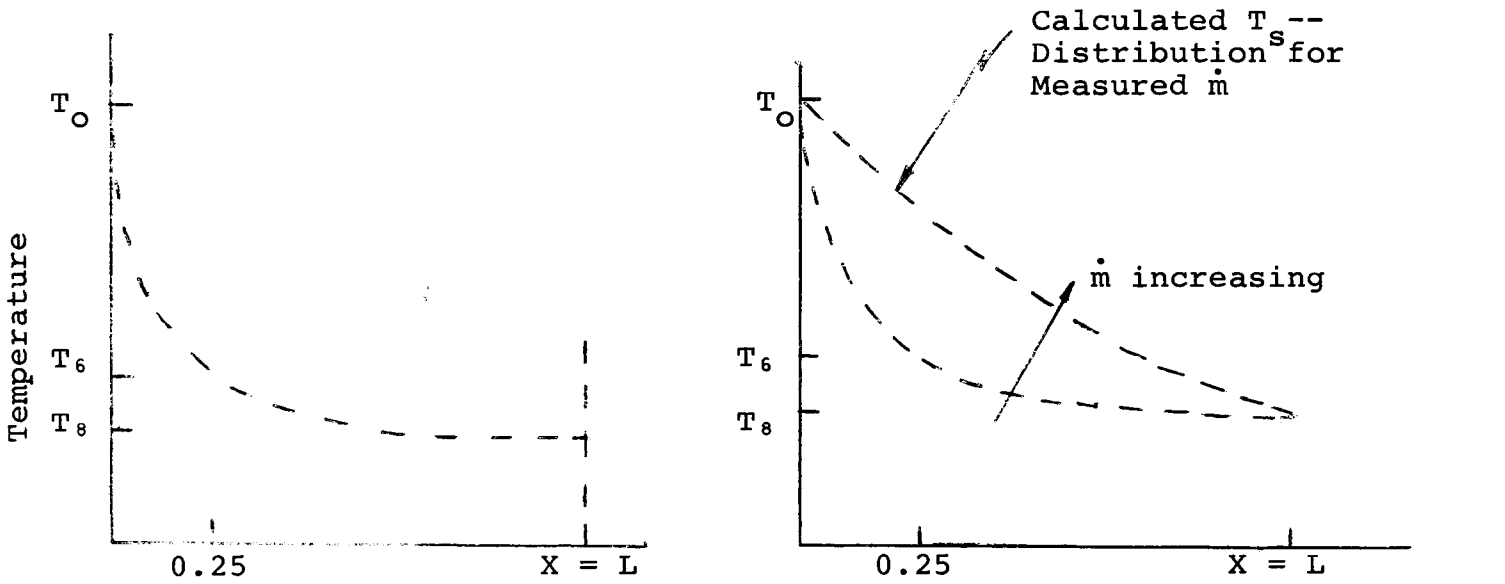
The following boundary conditions were applied:

$$x = 0; \qquad \theta = T_0 - T_E$$

$$x = L; \qquad \theta = T_8 - T_E \tag{B-9}$$

where $T_0 = T_1 + 25\ ^\circ F$ was found to be a reasonable approximation when compared with some more carefully extrapolated values.

The resulting temperature distribution for the measured mass flow, $\dot{m}$, was generally too high, as demonstrated in Figure 57. An iteration procedure varying the mass flow such that the curve would pass through the actual measured value T_6 at x = 0.25 inches yielded a temperature distribution which was found to be in good agreement with the experimental data. Figures 19 through 32, pages 61 through 74, give examples for such iterated temperature distributions.



(a) Typical Temperature Distribution (b) Calculated Temperature Distribution

Figure 57. Representation of actual temperature distribution by mass flow iteration.

APPENDIX C

DETERMINATION OF THE HEAT TRANSFER COEFFICIENT AT THE COOLANT-SOLID INTERFACE

From the analysis of Appendix B, the governing equation is:

$$\dot{m}c_p \frac{dT_f}{dx} = -Ph(T_s - T_f) \tag{C-1}$$

For a point "a" along the channel:

$$h_a(T_s - T_f)_a = -\frac{\dot{m}c_p}{P}\frac{dT_f}{dx}\bigg|_a = J_a \tag{C-2}$$

and similarly for another point "b" distance Δx away:

$$h_b(T_s - T_f)_b = -\frac{\dot{m}c_p}{P}\frac{dT_f}{dx}\bigg|_b = J_b \tag{C-3}$$

consider a fluid element of length Δx between these two points. The heat transfer from the solid can be written as:

$$dQ = hP(T_w - T_B) = -\dot{m}c_p\, dT_B$$

$$= -\rho u_m A c_p\, dT_B \tag{C-4}$$

Then:

$$\frac{1}{\rho u_m c_p}\int_x^{x+\Delta x} h(x)\,dx = \frac{A}{P}\int_{T_a}^{T_b}\frac{dT}{T_w - T_B} \tag{C-5}$$

If we assume constant properties over a small interval then:

$$h(x) = \bar{h}$$

$$T_w(x) = \bar{T} = \frac{T_{sa} + T_{sb}}{2} \tag{C-6}$$

and it can be integrated to obtain:

$$\frac{\bar{h}}{\rho u_m c_p}\Delta x = \frac{A}{P} \ln\left(\frac{T_w - T_a}{T_w - T_b}\right) \tag{C-7}$$

and thus,

$$\bar{h} = \rho u_m c_p \frac{A}{P\Delta x} \ln\left(\frac{T_w - T_a}{T_w - T_b}\right) \tag{C-8}$$

or with the Equations C-2 and C-3 approximately,

$$\bar{h} \simeq \frac{\dot{m}c_p}{P\Delta x} \ln\left(\frac{J_a}{J_b}\right) \tag{C-9}$$

Now as,

$$J = \dot{m}c_p \frac{dT_s}{dx} \tag{C-10}$$

and as from Equation B-6:

$$\theta = T_s - T_E = a_1 e^{\lambda_1 x} + a_2 e^{\lambda_2 x} \tag{C-11}$$

J can be expressed as:

$$J = \dot{m}c_p [\lambda_1 c_1 e^{\lambda_1 x} + \lambda_2 c_2 e^{\lambda_2 x}] \tag{C-12}$$

Thus, $\bar{h}$ in Equation C-9 can be determined incrementally along the flow channel which was carried out on a computer.

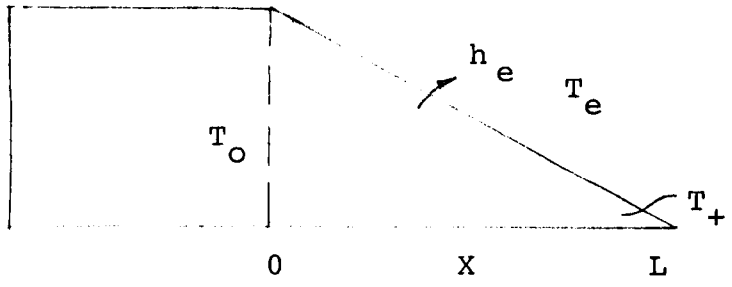
Plotting $\bar{h}$ in the form of a Nusselt number, $Nu = \frac{h\ D_H}{k_f}$ and Peclet number, $Pe = \frac{mD_H}{A\mu}\frac{c_p\mu}{k_f}$, gives the correlation shown in Figure 52, page 99.

APPENDIX D

DETERMINATION OF HEAT FLUX FROM HEATER POWER INPUT AND BLOCK TEMPERATURE

In some of the tests where two phase flow was present at the slot exit, it was not possible to calculate the heat flux into the land from the temperature gradient. It is then necessary to determine the heat flux by means of a correlation of heat flux with the power supplied to the heaters, the temperatures of the copper block and the land at the slot exit, the ambient temperature in the pressure vessel, and the heat transfer coefficient between the block surface and the vessel atmosphere.

The dimensionless parameters governing this process are determined as follows. A diagram of the block is shown below:



An energy balance on the block gives:

$$kA(x)\frac{d^2T}{dx^2} = -h_e P(x)[T(x) - T_e] \qquad (D\text{-}1)$$

Defining:

$$\theta(x) \equiv \frac{T(x) - T_e}{T_o - T_e} \tag{D-2}$$

and

$$x' \equiv x/L \tag{D-3}$$

Equation D-1 becomes:

$$\frac{kA(x)}{L^2}(T_o - T_e)\frac{d^e\theta}{dx'^2} = -h_e P(x)[T_o - T_e]\theta(x)$$

$$\frac{d^2\theta}{dx'^2} = -\frac{h_e P(x) L^2}{kA(x)}\theta(x) \tag{D-4}$$

Define:

$$Nu_x \equiv \frac{h_e P(x) L^2}{kA(x)}$$

$$\frac{d^2\theta}{dx'^2} = -Nu_x\theta(x) \tag{D-5}$$

At

$$x = L,\ T(L) = T_t,\ \theta = \theta_+ = \frac{T_+ - T_e}{T_o - T_e}$$

$$\left.\frac{d^2\theta}{dx'^2}\right|_{x'=1} = -Nu_L\theta_+ \tag{D-6}$$

Where:

$$Nu_L = \frac{h_e P(L) L^2}{kA(L)} \tag{D-7}$$

and h_e is a function of the vessel pressure.

At x = 0,

$$kA_o \frac{dT}{dx} = -P \qquad \text{(D-8)}$$

where P is the power supplied to the heaters.

Substituting D-2 and D-3 into Equation D-8 and rearranging:

$$\left.\frac{d\theta}{dx'}\right|_o = - \frac{PL}{kA_o(T_o - T_e)} \qquad \text{(D-9)}$$

At x = L, the heat conducted into the land is given by:

$$q = -k \left.\frac{dT}{dx}\right|_{x=L}$$

$$= -k \frac{T_o - T_e}{L} \left.\frac{d\theta}{dx'}\right|_{x'=1}$$

$$\left.\frac{d\theta}{dx'}\right|_{x'=1} = - \frac{qL}{k(T_o - T_e)}$$

The dimensionless groups are thus:

$$\frac{PL}{kA_o(T_o - T_e)}, \frac{qL}{k(T_o - T_e)}, \text{Nu, and } \theta_+$$

The ratio of heat flux to the heater power P should then correlate with:

$$Nu_L = h_e \frac{P(L)L^2}{kA(L)}$$

where h_e is a function of the vessel pressure and

$$\theta_+ = \frac{T_+ - T_e}{T_o - T_e}$$

APPENDIX E

THOMPSON SOLUTION WITHOUT ASSUMPTION $T_s = T_F$

Thompson proposed the following method of solution. The governing equations:

$$kA_s \frac{d^2T}{dx^2} = Ph(T_s - T_f) \tag{E-1}$$

and

$$\dot{m}c_p \frac{dT_f}{dx} = Ph(T_s - T_f) \tag{E-2}$$

lead to a general solution:

$$T_s - T_f = c_1 e^{r_1 x} + c_2 e^{r_2 x} = \Delta T \tag{E-3}$$

with,

$$r_{1/2} = \frac{1}{2}[-A \pm \sqrt{A^2 + 4B}]$$

where,

$$A = \frac{Ph}{\dot{m}c_p} \text{ and } B = \frac{Ph}{kA_s}$$

Combining Equations E-1 and E-2 and integrating twice yields:

$$T_s = B\left(\frac{c_1}{r_1^2} e^{r_1 x} + \frac{c_2}{r_2^2} e^{r_2 x}\right) + c_3 x + c_4 \tag{E-4}$$

Equation E-3 and E-4 together with the boundary conditions (Set I):

$x = 0;$ $\quad \Delta T = T_o - T_g;$ $\quad T_s = T_o$

$x = L;$ $\quad \Delta T = 0;$ $\quad T_s = T_g$

represent the first approach to solve for the temperature distribution.

The results obtained are qualitatively given in Figure 58. Comparing these with some typical data, as in Figure 57, page 128, it is seen that the values are too high. Attempts to influence the results by choosing suitable convection coefficients or changing the mass flow rate did not succeed. The effect of a variation of h is shown in Figure 59. The solution did not seem to be very sensitive to mass flow.

A second approach was tried by using Equation E-3 together with Equation E-2 which can be written after integration as:

$$T_c = A\left[\frac{c_1}{r_1} e^{r_1 x} + \frac{c_2}{r_2} e^{r_2 x}\right] + c_5 \qquad \text{(E-5)}$$

The following boundary conditions were used (Set II):

$x = 0;$ $\quad \Delta T = T_o - T_g;$ $\quad T_c = T_g$

$x = L;$ $\quad \Delta T = 0$

The results are again qualitatively given in Figure 60. As one boundary condition less than in the previous

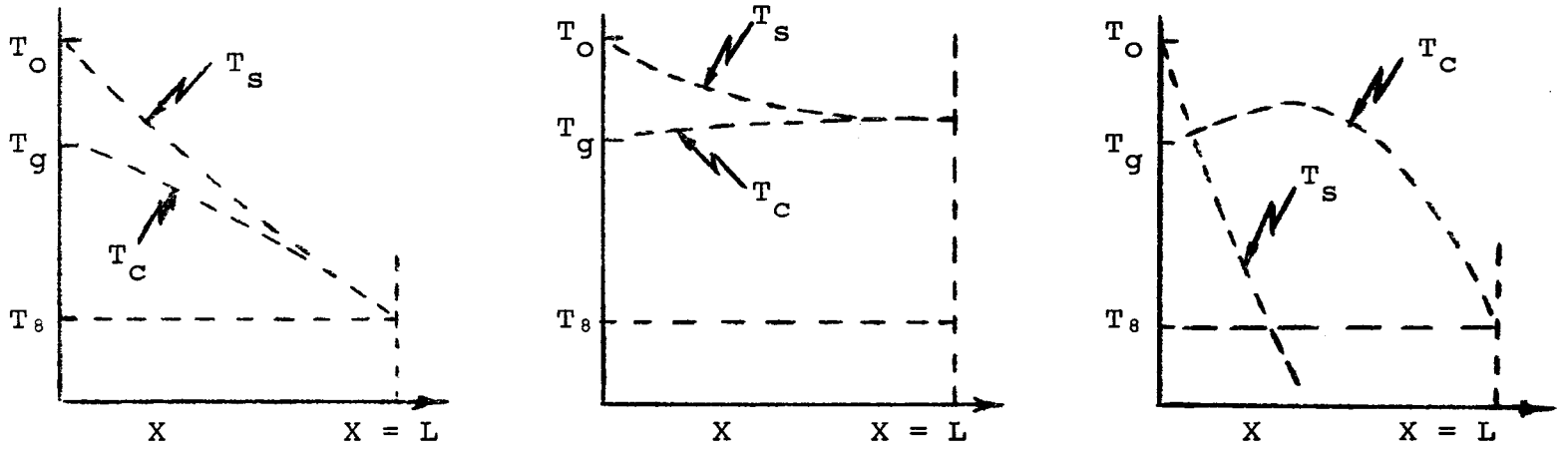


Figure 58. Qualitative solutions to approaches I-III.

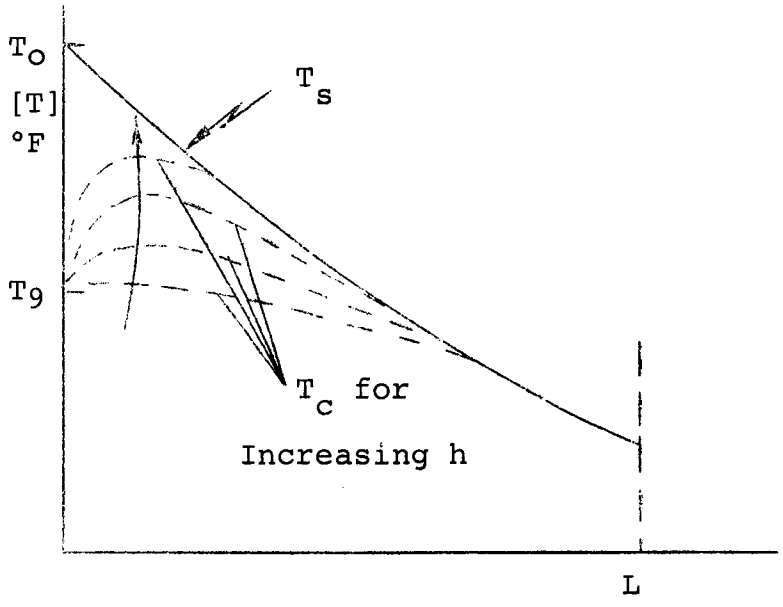


Figure 59. Influence of h--approach I.

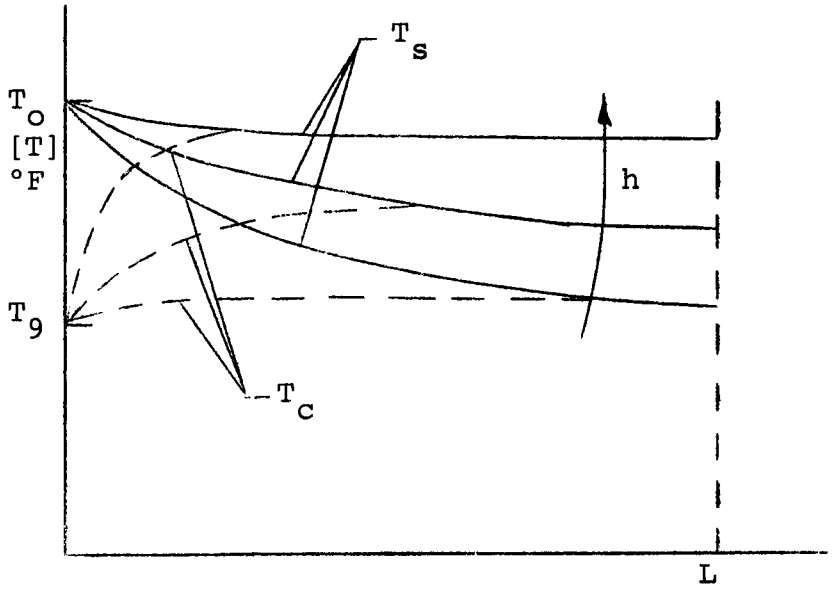


Figure 60. Influence of h--approach II.

case was used at x = L, a natural boundary condition, tending to shift the curve to higher temperatures was established at that end. The sensitivity to convection coefficient and mass flow rate was similar to the first case, Figure 59, and therefore their influence not big enough to change the temperature distribution to a typical one shown in Figure 58.

A third approach was carried out using Equation E-3 with new coefficients:

$$\Delta T = c_5 e^{r_1 x} + c_6 e^{r_2 x} \qquad \text{(E-6)}$$

and Equation E-5 with new coefficients to be determined from another set of boundary conditions:

$$T_c = A\left(\frac{c_5}{r_1} e^{r_1 x} + \frac{c_6}{r_2} e^{r_2 x}\right) + c_7 \qquad \text{(E-7)}$$

These boundary conditions were (Set III):

$x = 0;$ $\quad \Delta T = T_o - T_9;$ $\quad T_c = T_9$

$x = L;$ $\quad T_c = T_8$

Figure 59 shows this solution qualitatively. Again, it was not possible to find a suitable combination of convection coefficient h and mass flow rate, $\dot{m}$, to shift the distribution into the vicinity of the actual measured values.

The University of Tennessee Space Institute solutions for temperature distribution do not appear to lead to the

same conclusions obtained by Thompson. As it is believed, however, that the original UTSI solution based on $T_s = T_f$ and incorporating the experimentally determined leakage coefficient, h_e, is correct because of the excellent agreement with experimental results.

The conclusion that the limiting heat transfer coefficients correlate with:

$$Nu = \mu P_e^{\,2} \tag{E-8}$$

is a valid correlation for low mass flux.

Thompson begins with the equation:

$$q = k(T_o - T_f(x=c))r_2 \tag{E-9}$$

and derives Equation E-8. The present authors cannot obtain Equation E-9 analytically, however.

VITA

John H. Wickman was born in Elgin, Illinois, on March 12, 1949. He attended elementary schools in Barrington, Illinois, and graduated from Arcadia High School in Phoenix, Arizona in 1967. The following September he entered Arizona State University, and in June 1971, he received a Bachelor of Science degree in Mechanical Engineering. In the summer of 1971, he accepted a research assistantship at The University of Tennessee Space Institute and began study toward a Master's degree. He received this degree in August, 1973 while being employed since December, 1972 by Pratt and Whitney Aircraft in East Hartford, Connecticut.